

# **For Reference**


---

**NOT TO BE TAKEN FROM THIS ROOM**



Ex LIBRIS  
UNIVERSITATIS  
ALBERTAENSIS





Digitized by the Internet Archive  
in 2023 with funding from  
University of Alberta Library

<https://archive.org/details/Humphries1982>













THE UNIVERSITY OF ALBERTA

RELEASE FORM

NAME OF AUTHOR           JOSEPH A. HUMPHRIES  
TITLE OF THESIS         THE DIFFUSION OF BLUFF WALL JETS WITH  
                             FINITE TAILWATER DEPTH  
DEGREE FOR WHICH THESIS WAS PRESENTED   MASTER OF SCIENCE  
YEAR THIS DEGREE GRANTED   SPRING 1982

Permission is hereby granted to THE UNIVERSITY OF ALBERTA LIBRARY to reproduce single copies of this thesis and to lend or sell such copies for private, scholarly or scientific research purposes only.

The author reserves other publication rights, and neither the thesis nor extensive extracts from it may be printed or otherwise reproduced without the author's written permission.








THE UNIVERSITY OF ALBERTA

THE DIFFUSION OF BLUFF WALL JETS WITH FINITE TAILWATER DEPTH

by

 JOSEPH A. HUMPHRIES

A THESIS

SUBMITTED TO THE FACULTY OF GRADUATE STUDIES AND RESEARCH  
IN PARTIAL FULFILMENT OF THE REQUIREMENTS FOR THE DEGREE  
OF MASTER OF SCIENCE

CIVIL ENGINEERING

EDMONTON, ALBERTA

SPRING 1982





THE UNIVERSITY OF ALBERTA  
FACULTY OF GRADUATE STUDIES AND RESEARCH

The undersigned certify that they have read, and recommend to the Faculty of Graduate Studies and Research, for acceptance, a thesis entitled THE DIFFUSION OF BLUFF WALL JETS WITH FINITE TAILWATER DEPTH submitted by JOSEPH A. HUMPHRIES in partial fulfilment of the requirements for the degree of MASTER OF SCIENCE.





## Abstract

The theory of three dimensional turbulent wall jets with an infinite submergence is presented, followed by a brief discussion on how the theory can be adapted to the situation of a finite tailwater. The tailwater conditions were experimentally found to consist of three states. Firstly, shallow tailwater in which the theory is invalid. Secondly, moderate tailwater in which the theory is valid for a relatively short streamwise distance. Finally, deep tailwater state in which the theory remains valid. In the streamwise direction, the three dimensional turbulent wall jet with a finite tailwater was found to consist of three regions, firstly the potential core region, secondly the radial type decay region and thirdly an approximately "uniform" flow region, with a transition zone between the second and third regions.

An experimental investigation utilising a flow visualisation technique provided evidence that, except for very low tailwaters, the expansion of the jet was linear and dependent on the tailwater depth. The change of jet expansion with the change in tailwater depth was found to be described by a unique curve. From experimental measurements it was found that both the vertical and transverse velocity profiles were similar. The decay of maximum centreline velocity was shown to be less for shallower tailwaters than for deep tailwaters and using the concept of the virtual origin, the decay of maximum velocity has been presented in a





convenient form. The change in the length of the potential core and the surface velocity were found to be dependent on the tailwater depth. The length scales for the velocity profiles were studied and curves for their prediction have been developed. A preliminary investigation of the bed shear stress has shown that the centreline shear stress decay is reduced as the tailwater becomes shallower and that the transverse shear stress profiles are similar. Finally the scour hole produced by the bluff wall jet eroding a sand bed was found to be similar and that the presence of a scour hole seriously affected the jet expansion.





## Acknowledgements

The author would like to sincerely thank Dr N. Rajaratnam for his help and guidance throughout the course of this study.

The aid of Messrs S. Lovell and A. Lee in the construction and maintainance of the experimental apparatus is greatly appreciated. The help and advice offered by all the staff and students of the graduate Hydraulics Laboratory is acknowledged. The financial support for this study was provided by the Natural Science and Engineering Research Council through a grant to Dr N. Rajaratnam which is gratefully acknowledged.

The author would like to thank his parents for their support and understanding, Barbara for her patience and finally, Mike.



## Table of Contents

Chapter	Page
I. INTRODUCTION .....	1
A. Turbulent Jets .....	1
B. Practical Considerations .....	3
C. Existing Work .....	4
D. Outline of Proposed Work .....	5
E. Concept of the "Uniform Flow Region" .....	7
II. THEORETICAL DISCUSSION .....	10
A. Introduction .....	10
B. Equations of Motion .....	10
C. Deep submergence Theory .....	13
Simplified Equations of Motion .....	13
Similarity Analysis .....	14
Momentum Integral Equation .....	18
Dimensional Considerations .....	22
D. Adaptation to Finite Tailwater .....	23
Shallow Tailwater Condition .....	24
"Uniform Flow Region" .....	25
Moderate and Deep Tailwater Conditions .....	26
Dimensional Considerations .....	27
E. General Discussion .....	29
F. Summary .....	30
III. EXPERIMENTAL APPARATUS AND MEASUREMENT TECHNIQUES .....	32
A. Introduction .....	32





B. Jet tank .....	32
C. Lake Model .....	34
D. Photographic Procedures .....	38
E. Velocity Measurement .....	42
F. Bed Shear Stress Measurement .....	45
G. Scour Hole Measurement .....	50
IV. ANALYSIS OF EXPERIMENTAL RESULTS .....	53
A. PART I - JET EXPANSION .....	53
Introduction .....	53
Review of Existing Work .....	53
Experiments .....	56
Experimental Results .....	59
Correlation of the Transverse Expansion ....	73
Summary .....	73
B. PART II VELOCITY AND SHEAR STRESS ANALYSIS ....	76
Introduction .....	76
Review of Existing Work .....	76
Experiments .....	77
Typical Vertical Velocity Profiles .....	78
Similarity of Vertical Velocity Profile ....	82
Surface Velocity .....	85
Velocity Decay .....	88
Vertical Length Scale .....	94
Transverse Velocity .....	97
Centreline Bed Shear Stress .....	105
Transverse Shear Stress .....	110
Summary .....	114



C. PART III EROSION STUDIES .....	117
Introduction .....	117
Review of Existing Work .....	117
Experiments .....	118
Results and Analysis .....	118
Summary .....	127
V. CONCLUSIONS AND RECOMMENDATIONS FOR FURTHER STUDY .....	129
A. Conclusions .....	129
B. Recommendations for Further Study .....	130
LIST of REFERENCES .....	132
APPENDIX A - Experimental Data on the Transverse Expansion .....	A1
APPENDIX B - Velocity and Shear Stress data .....	B1
APPENDIX C - Jet with Scour data .....	C1





## List of Tables

Table 4.1 - Jet Expansion Classification .....	60
Table 4.2 - Details of Experiments .....	79
Table 4.3 - Important Flow Parameters .....	119
Table A1 - Significant Expansion Results .....	A20
Table B1 - Velocity Run Flow Parameters .....	B2
Table B2 - Centreline Shear Stress .....	B11
Table C1 - Scour Hole Parameters .....	C3



## List of Figures

Figure 1.1 - Flow regions for a moderate tailwater to nozzle height ratio .....	9
Figure 1.2 - Flow regions for a tailwater to nozzle height ratio approaching unity .....	9
Figure 2.1 - Definition sketch for three dimensional wall jets .....	11
Figure 3.1 - Jet tank (schematic representation) .....	35
Figure 3.2 - Lake model(schematic representation) .....	39
Figure 3.3 - Velocity measurement arrangement(schematic representation) .....	44
Figure 3.4 - Equivalent sand roughness .....	47
Figure 3.5 - Calibration curve for bed shear stress .....	52
Figure 4.1 - Definiton sketch a)Plan b)Section .....	55
Figure 4.2 - Nozzle dimensions .....	58
Figure 4.3 - Variation of $\tan\theta$ with Froude number for	





bluff nozzles and no tailwater .....	68
Figure 4.4 - Possible streamlines for a plunging jet .....	70
Figure 4.5 - Variation of $\hat{z}$ for bluff wall jets with very shallow tailwaters .....	71
Figure 4.6 - Expansion of bluff wall jets in the transverse direction with varying tailwater depths ...	74
Figure 4.7 - Typical vertical velocity profiles for the rectangular bluff nozzle with different tailwater depths .....	80
Figure 4.8 - Definition sketch for scales a) vertical b) transverse .....	83
Figure 4.9 - Typical reduced vertical velocity profiles for the rectangular bluff nozzle .....	84
Figure 4.10 - Dimensionless vertical velocity profile for the bluff wall jet with finite tailwater depth ...	86
Figure 4.11 - Variation of centreline surface velocity with tailwater depth for bluff nozzles .....	87
Figure 4.12 - Variation of centreline surface velocity	



with tailwater and longitudinal distance .....	87
Figure 4.13 - Definition sketch for velocity decay with shifted origin .....	90
Figure 4.14 - Centreline maximum velocity decay of bluff wall jets with finite tailwater, using the shifted origin .....	91
Figure 4.15 - Variation of a) $C$ and b) $x^*$ , for the centreline velocity decay .....	93
Figure 4.16 - Growth of non-dimensional potential core length with increasing tailwater .....	95
Figure 4.17 - Vertical length scale parameters a) Change in $db/dx$ b) Change in $\hat{b}/y_0$ .....	98
Figure 4.18 - Typical bluff wall jet transverse velocity profile .....	100
Figure 4.19 - Typical reduced transverse velocity profile for a bluff wall jet with finite tailwater depth .....	101
Figure 4.20 - Dimensionless transverse velocity profile for bluff wall jets with finite tailwater .....	102





Figure 4.21 - Change in transverse length scale parameters a)Variation of $db_z/dx$ b)Variation of $\hat{b}_z/z_0$ .	106
Figure 4.22 - a)Variation of $C_F$ with longitudinal downstream distance b)Variation of $C'_F$ with longitudinal downstream distance .....	108
Figure 4.23 - a)Typical transverse shear stress profile for a bluff wall jet with finite tailwater depth b)Typical reduced transverse shear stress profile for a bluff wall jet with finite tailwater depth ....	112
Figure 4.24 - Transverse shear stress similarity .....	113
Figure 4.25 - a)Variation of transverse shear stress length scale gradient b)Variation of transverse shear stress of length scale intercept .....	115
Figure 4.26 - Definition sketch a)Plan b)Sectional .....	122
Figure 4.27 - Scour hole centreline profiles for a bluff wall jet with a tailwater approximately equal to the outlet depth .....	123
Figure 4.28 - Dimensionless scour hole centreline profile for a bluff wall jet with a tailwater approximately equal to the outlet depth .....	125



Figure 4.29 - Variation of the scour hole centreline profile length scales a) $\epsilon_{m\infty}$ b) $x_\infty$ .....	128
Figure A1 - Jet expansions .....	A2
Figure B1 - Proportionality of velocity decay .....	B6
Figure B2 - Vertical length scale .....	B8
Figure B3 - Transverse length scale .....	B10
Figure B4 - Centreline shear stress .....	B13
Figure B5 - Inverse proportionality of shear stress with $x^2$ .....	B14
Figure B6 - Lack of correlation of shear stress decay with tailwater depth .....	B16
Figure B7 - Growth of length scale $b^*$ .....	B17
Figure C1 - Jet expansion .....	C2





## List of Plates

Plate 3.1 - General view of jet tank arrangement .....	36
Plate 3.2 - Nozzle outlet and aluminum bed .....	36
Plate 3.3 - Adjustable constant head standpipe and velocity apparatus .....	37
Plate 3.4 - Adjustable constant tailwater standpipe .....	37
Plate 3.5 - General view of lake model .....	40
Plate 3.6 - Test section details .....	40
Plate 4.1 - Run 1g .....	61
Plate 4.2 - Run 2a .....	61
Plate 4.3 - Run 3a .....	62
Plate 4.4 - Run 3g .....	62
Plate 4.5 - Run 4g .....	63
Plate 4.6 - Run 4o .....	63



Plate 4.7 - Run 5m .....64

Plate 4.8 - Run 5r .....64

Plate 4.9 - Run 5ax .....65

Plate 4.10 - Run 6h .....65

Plate 4.11 - Run 6o .....66

Plate 4.12 - Run 7g .....66

Plate 4.13 - Run S4 .....121

Plate 4.14 - Run S8 .....121



## List of Symbols

$a_1$	empirical constant
$A$	cross-sectional area of nozzle
$b$	vertical length scale
$b_y$	vertical half length
$b_z$	transverse half length
$b^*$	transverse half length, shear stress
$\hat{b}$	point of intersection on vertical axis
$\hat{b}_z$	point of intersection on transverse axis
$\hat{b}^*$	point of intersection on transverse axis
$C$	empirical constant
$C_f$	empirical constant
$C_1$	empirical constant
$C_F$	local skin friction coefficient
$C'_F$	skin friction coefficient
$d$	diameter of Prandtl-type pitot static tube
$D$	mean diameter of bed material
$e$	exponential
$f, f_1, f_2,$	functional relationships
$f_3, f_4, f_5$	
$F$	functional relationship
$F_o$	Froude number
$F_d$	densimetric Froude number
$g_1, g_2, g_3$	functional relationship
$g_4, g_5$	
$g$	acceleration due to gravity
$\Delta h$	static and dynamic pressure head difference ( $H_2O$ )





$k_s$	equivalent sand roughness
$L$	non-dimensional length of potential core
$L_1$	length of potential core
$M_o$	initial jet momentum
$p$	piezometric pressure
$\Delta p$	dynamic pressure
$\Delta p_p$	Preston tube reading
$\Delta p_*$	dimensionless Preston tube reading
$q_1, q_2$	exponents
$R$	Reynolds number
$Re$	Reynolds number
$u$	turbulent mean velocity in x direction
$u'$	fluctuating velocity component in x direction
$U_o$	uniform initial velocity
$u_m$	centreline velocity
$u_{mo}$	local maximum velocity
$U_s$	surface velocity in x direction
$v$	turbulent mean velocity in y direction
$v'$	fluctuating velocity component in y direction
$w$	turbulent mean velocity in z direction, also distance between bed ridges
$\Delta w$	breadth of bed ridge
$w'$	fluctuating velocity component in z direction
$x$	longitudinal distance from nozzle
$\bar{x}$	longitudinal distance from virtual origin
$x^*$	longitudinal distance between $x$ and $\bar{x}$ , also



	non-dimensional variable
$\hat{x}$	longitudinal distance to shear stress virtual origin from $x=0$
$x'$	longitudinal distance from shifted origin
$x_{\infty}$	longitudinal distance to position of maximum scour
$y$	normal distance from bed
$y_0$	nozzle height
$y_t$	depth of tailwater
$y^*$	non-dimensional variable
$z$	transverse direction measured from jet central axis
$z_0$	width of nozzle
$\hat{z}$	point of intersection on transverse axis
$\xi$	$=z/x$
$\epsilon$	depth of scour
$\epsilon_{m\infty}$	depth of maximum scour
$\delta$	height of maximum velocity above bed
$\theta'$	angle of growth of $b_z$
$\theta$	angle of growth of nominal jet boundary
$\emptyset$	functional relationship
$\rho$	fluid density
$\Delta\rho$	difference in density between bed material and fluid
$\tau_0$	bed shear stress
$\tau_{mo}$	centreline bed shear stress
$\tau_{0,0}$	bed shear stress at nozzle



v                      kinematic viscosity                      .





## I. INTRODUCTION

### A. Turbulent Jets

When a jet of water enters a large body of water or a jet of air enters into a large expanse of air, surfaces of discontinuity or separation appear. The separation surfaces are very unstable and result in the formation of eddies that move in a random fashion, both along and across the jet. This motion causes a transfer of momentum between adjoining layers and results in a finite region that has a continuous velocity distribution and is known as a shear layer. For large Reynolds numbers, as is the case in most practical situations, this shear layer is turbulent. The turbulent mixing gradually extends into both the jet and the surrounding fluid causing on one hand, after a short distance, a fully turbulent jet and on the other, an expansion of the jet.

If a jet diffuses into the ambient fluid unaffected by any solid boundary, the jet is known as a free jet. Commonly investigated free jets are the plane jet and the axisymmetric jet. A plane jet is one issuing from a nozzle that is (theoretically) infinitely long, while an axisymmetric jet is one issuing from a circular nozzle.

The wall jet is defined as a jet of fluid issuing tangentially to a boundary surrounded by stationary (or moving) fluid (Rajaratnam, 1965). The classical wall jet is a



plane turbulent wall jet issuing into the same stationary fluid of semi-infinite extent on a smooth boundary and has been fairly extensively researched(Rajaratnam,1976).

The third type of turbulent jet,either free or wall, is the three dimensional jet.A jet issuing from a nozzle that is neither axisymmetric nor rectangular(with a large aspect ratio,that is the ratio of the width of the slot to the height)is known as a three dimensional jet.Three dimensional jets can be free or wall jets but the only type to be considered here in detail is the wall jet.

Three dimensional wall jets can be either slender or bluff wall jets.If a jet with a fairly large aspect ratio issues tangentially onto a smooth plate,the jet is found to consist of three distinct regions. Near the nozzle there is a region called the potential core,in which the maximum velocity along the central plane,normal to the bed, remains constant and equal to the initial velocity.However as the shear layer on the upper side and the boundary layer on the bed grow ,the potential core is reduced until it disappears completely .From this point on downstream the maximum velocity decays. Initially the velocity decay is affected by the characteristics of the nozzle and was termed by Viets and Sforza(1966) the characteristic decay region.After a certain distance downstream of the nozzle the shear layers from the sides meet and the velocity decay becomes independent of the nozzle characteristics .This region is referred to as the radial-type decay because the velocity



decays approximately with  $1/x$ , where  $x$  is the axial distance from the outlet, which is similar to the radial wall jet (Glauert, 1956). A wall jet with these three pronounced regions is called a slender jet.

For a nozzle with an aspect ratio which is close to unity, it has been found (Sforza and Herbst, 1970; Newman et al., 1972; Pani, 1972) that the velocity decay passes from the potential core straight into the radial type decay region. This type of jet is classified as a bluff wall jet.

## B. Practical Considerations

It is a common engineering problem to have a situation where a turbulent jet enters an ambient fluid of limited depth. Such situations occur when a pipe, culvert or control gate structure discharges into a shallow pond, lake or reservoir, especially in the littoral regions. The prairie lake is a notable case where the depth remains very shallow for most, if not all, of the lake. The Athabasca-Peace Delta region in northern Alberta is a prime example, where the depth is approximately two metres for the whole delta region, extending over an area of over  $2,500 \text{ km}^2$  (Kellerhals, 1971).

In these situations the outlet will normally discharge on or very close to, and tangentially along, the bed of the lake. This problem can possibly be modelled as a turbulent wall jet with a finite tailwater, for the outlets described





above the aspect ratio will be small and therefore a bluff wall jet. In some cases, such as a gorge, a river entering a reservoir or lake may also be classified as a bluff wall jet, although in most cases the aspect ratio will probably put a river into the slender jet range.

### C. Existing Work

Although not many investigations of three dimensional wall jets have been undertaken, the studies that have been carried out are quite comprehensive. Viets and Sforza (1966) and Sforza and Herbst (1970) carried out experimental investigations of both slender and bluff wall jets. Pani (1972) carried out both a theoretical prediction and experimental work on bluff wall jets. Pani (1972) also did some work on circular wall jets with swirl. Newman et al. (1972) conducted a series of experiments with a circular nozzle resting on top of a smooth wall, while Chandrasekhara Swamy and Bandyopadhyay (1975) researched a circular air jet passing over a plate placed along the central axis but a short distance from the nozzle. Summaries of the state of knowledge on bluff wall jets are given by Rajaratnam (1976) in his book "Turbulent Jets" and by Launder and Rodi (1981).

Some work concerning erosion due to turbulent wall jets has been recently carried out. Rajaratnam and Berry (1977) studied the erosion due to a circular turbulent wall jet for the case when the tailwater was much deeper and the channel



much wider than the jet. Rajaratnam and Diebel(1981) extended this work to the case of very low tailwater and variation of channel width, while Rajaratnam(1981) and Rajaratnam and Macdougall(1981) have investigated erosion caused by a plane turbulent water wall jet with both deep tailwater and tailwater of the same depth as the jet thickness.

The only published work on a turbulent jet with limited tailwater depth appears to be a study by Rajaratnam and Subramanya(1968) investigating hydraulic jumps below abrupt symmetrical expansions. In that paper the downstream channel was of limited width, unlike the channel of the present study.

#### D. Outline of Proposed Work

Due to the lack of knowledge on the study of three dimensional turbulent wall jets with finite tailwater depth, the experiments carried out were of a very exploratory nature. In order to keep the investigation simple and prevent confusion in the data due to different jet conditions, the experiments were limited to a study of bluff nozzles. Also, as will be discussed later, the downstream distances involved in the work are, for jet flows, relatively short, only to a distance of approximately thirty times the nozzle height.

The experimental work was divided into three sections. Firstly a flow visualisation study of the change on the



expansion of the jet due to the change of tailwater depth was investigated, with tailwater to nozzle thickness ratios between zero and approximately fourteen (approaching infinite submergence condition), using five different aspect ratios.

Secondly a series of velocity measurements, both vertical and transverse were taken, along with bed shear stress measurements. The results were analysed with respect to similarity of profiles, velocity and shear stress decay and surface velocity, along with any related length scales. Tailwater to nozzle thickness ratios varied from approximately one to about five. Two aspect ratios were used.

Thirdly a smaller piece of work investigated the erosion of a fine sand bed due to slow moving jets. The centreline scour hole profile was measured and analysed for similarity. The tailwater to outlet depth ratio was approximately one and only one aspect ratio was used.

A short discussion on the theoretical analysis of a three dimensional turbulent wall jet and the difficulties in adapting it to the case of a finite tailwater is also presented.

The experimental investigations were carried out at the T. Blench Hydraulics Laboratory of the University of Alberta, Edmonton, Canada during the spring, summer and autumn of 1981.





## E. Concept of the "Uniform Flow Region"

As discussed earlier a bluff wall jet issuing into a semi-infinite stationary body of the same fluid has two distinct regions, the potential core region and the radial-type decay region. However it was found, during the course of the investigation, that this was not the case for the situation of a finite tailwater and in order to promote a better understanding of the problem, a qualitative description of the jet will now be presented.

Once the jet has entered the shallow body of fluid it is obvious that the jet will expand as discussed earlier. It is also easy to envision that due to the limited tailwater the jet will quickly fill the whole depth of tailwater. Once the potential core region has disappeared, the maximum velocity will begin to decay in the normal radial decay fashion. However, as soon as the jet fills the complete depth the only stress decelerating the upper surface is the shear stress due to the (in this case) air-water interface, which is negligible compared to the flow deceleration and that due to the bed (or wall) shear stress. Therefore, the maximum velocity is decaying faster than the surface velocity and eventually a region of (approximately) uniform vertical flow is reached.

In order to pass from the vertical velocity profile found in the radial type flow region to an (approximately) uniform vertical velocity profile a transition zone is



formed.

As the tailwater depth decreases, then the jet expands more rapidly into the whole depth and therefore the "uniform" flow transition zone encroaches upon the radial type decay region, thereby shortening the potential core region. When the tailwater depth to nozzle height ratio approaches unity the jet seems to expand abruptly into the whole depth and the radial type decay region no longer exists. The jet appears to pass from a shortened potential core into the uniform flow transition region.

It is obvious that once in the the uniform flow region, the normal methods of analysing the similarity of velocity profiles will no longer be correct because the maximum velocity will occur at an infinite number of locations, even towards the end of the transition zone the choosing of the correct position of the maximum velocity would probably become difficult and this is one of the reasons why measurements were restricted to a fairly short downstream distance.

No attempt was made to measure velocity profiles when the tailwater to nozzle ratio was less than unity and no attempt will be made to predict the flow patterns, these are areas which require further detailed investigation.

Figures 1.1 and 1.2 give a schematic representation of the ideas proposed. Reference should also be made to the vertical velocity profiles obtained from Run1 and Run7. (figure 4.7)



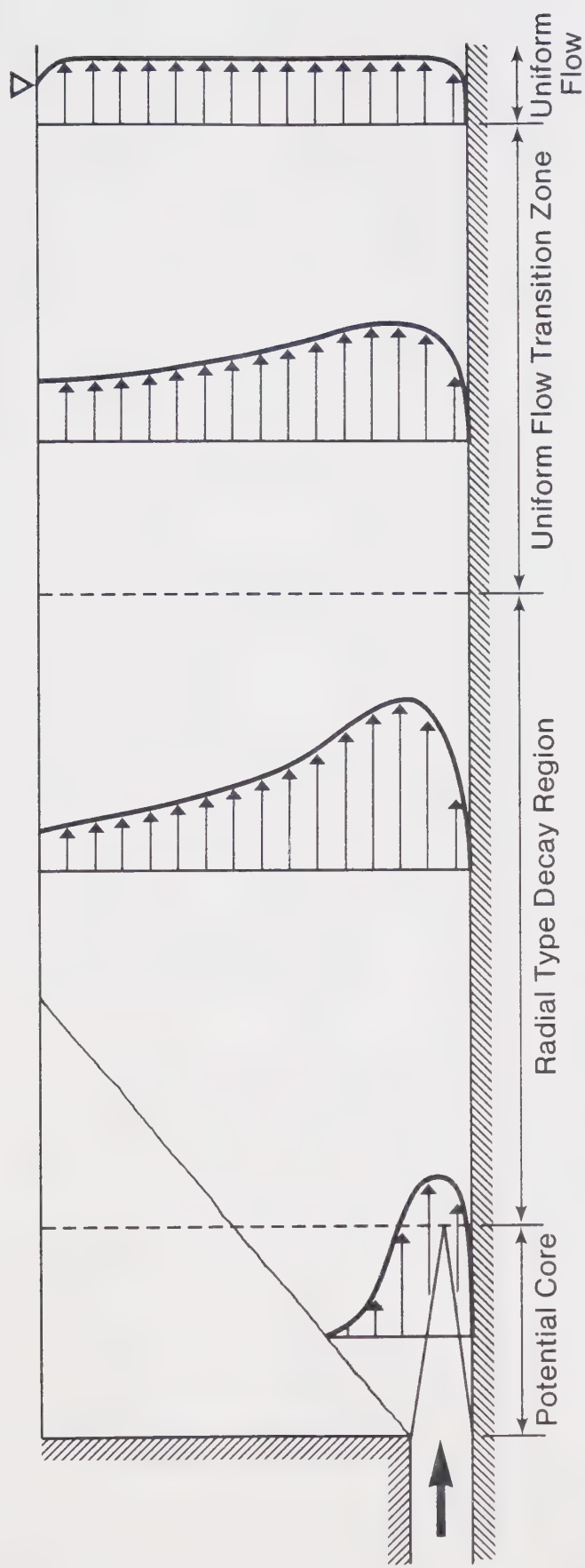


Figure 1.1. Flow regions for a moderate tailwater to nozzle height ratio

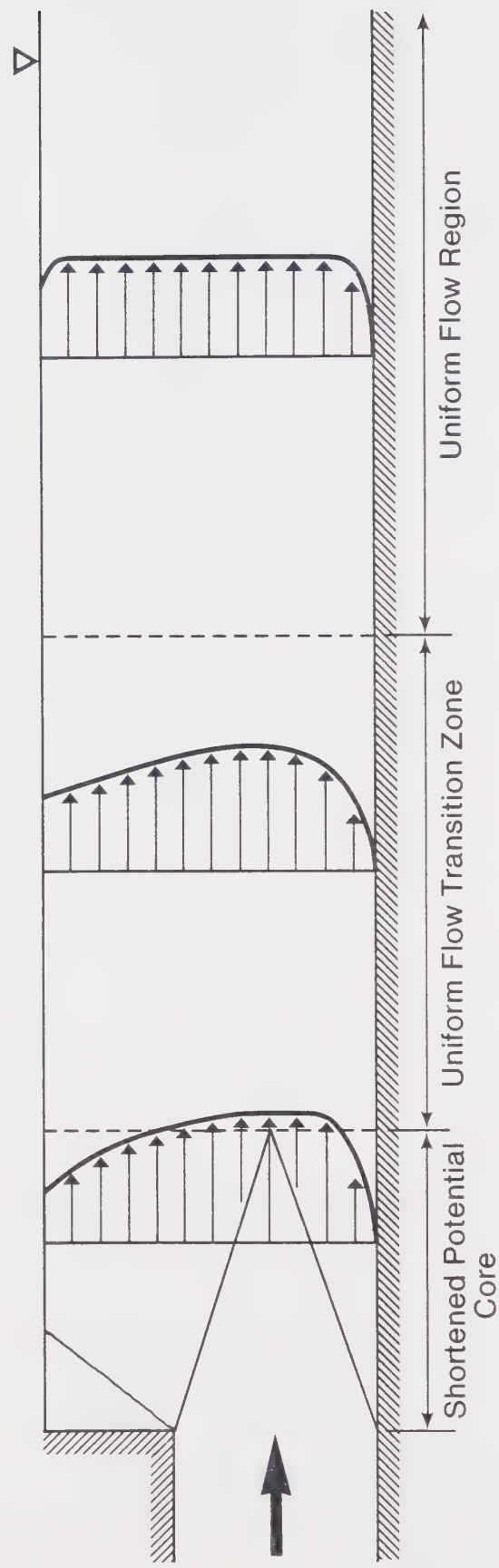


Figure 1.2. Flow region for a tailwater to nozzle height ratio approaching unity.



## II. THEORETICAL DISCUSSION

### A. Introduction

Presented within this chapter is an outline of the theory of three dimensional wall jets issuing into an infinite half space of the same fluid. This is followed by a discussion on how the theory may be adapted for the condition of a finite tailwater depth and how under certain circumstances the assumptions made in the theory are invalid. Also presented is a short discussion on the use of dimensional analysis in this study. In this chapter, and the study as a whole, the cartesian system of co-ordinates is used. The x axis is along the bed and central plane of symmetry of the jet, the y direction is normal to the bed and the z axis is in the third orthogonal direction, as shown in figure 2.1.

### B. Equations of Motion

The Reynolds equations for steady flow in the cartesian co-ordinates can be written as (Schlichting, 1968);

$$u \frac{\partial u}{\partial x} + v \frac{\partial u}{\partial y} + w \frac{\partial u}{\partial z} = - \frac{1}{\rho} \frac{\partial p}{\partial x} + \nu \left[ \frac{\partial^2 u}{\partial x^2} + \frac{\partial^2 u}{\partial y^2} + \frac{\partial^2 u}{\partial z^2} \right] - \left[ \frac{\partial}{\partial x} \overline{u'^2} + \frac{\partial}{\partial y} \overline{u'v'} + \frac{\partial}{\partial z} \overline{u'w'} \right] \quad (2.1)$$





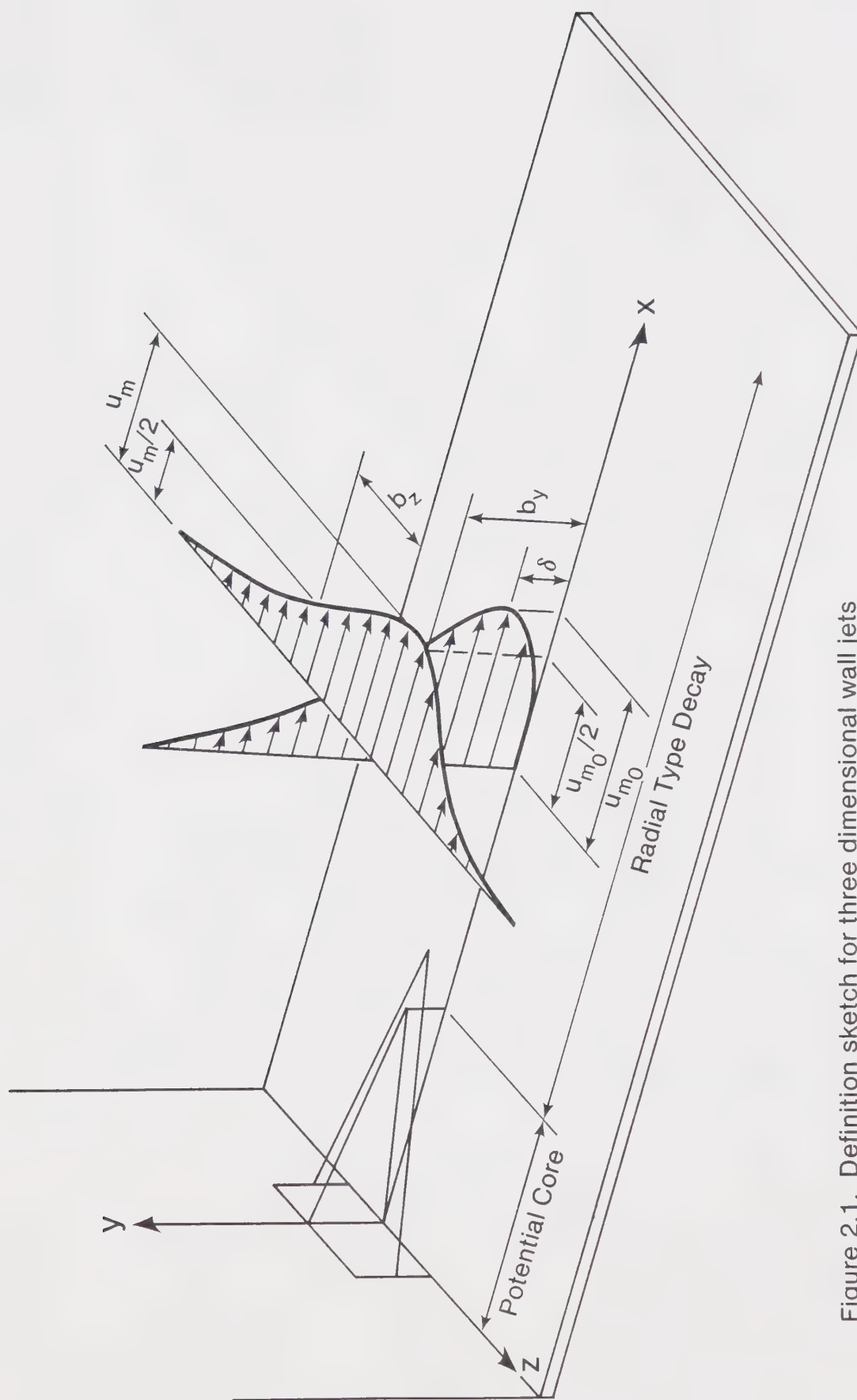


Figure 2.1. Definition sketch for three dimensional wall jets



$$u \frac{\partial v}{\partial x} + v \frac{\partial v}{\partial y} + w \frac{\partial v}{\partial z} = -\frac{1}{\rho} \frac{\partial p}{\partial y} + \nu \left[ \frac{\partial^2 v}{\partial x^2} + \frac{\partial^2 v}{\partial y^2} + \frac{\partial^2 v}{\partial z^2} \right] - \left[ \frac{\partial}{\partial x} \overline{u'v'} + \frac{\partial}{\partial y} \overline{v'^2} + \frac{\partial}{\partial z} \overline{v'w'} \right] \quad (2.2)$$

$$u \frac{\partial w}{\partial x} + v \frac{\partial w}{\partial y} + w \frac{\partial w}{\partial z} = -\frac{1}{\rho} \frac{\partial p}{\partial z} + \nu \left[ \frac{\partial^2 w}{\partial x^2} + \frac{\partial^2 w}{\partial y^2} + \frac{\partial^2 w}{\partial z^2} \right] - \left[ \frac{\partial}{\partial x} \overline{u'w'} + \frac{\partial}{\partial y} \overline{u'w'} + \frac{\partial}{\partial z} \overline{w'^2} \right] \quad (2.3)$$

$$\text{and } \frac{\partial u}{\partial x} + \frac{\partial v}{\partial y} + \frac{\partial w}{\partial z} = 0 \quad (2.4)$$

where  $x, y$  and  $z$  axis are defined in section A

$u, v, w$  = the turbulent mean velocity components in the  $x, y$  and  $z$  directions respectively

$u', v', w'$  = the fluctuating component of the velocities in  $x, y$ , and  $z$  directions respectively

$p$  = mean piezometric pressure at the point of consideration

$\rho$  = mass density of the fluid and

$\nu$  = kinematic viscosity of the fluid



### C. Deep submergence Theory

Presented in this section is a brief review of the theory of three dimensional turbulent wall jets. The theory is not dealt with in great detail and only the salient points are noted; for a detailed discussion the reader should refer to Pani(1972) or Rajaratnam(1976).

#### Simplified Equations of Motion

The following assumptions are made;

- (i) Beyond an initial reach from the nozzle  $y \ll x$  and  $z \ll x$
- (ii) In a major portion of the flow,  $u \gg v$  and  $u \gg w$ .
- (iii) The fluctuating velocity components are small compared to the mean values.
- (iv) Gradients in the  $y$  and  $z$  directions are much larger than in the corresponding gradients in the  $x$  direction.
- (v) The piezometric pressure gradients in all three directions are small.

In estimating the order of magnitude of each term, the order of magnitudes for the dimensional forms of equations 2.1 to 2.4 were assigned as

$$u \sim 1, x \sim 1, y \sim \Delta \text{ and } z \sim \Delta$$

where  $\Delta$  is a quantity of order much less than unity. It is possible to carry out an order of magnitude analysis on the equations of motion. Deleting terms of smaller order than the equations of motion are reduced to



$$u \frac{\partial u}{\partial x} + v \frac{\partial u}{\partial y} + w \frac{\partial u}{\partial z} = \nu \left[ \frac{\partial^2 u}{\partial y^2} + \frac{\partial^2 u}{\partial z^2} \right] - \left[ \frac{\partial}{\partial y} \overline{u'v'} + \frac{\partial}{\partial z} \overline{u'v'} \right] \quad (2.5)$$

$$\text{and } \frac{\partial u}{\partial x} + \frac{\partial v}{\partial y} + \frac{\partial w}{\partial z} = 0 \quad (2.6)$$

### Similarity Analysis

If, when the ratio of the local velocity to the local maximum velocity is plotted against the ratio of the distance from the jet axis to some characteristic length, the velocity profiles collapse onto a single curve, the velocity profiles are termed "similar". In a wall jet the distance in the y direction is measured from the wall (or boundary). The characteristic length has usually been taken as the distance to where the velocity becomes half that of the local maximum and  $\frac{\partial u}{\partial y} < 0$ , and is known as the "half length".

Glauert(1956) has shown theoretically that complete similarity of velocity profiles is not possible due to a thin layer existing near the wall where viscosity is important. However the experience of many investigators has shown that a single velocity scale and a single length scale correlates the data well. Therefore while it is not theoretically feasible, it is possible to have experimental





similarity. It should be noted that similar profiles are independent of the x co-ordinate.

Assuming that from similarity

$$\frac{u_m}{u_{mo}} = f_1 \left( \frac{y}{b_y} \right) \quad (2.7)$$

where  $u_m$  = turbulent mean velocity in the x direction at a distance y from the bed in the z=0 plane

$u_{mo}$  = the local maximum velocity

$b_y$  = the half length in the y direction

$f_1$  = a functional relation

and that in the x-z plane

$$\frac{u}{u_m} = g_1 \left( \frac{z}{b_z} \right) \quad (2.8)$$

where  $u$  = turbulent mean velocity in the x direction at a distance z from the axis

$b_z$  = the half length in the z direction

$g_1$  = a functional relation

From experience with other jet flows it is possible to make the assumptions (Rajaratnam, 1976)

$$\frac{v}{u_m} = g_2 \left( \frac{z}{b_z} \right) \quad , \quad \frac{w}{u_m} = g_3 \left( \frac{z}{b_z} \right)$$



$$\frac{\overline{u'v'}}{u_m^2} = g_4\left(\frac{z}{b_z}\right), \quad \frac{\overline{u'w'}}{u_m^2} = g_5\left(\frac{z}{b_z}\right) \quad (2.9)$$

where  $g$  denotes a functional relationship.

If it is further assumed that

$$u_{m0} \propto x^p \quad b_y \propto x^{q_1} \quad \text{and} \quad b_z \propto x^{q_2} \quad (2.10)$$

where  $p$ ,  $q_1$  and  $q_2$  are unknown exponents. Then it can be shown that by manipulation of the above set of assumptions Eq 2.5 becomes

$$\begin{aligned} 2f_1 f_1' g_4 &= \frac{y}{u_{m0} b_y} g_1 f_1'' + \frac{v}{u_{m0} b_y} \left(\frac{b_y}{b_z}\right)^2 f_1 g_1'' - \frac{b_y}{b_z} f_1^2 g_5' \\ &\quad - \frac{b_y u_{m0}'}{u_{m0}} f_1^2 g_1^2 + b_y' \left(\frac{y}{b_y}\right) f_1 f_1' g_1^2 \quad (2.11) \\ &\quad + \frac{b_y b_z'}{b_z} \left(\frac{z}{b_z}\right) f_1^2 g_1 g_1' - f_1 f_1' g_1 g_2 - \frac{b_y}{b_z} f_1^2 g_1' g_3 \end{aligned}$$

where, for convenience,  $(y/b_y)$  and  $(z/b_z)$  have been dropped from Eq 2.7 to 2.9 on the understanding that  $f$  is a function of  $(y/b_y)$  and  $g$  is a function of  $(z/b_z)$ .

and where

$$u_{m0}' = \frac{\partial u_{m0}}{\partial x} = \frac{d u_{m0}}{d x}$$

$$b_y' = \frac{\partial b_y}{\partial x} = \frac{d b_y}{d x} \quad \text{and} \quad b_z' = \frac{\partial b_z}{\partial x} = \frac{d b_z}{d x}$$



also the prime on the  $f$  function denotes differentiation with respect to  $(y/b_y)$  and on the  $g$  functions denotes differentiation with respect to  $(z/b_z)$ .

In turbulent jets  $\frac{y}{u_{m0} b_y}$  is generally small and so the first term on the right hand side of Eq 2.11 could be neglected, this assumption will only run into difficulties near the wall. Also for wall jets  $b_y/b_z$  is less than unity, so that the second term on the right could also be dropped. For similarity, since the left side is independent of  $x$ , the right must also be independent of  $x$ . Therefore

$$\frac{b_y}{b_z} \propto x^0 \Rightarrow q_1 = q_2 \quad (2.12)$$

$$\text{and } \frac{b_y u'_{m0}}{u_{m0}} \propto x^0$$

$$\Rightarrow x^{(q_1 + p - 1 - p)} \propto x^0 \therefore q_1 = 1 \quad (2.13)$$

$$\text{also } b_y' \propto x^0 \Rightarrow q_1 - 1 = 0 \quad (2.14)$$

$$\text{finally } \frac{b_y b'_z}{b_z} \propto x^0 \Rightarrow x^{(q_1 + q_2 - 1 - q_2)} \propto x^0 \text{ \& } q_1 = 1 \quad (2.15)$$



Therefore  $q_1=1$ ,  $q_2=1$  but the value of exponent  $p$  is still unknown.

### Momentum Integral Equation

To evaluate the exponent  $p$  the momentum integral equation can be utilised. From Eqs 2.5 and 2.6

$$\frac{\partial}{\partial x}(u^2) + \frac{\partial}{\partial y}(uv) + \frac{\partial}{\partial z}(uw) = \nu \left( \frac{\partial^2 u}{\partial y^2} + \frac{\partial^2 u}{\partial z^2} \right) - \left( \frac{\partial}{\partial y} \overline{u'v'} + \frac{\partial}{\partial z} \overline{u'w'} \right) \quad (2.16)$$

The boundary conditions for deep submergence are,

$$\text{at } y = 0 \quad u = v = w = 0$$

$$u' = v' = w' = 0$$

$$y = \infty \quad u = 0 \quad \frac{\partial u}{\partial y} = 0$$

$$u' = 0$$

$$\text{and at } z = \pm\infty \quad u = 0 \quad \frac{\partial u}{\partial z} = 0$$

$$u' = 0$$

Eq 2.16 is integrated over the infinite half-space bounded by  $y=0$  plane and reduces to

$$\int_{-\infty}^{\infty} \int_0^{\infty} \frac{\partial}{\partial x}(u^2) \, dy \, dz = \nu \int_{-\infty}^{\infty} \left( \frac{\partial u}{\partial y} \right)_0^{\infty} dz$$





$$\rightarrow \frac{d}{dx} \int_{-\infty}^{\infty} \int_0^{\infty} u^2 dy dz = -\frac{1}{\rho} \int_{-\infty}^{\infty} \tau_0 dz \quad (2.17)$$

where  $\tau_0$  is the shear stress on the boundary

Rewriting the right hand side of Eq 2.17 as

$$-\frac{1}{\rho} \int_{-\infty}^{\infty} \tau_0 dz = -\frac{1}{\rho} \tau_{0m} x \int_{-\infty}^{\infty} \left( \frac{\tau_0}{\tau_{0m}} \right) d\xi \quad (2.18)$$

where  $x$ =distance measured from the nozzle in the  $x$  direction

$\tau_{0m}$ =boundary shear stress on the centreline and is in the  $x$  direction

$$\xi = z/x$$

and assuming that

$$\int_{-\infty}^{\infty} \frac{\tau_0}{\tau_{0m}} d\xi = a_1 \quad (2.19)$$

$$\frac{\tau_{0m}}{\frac{1}{2} \rho u_{m0}^2} = C_f \quad (2.20)$$

$$\frac{u_{m0}}{U_0} = \left( \frac{C}{x/\sqrt{A}} \right) \quad (2.21)$$



where,  $a_1, C_f$  and  $C$  are empirical constants found from experimental data.  $U_0$  is the efflux velocity and  $A$  is the cross-sectional area of the nozzle. Eq 2.21 is only a simplified version that does not fit the experimental data very well.

Then it is possible that by substitution and integration to obtain the equation

$$\int_{-\infty}^{\infty} \int_0^{\infty} \rho u^2 dy dz = M_0 \left[ 1 - a_1 \frac{C_f C^2}{2} L_n \frac{x}{x_0} \right] \quad (2.22)$$

where  $M_0 = \rho A U_0^2$  = efflux momentum of the nozzle and  $x_0$  = the value of  $x$  at the virtual origin.

Based on his experimental results Pani(1972) was able to evaluate  $a_1$ ,  $C_f$  and  $C$  and simplify Eq 2.22. Pani(1972) then demonstrated that the momentum loss in a distance of one hundred times the nozzle thickness was around 11%. Therefore for a rough approximation the three dimensional wall jet momentum is conserved and Eq 2.22 reduces to

$$\int_{-\infty}^{\infty} \int_0^{\infty} \rho u^2 dy dz = M_0 \quad (2.23)$$

Differentiation of Eq 2.23 gives

$$\frac{d}{dx} \int_{-\infty}^{\infty} \int_0^{\infty} \rho u^2 dy dz = \frac{d(M_0)}{dx} = 0 \quad (2.24)$$



$$\text{or } \frac{d}{dx} \rho u_{m0}^2 b_y b_z \int_{-\infty}^{\infty} \int_0^{\infty} f_1^2 g_1^2 d\left(\frac{y}{b_y}\right) d\left(\frac{z}{b_z}\right) = 0 \quad (2.25)$$

In Eq 2.25 the integrand is a constant, implying that

$$\frac{d}{dx} \left[ \rho u_{m0}^2 b_y b_z \right] = 0 \quad (2.26)$$

that is

$$x^{2p+q_1+q_2} \propto x^0 \quad (2.27)$$

$$\therefore 2p+q_1+q_2 = 0 \quad \rightarrow \quad p = -1$$

Therefore for a three dimensional wall jet

$$u_{m0} \propto 1/x$$

$$b_y \propto x$$

$$\text{and } b_z \propto x \quad (2.28)$$



## Dimensional Considerations

The use of dimensional analysis always involves engineering judgement and experience in order to choose the important variables. For a three dimensional wall jet with deep submergence the following results have been successfully vindicated by experimental observations Pani(1972).

Generally, Reynolds numbers in jets are over a few thousand and therefore it is reasonable to neglect the effect of viscosity. Therefore the maximum velocity along the centreline is a function of the initial momentum flux (because of conservation of momentum), the fluid density and the distance  $\bar{x}$  measured from a virtual origin (refer to chapter 4 for detailed discussion).

$$u_{m0} = \phi(M_0, \rho, \bar{x}) \quad (2.29)$$

Using Buckingham's Pi theorem it is possible to obtain that

$$\frac{u_{m0}}{\sqrt{(M_0/\rho\bar{x})}} = C \quad (2.30)$$

where C is an empirical constant

$$\text{but } M_0 = \rho A U_0^2$$





$$\therefore \frac{u_{mo}}{U_0} = \frac{C}{(\bar{x}/\sqrt{A})} \quad (2.31)$$

The centreline shear stress can be expressed as

$$\tau_{om} = \phi(M_0, \rho, x, \nu) \quad (2.32)$$

again the use of Buckingham's Pi theorem leads to the result

$$\frac{\tau_{om}}{\rho U_0^2} \left( \frac{\bar{x}}{A} \right)^2 = F \left( \frac{U_0 \sqrt{A}}{\nu} \right) \quad (2.33)$$

For a given Reynolds number,  $\tau_{om} \propto \frac{1}{\bar{x}^2}$

Because the shear stress is a function of the jet velocity, it is reasonable to expect that if the transverse velocity profiles are similar then the transverse bed shear stress profiles are also similar.

$$\frac{\tau_0}{\tau_{om}} = f \left( \frac{z}{b^*} \right) \quad (2.34)$$

and also that  $b^*$ , the shear stress half length,  $\propto x$ .

#### D. Adaptation to Finite Tailwater

The following paragraphs attempt to show how the theory of three dimensional wall jets in some cases remains to a



reasonable approximation valid, while under other conditions some of the assumptions made in the theory are no longer viable and the theory breaks down.

### Shallow Tailwater Condition

From observations made of the flow, it became obvious that for tailwaters approaching the same depth as the nozzle height (and tailwaters less than the nozzle height) the surface of the water no longer remained flat. The waves and ripples formed on the surface were unsteady, sharp-crested and localised. Therefore, for a shallow tailwater it can no longer be assumed that the pressure gradients are negligible, nor that any gradients in the x direction are smaller than those in the y and z planes. It is also possible that fluctuating velocity components may no longer be small compared to the mean velocity. These factors lead to the conclusion that the equations of motion can no longer be simplified as discussed above. Because the flow pattern has become so complex no attempt has been made to simplify the equations of motion and the theory for infinite submergence can no longer be accepted.

The actual definition of a shallow tailwater is unclear and, from observations, is dependent on the Froude number  $F_0$  defined as

$$F_0 = \frac{U_0}{\sqrt{gy_0}} \quad (2.35)$$



where  $y_0$  =nozzle height

However, for the range of Froude numbers considered in this present study it appears that the surface disturbances become small for a tailwater one third greater than the nozzle height. It should also be considered that for a shallow tailwater the jet expansion in the transverse direction becomes very small(see chapter 4) and therefore the ratio of  $b_y/b_z$  can no longer be assumed to be much less than unity, further invalidating the theory.

### "Uniform Flow Region"

In chapter 1 the concept of an (almost) uniform flow region was discussed and it was stated that within this region the similarity of vertical velocity profiles would become undefined. It was also discussed that this region occurs in both shallow and moderate tailwaters. Therefore, at a certain distance downstream of the nozzle outlet, the similarity analysis used earlier can no longer be true and again the theory fails. Again the definition of a moderate tailwater is unclear and is dependent on  $F_0$  but in the present study a tailwater to nozzle height ratio of approximately four appears to be a reasonable upper limit. The distance downstream to where the (approximately) uniform flow region starts is undefined and is dependent on the



tailwater depth and probably the Froude number. It should also be noted that even for quite deeply submerged flow conditions, the jet expansion still reaches the the water surface. When the jet expansion reaches the surface some surface disturbances do occur but are not thought to be significant.

### Moderate and Deep Tailwater Conditions

Within the remaining flow situations, that is, for a moderately deep tailwater, fairly close to the nozzle outlet and for the deep submergence condition it is possible to investigate the theory of three dimensional turbulent wall jets to discover whether it can still be used.

The assumptions made in simplifying the equations of motion are still valid, as is the similarity analysis providing that Eq 2.10 is modified slightly. For a finite tailwater it is reasonable to assume that

$$\begin{aligned} u_{m0} &\propto x^p \\ b_y &\propto x^{q1} \\ b_z &\propto x^{q2} \end{aligned}$$

but that the coefficient of proportionality is different for each tailwater. That is, Eq 2.10 is true for any given tailwater depth. This, therefore, leads to the same conclusion that  $q_1=1$  and  $q_2=1$  or in other words, the





variation of the length scales are linear with the distance downstream from the nozzle but the equation of the line relating the two variables changes with the variation of the tailwater depth.

Considering the momentum integral equation, this equation remains valid but the boundary condition for  $y=\infty$  is no longer correct. At the water surface there is an air-water interface, on this interface it is reasonable to assume "no-slip" condition and within the bounds of accuracy used in the above work the shear stress on the interface can be neglected. Therefore the boundary condition for Eq 2.16 becomes

$$y=y_t, \quad \begin{matrix} u=U_s \\ u'=U'_s \end{matrix} \quad \cdot \quad \frac{\partial u}{\partial y} = 0$$

and the approximation of conservation of momentum is still correct. So again  $u_{mo} \propto 1/x$  for any given tailwater but, as before, the equation of the line is a function of the tailwater depth.

## Dimensional Considerations

As stated in section C the use of dimensional analysis involves the use of considerable engineering judgement. One obvious approach is to use the knowledge of three dimensional turbulent wall jets with infinite submergence as



a starting position and to make adjustments to account for a finite tailwater.

For example the centreline velocity decay can be considered as

$$u_{m0} = \phi (M_0, \rho, \bar{x}, y_t, y_0) \quad (2.36)$$

where  $y_t$  = tailwater depth

$y_0$  = nozzle height

Buckingham's Pi theorem gives the dimensionless groups

$$u_{m0} = F \left[ \sqrt{\frac{M_0}{\rho \bar{x}}}, \frac{y_t}{y_0} \right] \quad (2.37)$$

$$\text{or} \quad \frac{u_{m0}}{U_0} = \frac{C}{(\bar{x} / \sqrt{A})}$$

$$\text{where} \quad C = f \left( \frac{y_t}{y_0} \right) \quad (2.38)$$

Similarly the centreline shear stress could be expressed as

$$\tau_0 = \phi (M_0, \rho, \bar{x}, \nu, y_t, y_0) \quad (2.39)$$

and, as shown earlier, for a given Reynolds number  $\tau_0 \propto 1/\bar{x}^2$ , but now the proportionality is a function of the tailwater.



The transverse shear stress profile can be expected to be similar but again the half width,  $b^*$ , will be a function of the distance  $x$  and the tailwater depth  $y_t$ .

It must also be recognised that the correctness of dimensional analysis is very sensitive to the variables originally thought to be involved in the function. If, for instance, the wrong length scale is used then the dimensionless groups will be formed around the incorrect assumption.

## E. General Discussion

As has been shown, the theory of three dimensional turbulent jets with a finite tailwater depth is not complete and in some areas non-existent. It is therefore necessary to complement theory by empirical relationships. This development of empirical correlations is attempted in the following chapters, using the results obtained from experiments performed on bluff jets with a finite tailwater depth.

It must be recognised that experiments can only cover a limited range and this is true for the studies presented here. Also the development of empirical relationships involves a great amount of judgement, experience, trial and error and dimensional consideration. Therefore, the relationships and correlations presented in this study must be treated with caution and may need to be adjusted as more



data become available. Nor should they be applied to situations which have different boundary conditions, for example when the jet is slender or when the jet discharges into a channel of restricted width. However the empirical results contained in this study do provide a far better estimate than trying to apply infinite depth theory to finite tailwater cases and a better estimate than anything that, to the author's knowledge, is currently available.

#### F. Summary

An outline of the theory for infinite tailwater has been presented. The equations of motion were simplified using an order of magnitude analysis. Then using a similarity analysis and the momentum integral equation it was shown that the jet grows linearly and the centreline velocity decay is proportional to the inverse of the distance from a virtual origin. Using dimensional considerations it was shown that the centreline shear stress decay is proportional to the inverse of the square of the distance from a virtual origin for any given Reynolds number.

It was then discussed how the theory became invalid for tailwater to nozzle height ratios of less than approximately  $1\frac{1}{3}$  and how the theory became invalid when the jet entered the (approximately) uniform flow region. Finally the theory was found to be still valid, although with additional





dependence on the tailwater, for flow situations in which the tailwater was deep, i.e. a tailwater to nozzle height ratio greater than approximately four or in moderate depth tailwater when restricted to relatively close to the nozzle.



### III. EXPERIMENTAL APPARATUS AND MEASUREMENT TECHNIQUES

#### A. Introduction

This chapter describes the apparatus used in the study and discusses the various measurement methods used. The limitations due to the apparatus and experimental procedures are also dealt with. The experiments were carried out in two flumes. The first flume, called the jet tank, was the smaller of the two but more versatile. The second and much larger flume, referred to (for the want of a better description) as the lake model, had a fixed tailwater condition and a free surface inlet (nozzle). The photographic study was carried out in both flumes, while velocity measurements were restricted to the jet tank and the scour investigation to the lake model.

#### B. Jet tank

The jet tank was of a rectangular shape, 3.55m long, 1.11m wide and 1.22m deep, with plexiglass sides. A false bed was provided approximately at half depth. This bed was provided by a 5mm thick aluminum plate, 1.10m wide and 2.44m long, stiffened by two channel sections, running lengthwise, 26cm from each edge. The plate was suspended at the upstream end by two, threaded, 5mm diameter steel rods, one in each corner. The rods passed through flanges attached to the top



of the tank ,thus enabling the upstream end of the plate to be leveled for each nozzle used. The downstream end of the plate was supported by hollow concrete construction blocks and a system of wedges, which allowed the plate to be set at the desired level. The test section of the bed was sprayed with white paint and a 1cm grid was etched into the paint, running parallel and normal to the nozzle central axis.

The inflow was fed, primarily from the laboratory sump but was supplemented by the city water supply when necessary, into a 150mm diameter standpipe. The standpipe could be varied in height to provide different constant head conditions. An overflow box collected the waste water and returned it to the sump. The standpipe turned through 90 degrees into the horizontal plane and after a length of 76cm entered the nozzle. In the horizontal section of the pipe "hogs hair" was positioned to act as a baffle and reduce any fluctuations or secondary flow. The nozzles were well formed and the contraction took place over a 30.5cm length. A circular nozzle of 2.54cm diameter and a small rectangular nozzle 0.64cm high by 1.58cm wide were turned from solid brass cylinders .A larger nozzle 2.5cm high and 4cm wide was shaped out of wood and sealed against water.

The tailwater conditions were controlled by an adjustable standpipe 13.7cm in diameter. The outflow was collected and either returned to the sump or, if dye was being used, into the city sewer system.



Figure 3.1 gives a schematic diagram of the jet tank arrangement and plates 3.1, 3.2, 3.3, 3.4 show details of the actual experimental setup.

### C. Lake Model

The second flume was constructed from hollow construction blocks and was 15.25m long, 4.57m wide and 0.61m deep. The inflow was provided from the laboratory sump and entered at the bottom of a head reservoir which was 0.61m long, 0.405m wide and 0.61m deep. From the reservoir the inflow passed over a V notch weir and into a head canal 0.91m long, 0.405m wide and 0.405m deep. The head in the reservoir was measured by a staff point gauge with an accuracy of 0.025mm and the discharge could be accurately calculated from the calibration curve of the weir (Hydraulics laboratory records). The inflow entered the lake model through a well formed constriction. The nozzle was 50mm wide and the upper surface was unrestricted. The water level in the model was controlled by sharp-edged tailgates that were sealed at a height of 0.406m. The water returned to the laboratory sump, and a plugged 15cm diameter pipe passed underneath the tailgate, along the bed of the model, allowing the model to be drained if necessary.

A 2.4m long by 2.4m wide sandbox of 15mm plywood was placed around the entrance to the model, the top of the sandbox was level with the bottom of the nozzle. The sandbox





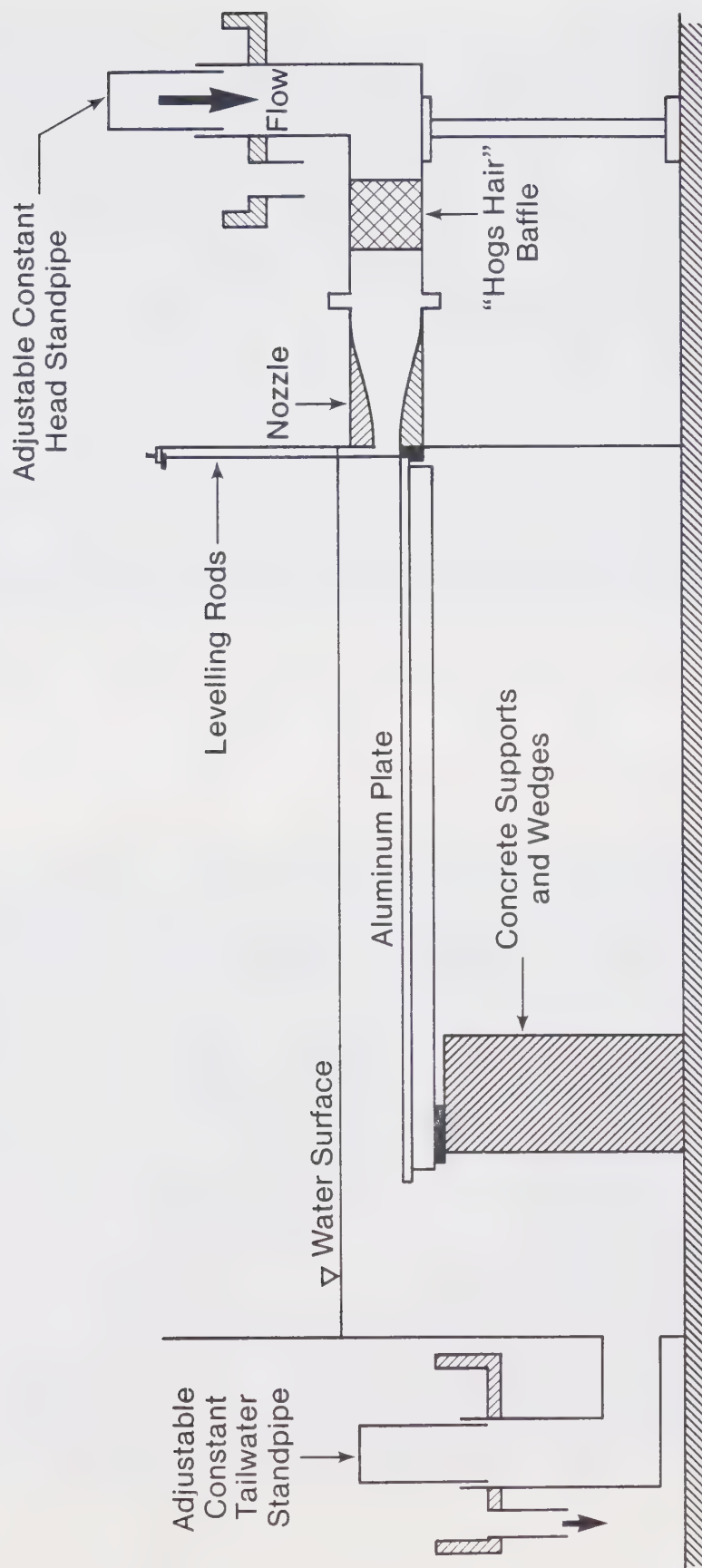


Figure 3.1. Jet Tank (schematic representation, sectional view)





Plate 3.1 - General view of jet tank arrangement



Plate 3.2 - Nozzle outlet and aluminum bed



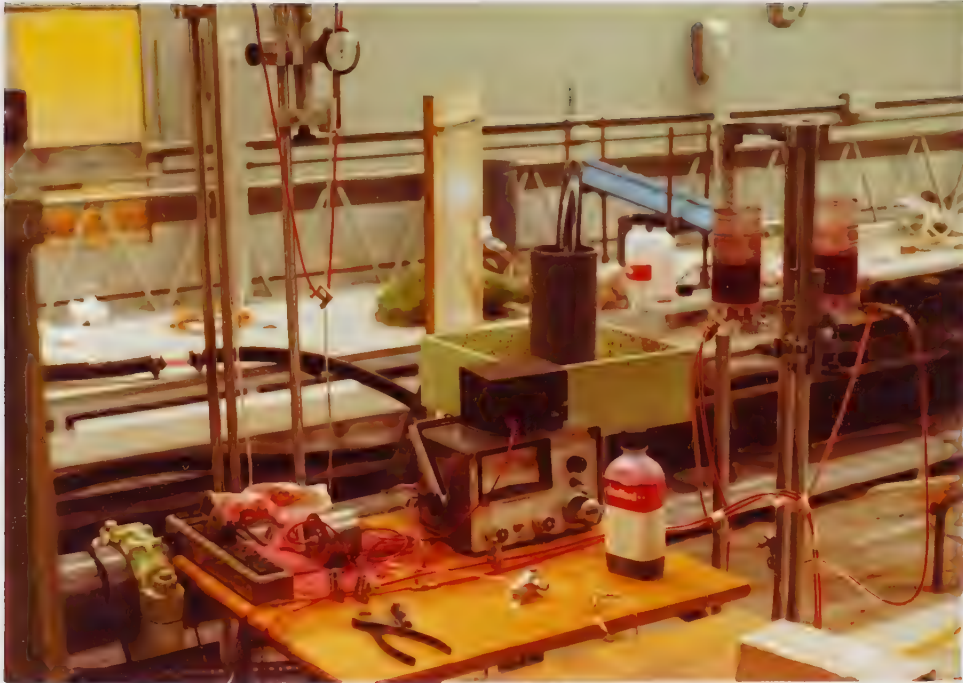


Plate 3.3 - Adjustable constant head standpipe and velocity apparatus



Plate 3.4 - Adjustable constant tailwater standpipe





contained 0.11mm mean diameter fine sand. For the experiments not involving scour investigations, a 3.66m long by 1.22m wide aluminum plate was placed over the sandbox and the entrance constriction was reshaped with plasticine. The downstream end of the plate was supported using hollow concrete construction blocks and wedges to ensure that the plate was level.

Figure 3.2 shows a schematic representation of the lake model and Plates 3.5 and 3.6 show details of the actual arrangement.

#### D. Photographic Procedures

The photographic work was carried out in both flumes, and a Pentax MX 35mm camera was used throughout. Kodacolor II C135 print film was used with an ASA 100 setting and a shutter speed of 1/30 second.

For the jet tank series of experiments, the camera was supported by two horizontal angle bars running across the width of the tank. This enabled the camera to be set at a constant height of 1.57m above the bed for all the experimental runs. A food dye injection technique into the head pipe coloured the jet, allowing a photographic study of the jet expansion in the transverse direction to be made. Initially the dye was fed, under gravity, along 5mm diameter plastic tubing into the jet flow. However this proved unsatisfactory and was later modified to allow a greater





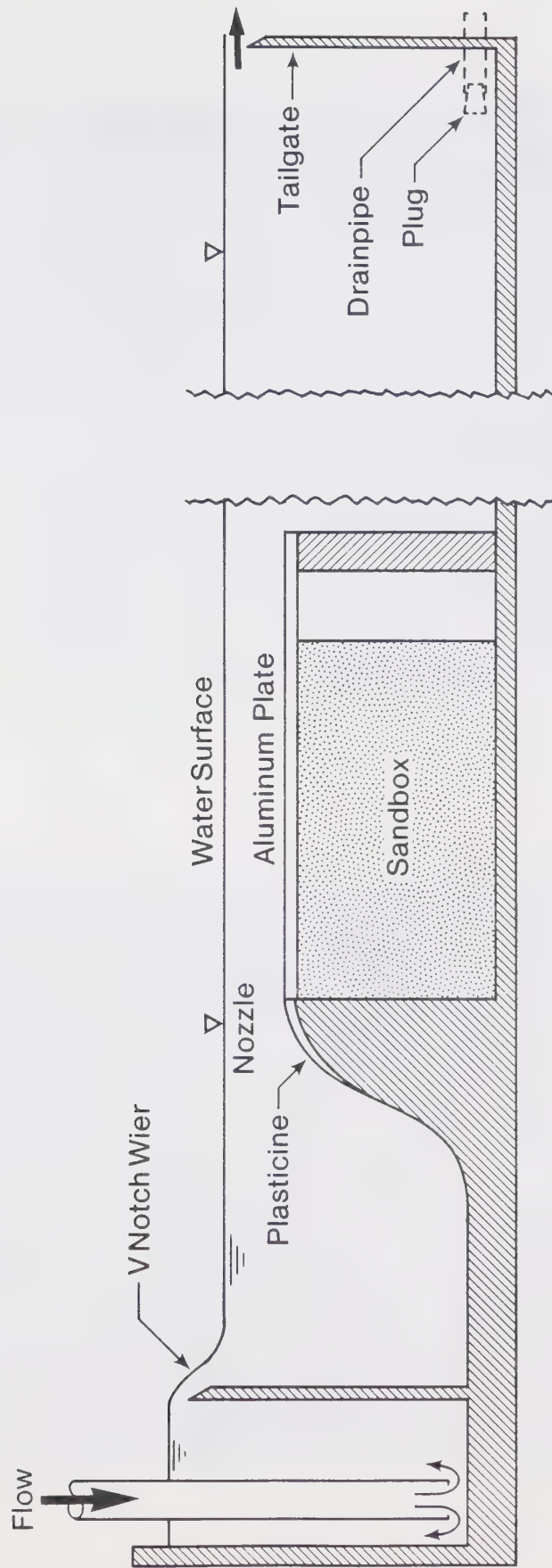


Figure 3.2. Lake model (schematic representation, sectional view)



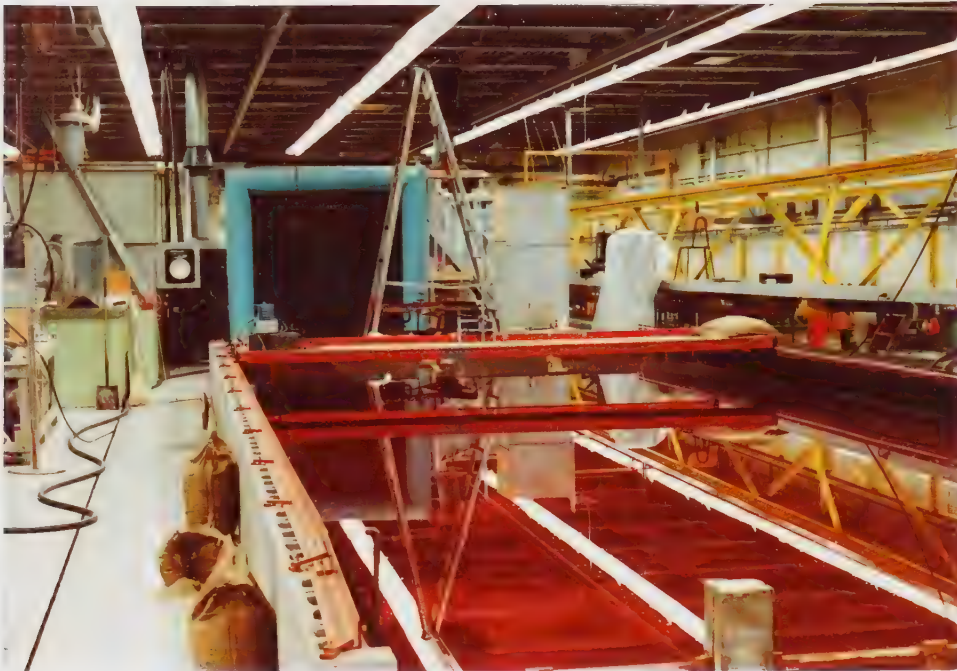


Plate 3.5 - General view of lake model



Plate 3.6 - Test section details



amount of dye to be injected under pressure. Initially it was hoped to take time averaged photographs with a slow shutter speed but due to the rapid discolouration of the tailwater by the food dye it was found necessary to increase the shutter speed. In order to obtain a true representation of the jet, at least three photographs were taken for each run and the values measured were averaged. The 1cm grid etched onto the bed allowed an accuracy of  $\pm 2\text{mm}$  but there was considerable judgement needed in estimating the position of the nominal jet boundary. The jet exit velocity was measured using a pitot-static tube, which will be discussed later in detail and the tailwater was measured using a point gauge mounted to a traverse that was capable of moving in both horizontal directions. The point gauge could be moved vertically by a mechanical cog system, the gauge could be read to an accuracy of 0.025mm but play in the cogs reduced the accuracy of the reading to approximately 0.1mm. The lack of camera lense angle and the need for a clear grid, meant that the section of the tank photographed was quite short.

For the lake model the camera was mounted on an angle beam, that in turn was bolted to a 3.5m high step ladder. The ladder was positioned over the head canal so that the camera was positioned approximately 3m above the sandbox test section. A scale was obtained by constructing a 10cm grid, of elasticated string with an aluminum frame, as shown in Plate 3.6. The grid was photographed on top of the sandbox and the metal plate before being removed for the



experimental runs. Because the camera was kept in the same position for all the runs, the grid photographs could be used as a scale for all the photographs obtained from the study. Dye colouration was achieved by adding the food dye into the head canal. Again at least three photographs for each run were taken and the average value calculated. The mean outlet velocity was found from the discharge obtained from the V notch weir and the area of the nozzle. The depth of tailwater and the nozzle depth were measured using a point gauge, similar in construction to that described earlier for the jet tank and was mounted on a traverse capable of movement in both horizontal directions. The traverse could be positioned to  $\pm 1.59\text{mm}$  in both directions. Plate 3.5 shows the camera mounting apparatus, while Plate 3.6 illustrates the point gauge.

### E. Velocity Measurement

Velocity readings from the jet tank were obtained using a commercially available Prandtl-type pitot static tube and commercially available pressure transducers. The pitot static tube had an external diameter of 1.59mm (1/16 in) and a hemispherical nose. The tube was clamped to the staff gauge on the traverse described above and is shown in Plate 3.2. The tube was positioned manually and the etched grid was used as a position reference.







The pitot-static tube was connected to the pressure transducer using 5mm diameter plastic tubing. The pressure transducer used for lower heads was a Celesco type P900, which had a full scale deflection of  $\pm 2.54\text{cm}$  water, although when tested it was found that the readings were still accurate to  $\pm 8.0\text{cm}$ . For larger heads (greater than  $2.54\text{cm}$  water) a Validyne model KP15, with a diaphragm full scale deflection of  $\pm 0.5\text{psi}$  was used. This transducer had a full scale deflection of  $\pm 35.0\text{cm}$  of water and, according to manufacturers specification, an accuracy of  $0.5\%$  and an ability to withstand an overload of  $200\%$ . The system also used either a Pace CD25 transducer indicator or a Validyne CD15 carrier demodulator, both linked to a digital indicator that had two decimal places and was therefore capable of reading to  $\pm 0.01\text{mV}$ . Plate 3.3 shows the pitot-static tube, the Celesco transducer and the Pace CD25 transducer indicator and digital indicator. The apparatus was calibrated using calibration reservoirs, also shown in Plate 3.3, the movable reservoir could be positioned to within  $\pm 0.025\text{mm}$ . The whole network system was filled with de-aired water that was coloured to facilitate the easy detection of air bubbles, which would invalidate any observations. A diagram of the system is shown in Figure 3.3

It was usually necessary to take an average value for the velocity head due to the fluctuations in the flow. For large velocity heads, as was usually the case, this would lead to negligible error but in areas of very slow flow an



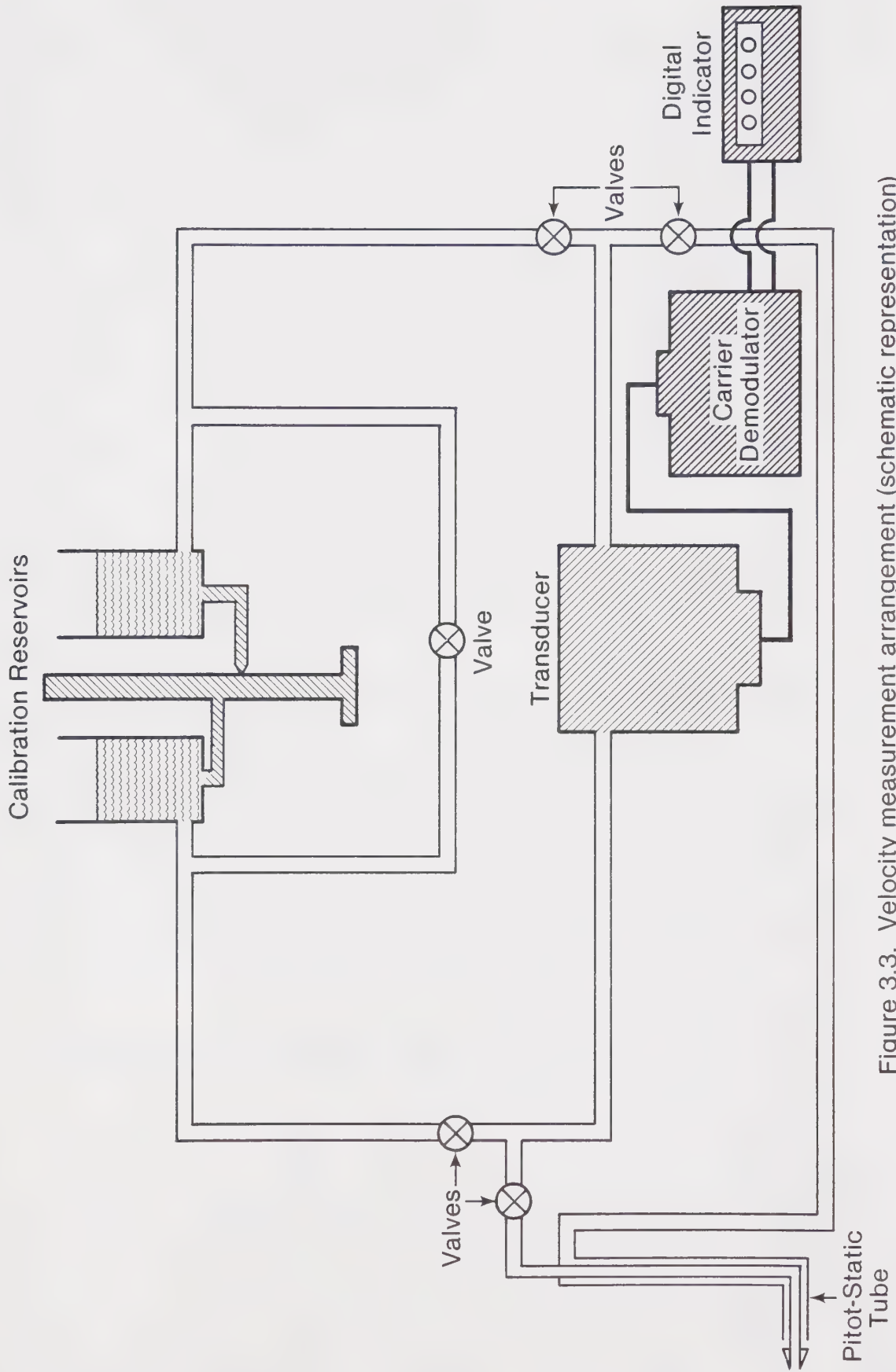


Figure 3.3. Velocity measurement arrangement (schematic representation)



error of 0.01mV could be quite significant (greater than 50%) and in the "uniform flow region" of the jet, with small differences in velocity in the vertical plane, the fluctuations of the readings could lead to significant error. This was another reason why the investigation only studied the jet relatively close to the nozzle. The low head transducer was calibrated to give a reading of 0.1mm of water for every 0.01mV, while the high head transducer gave a reading of 0.508mm of water for every 0.01mV shown on the digital indicator. It should also be noted that the pitot-static tube gives errors of less than 1% in velocity for misalignments to the direction of flow up to about 15 degrees (Massey, 1975).

As shown earlier, the velocity in the lake model was calculated by an indirect method. The discharge was found from the V notch weir and the nominal cross-sectional area of the nozzle was computed. Using the one dimensional continuity equation the mean initial velocity of the jet could be calculated.

#### F. Bed Shear Stress Measurement

A very simple way to measure the boundary shear stress is to use a Preston tube (Preston, 1954). A Preston tube is a total head tube resting on the boundary, for which the difference between the dynamic pressure on the tube and the static pressure on the boundary is correlated with the shear



stress. It has been shown (Rajaratnam, 1965; Rajaratnam and Muralidhar, 1968) that a Prandtl-type pitot static tube with a hemispherical nose behaves exactly like a Preston tube for boundary shear stress measurement. V.C. Patel (1965) has given a very accurate calibration curve for the Preston tube on smooth boundaries, while A.B. Hollingshead and N. Rajaratnam (1980) have produced calibration curves for the Preston tube on rough boundaries.

In the jet tank the bed was painted, with an engraved grid. This grid obviously produced some uniform roughness and before any shear stress measurements could be made it was necessary to make an estimate of the roughness.

It has been shown (Schlichting, 1968) that the increase in drag due to a circular cavity is the same or less than that given by small protrusions. It is therefore reasonable, for the lack of any other information, to assume that this is true for grooves as well as circular depressions.

For a uniform protuberance, a simple relationship for the equivalent sand roughness is;

$$k_s = \frac{\text{cross-sectional area A}}{\text{cross-sectional area B}} \quad (3.1)$$

where  $k_s$  = equivalent sand roughness and areas A and B are defined in Figure 3.4

For the case of a ridge of unit width and constant height, equation 3.1 reduces to





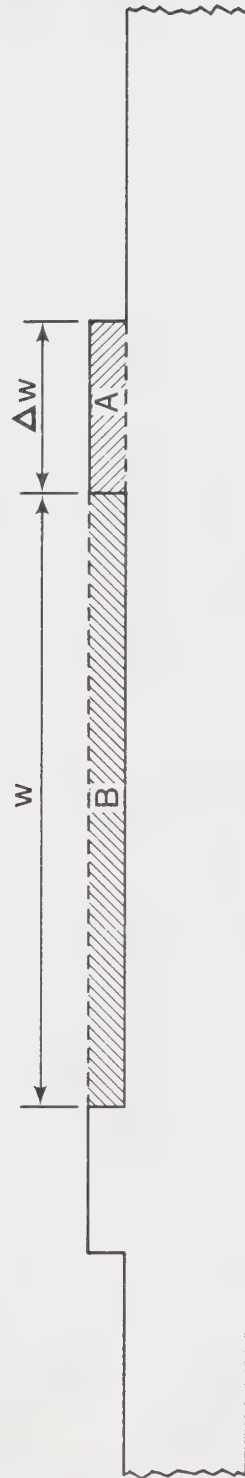


Figure 3.4. Equivalent sand roughness



$$k_s = \frac{\Delta w}{w} \quad (3.2)$$

where  $\Delta w$ =breadth of ridge

$w$ =distance between ridges

So, assuming that the grooves due to the grid can be replaced by equivalent ridges and that the grooves are nominally 1mm wide, leads to a  $k_s$  value of approximately

$$k_s \approx 1/9 \approx 0.11 \text{ mm/unit length} \quad (3.3)$$

For a pitot static tube of external diameter of approximately 1.6mm, the value of

$$\frac{d}{k_s} = \frac{1.6}{0.11} \approx 15 \quad (3.4)$$

where  $d$ =external diameter of pitot static tube

From the work of Hollingshead and Rajaratnam (1980), it can be found that the calibration curve for a  $d/k_s$  value of 15 follows Patel's curve until  $\Delta p_*$  is approximately  $4 \times 10^4$  and then enters a transition zone and becomes fully rough at  $\Delta p_*$  approximately  $1 \times 10^5$

where  $\Delta p_*$  is defined as

$$\Delta p_* = \frac{\Delta p d^2}{4 \rho v^2} \quad (3.5)$$



$\rho$ =mass density,  $\nu$ =kinematic viscosity of the fluid

$\Delta p$ =dynamic pressure

For the vast majority of the measurements made during the experimental runs, the boundary was smooth but for the two high velocity runs (runs 11 and 12), around the nozzle the boundary was probably transitional. However because of the assumptions and approximations used for the analysis it was considered reasonable to assume that the boundary was smooth for all measurements.

Using the approximation of a smooth boundary it was possible to use Patel's calibration curve for the ranges covered:

$$\text{Range} \quad 3.5 < \log_{10} \frac{\tau_0 d^2}{4\rho\nu^2} < 5.3$$

$$x^* = y^* + 2 \log_{10} (1.95y^* + 4.10) \quad (3.6)$$

$$\text{where } x^* = \log_{10} \left( \frac{\Delta p_p d^2}{4\rho\nu^2} \right) = \log_{10} \left( \frac{\Delta h g d^2}{4\nu^2} \right) \quad (3.7)$$

$$\text{and } y^* = \log_{10} \left( \frac{\tau_0 d^2}{4\rho\nu^2} \right) \quad (3.8)$$

$$\text{Range} \quad 1.5 < y^* < 3.5$$

$$y^* = 0.8287 - 0.1381 x^* + 0.1437 x^{*2} - 0.0060 x^{*3} \quad (3.9)$$



$$\begin{aligned} \text{Range } y^* &< 1.5 \\ y^* &= 1/2 x^* + 0.037 \end{aligned} \quad (3.10)$$

and  $\Delta p_p$  = Preston tube reading (the difference between Pitot and static pressures)

$\tau_o$  = wall shear stress

$\Delta h$  = head of water equivalent to pressure difference

$g$  = acceleration due to gravity

From temperature measurements taken of the water used in the jet tank, it was found to be of the order of  $10^\circ\text{C}$ , therefore the value of the kinematic viscosity was taken as  $1.3\text{mm}^2/\text{s}$  (Massey, 1975)

Using the equations given above it was possible to construct a calibration curve, converting the readings from the transducer in mm of water directly into shear stress ( $\text{N/m}^2$ ). This curve is given in Figure 3.5.

### G. Scour Hole Measurement

A fairly elementary study of the scour hole formed by the jet issuing across the sandbox in the lake model was performed. The model was left in operation for a minimum of 18 hours and occasionally for as long as 56 hours in order that the scour hole reached the asymptotic state (Rajaratnam





and Berry, 1977).

Once the scour had reached the asymptotic state, the flume was drained and the scour hole measured along its central axis, using the point gauge described in section C. The flume was refilled before the scour hole was filled in and leveled. The periodic draining of the lake model ensured that there was no temperature difference between the body of water contained in the flume and the water of the jet. This was also confirmed by temperature readings taken in the head canal and the lake model.



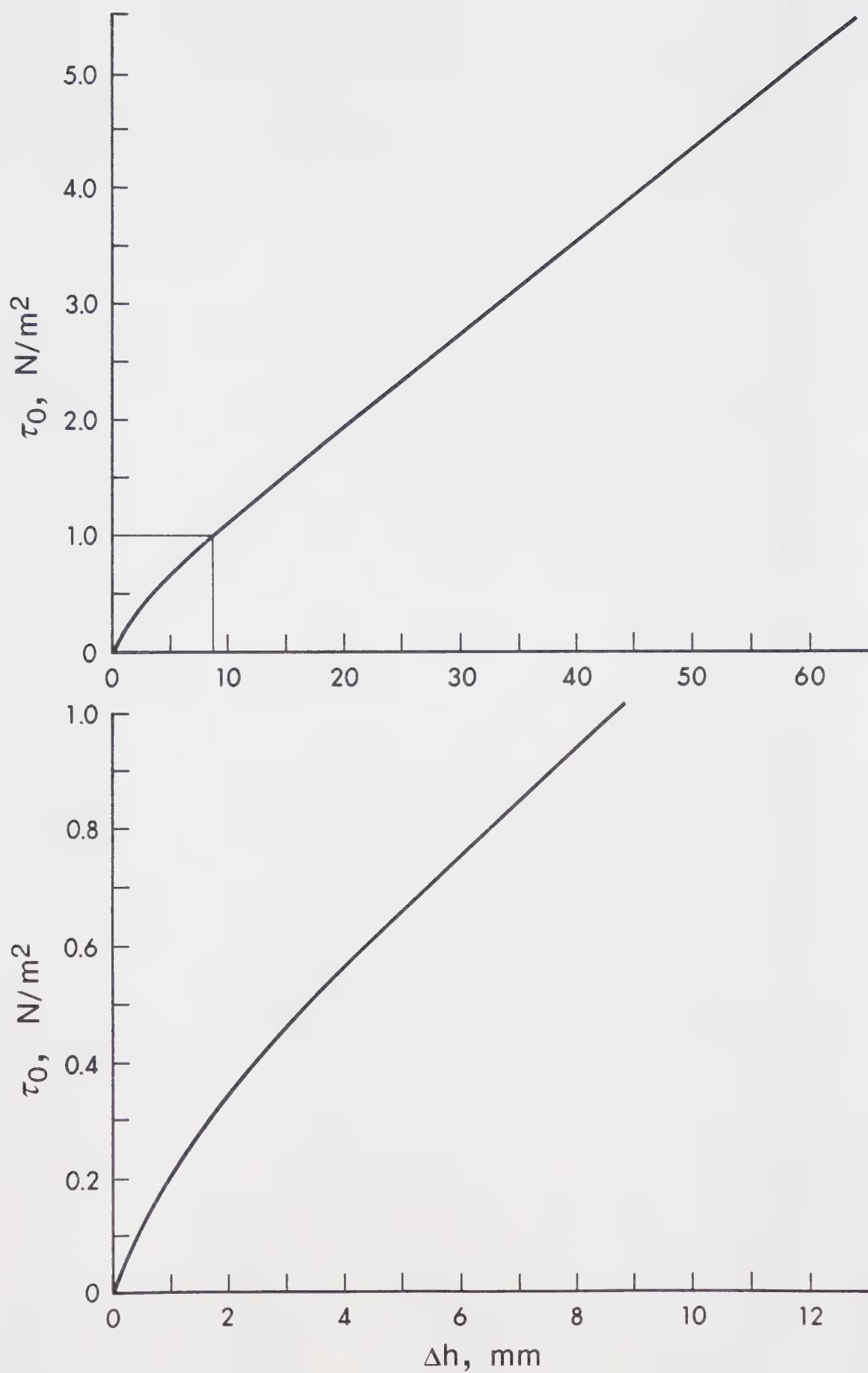


Figure 3.5 Calibration curve for bed shear stress



## IV. ANALYSIS OF EXPERIMENTAL RESULTS

### A. PART I - JET EXPANSION

#### Introduction

This section presents the results obtained from the photographic study made of the three dimensional turbulent bluff wall jet with varying finite tailwater conditions. Based on the present observations, a relationship for the change of the angle of the jet expansion is presented in a suitable form.

#### Review of Existing Work

Unfortunately there appears to be no previous studies made on the problem of the change of expansion of a bluff wall jet due to variations of the tailwater depth. However some results have been obtained for the limiting case of an infinitely deep tailwater.

Due to the problem of defining the exact position of the jet boundary, past investigators have only looked at the growth of the half width, ie the position where the local velocity is half the maximum velocity. This half width has been found to grow linearly with  $x$ , the distance downstream of the nozzle, and for wall jets the growth is much larger parallel to the bed than normal to it (Rajaratnam and



Pani, 1970; Newman et al., 1972). Using the terminology shown in the definition sketch Figure 4.1, Newman et al. (1972) obtained a value for  $\tan\theta'$ ,  $\theta'$  being the angle of half width growth, of 0.278, while Pani (1972) measured a value of 0.20 and Chandrasekhara Swamy and Bandyopadhyay (1975) arrived at a value of 0.166. However the experimental conditions of Pani were the closest to those of the present investigation and a value of 0.20 for  $\tan\theta'$  can be accepted. It is necessary to find a relationship between  $\tan\theta'$  and  $\tan\theta$ , where  $\theta$  is the angle of growth for the nominal jet boundary. Pani (1972) has shown that the velocity profiles in the transverse direction are similar and that the error function curve can be fitted to the data with reasonable accuracy, although the data tend to lie above the curve for larger values of  $z/b_z$ ,  $z$  being the transverse distance measured from the centre of the jet and  $b_z$  the half width in the transverse direction. Rajaratnam (1965), while investigating the modelling of the hydraulic jump by wall jets, used an approximate value of 2.25 for the non-dimensional length when the velocity became zero. Using a slightly higher estimate of 2.50, because the data lie just above the error function curve, leads to the result that the value of  $\tan\theta$  for an infinite tailwater is of the order of 0.50.

The other limiting condition is that of no tailwater. The situation can now be described as a stream expanding past an abrupt expansion and as such the expansion, of the stream, has been found to be dependent on the Froude number





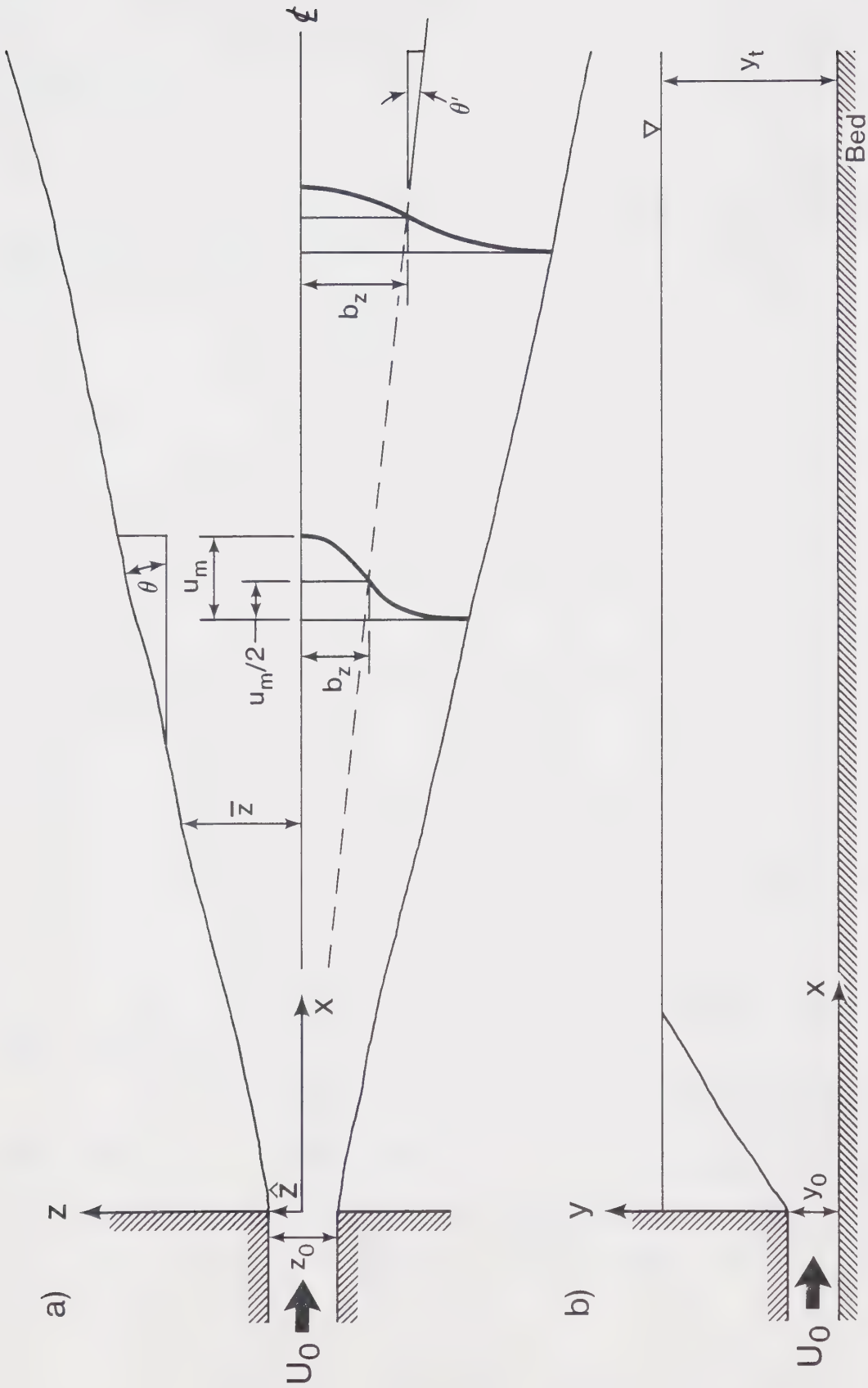


Figure 4.1. Definition sketch a) plan b) section



and linear (Rouse,1949).

## Experiments

It was found that the injection of dye into the jet produced a visual demarcation between the jet and surrounding fluid. From photographs taken of the coloured jet, it was observed that the jet was basically linear in its expansion, and that the expansion of the nominal jet boundary could be measured directly and with greater accuracy than by velocity measurements.

In total approximately one hundred different combinations of tailwater depth, initial velocity, nozzle aspect ratio and shape were investigated. Photographs were obtained and analysed for each run. In the jet tank, three different nozzles were used,

- 1) Round nozzle, diameter of 2.54cm, aspect ratio=1.0
- 2) Rectangular nozzle, 4cm wide by 2.5cm high, aspect ratio=1.6
- 3) Small rectangular nozzle, 1.58cm wide by 0.64cm high, aspect ratio=2.47

In the lake model, a study was made when the bed was fine sand ( $D_{50} = 0.11\text{mm}$ ) and the velocity was small enough that no scour was observed. A second study was made when the aluminum plate was placed over the sand bed. The outlet sizes for the two studies were

- 1) Rectangular outlet, 5cm wide by 3.1cm high, aspect



ratio=1.61

2) Rectangular outlet, 5cm wide by 2.00cm high, aspect ratio=2.50

The initial jet velocity range covered was extensive, the lowest being 1.79cm/s and the largest velocity was 265.0cm/s, although this upper velocity was for the no tailwater condition. The largest velocity investigated for a run with a tailwater was 256.1cm/s.

The tailwater range was varied from no tailwater to a tailwater to nozzle height ratio of 13.6, which is approaching the infinite tailwater condition. Most of the tailwater to nozzle height ratios were, however, in the range 0.6 to 6.0.

It should be noted that towards the downstream end of the plate, in the jet tank, the jet sometimes became unstable and oscillated. This may have been caused by the jet entering the deep water at the end of the tank, but while investigating hydraulic jumps below abrupt symmetrical expansions, Rajaratnam and Subramanya (1968) noticed that for a certain range of small tailwaters the jet tended to oscillate. The instability experienced in the present study may have similarities to that found by Rajaratnam and Subramanya but further study needs to be done before any conclusion can be reached. However due to the relatively short test section used in the present work any instability did not affect the results observed and presented here.



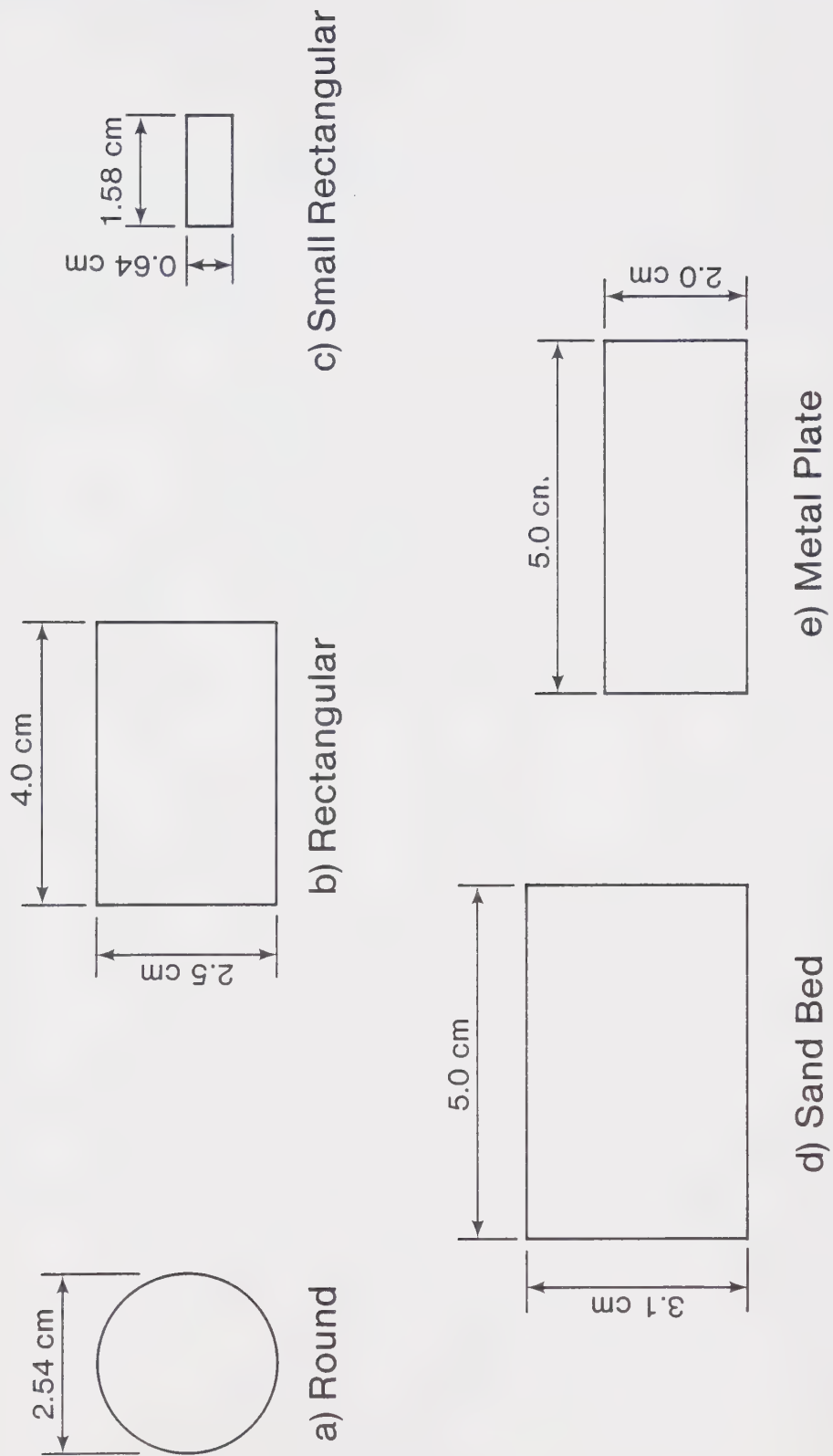


Figure 4.2. Nozzle dimensions: a, b, c - jet tank : d, e - lake model (full size)





## Experimental Results

From the photographic study undertaken it was found possible to classify the jet characteristics into five separate sets. These five classifications are defined in Table 4.1.

It will be noticed that Table 4.1 also contains two other classifications however these are the results from the lake model and are only separated for ease of identification, they are really part of Set 5. Plates 4.1 through to Plate 4.12 show typical jet profiles from each classification.

### Set 1

Set 1 was the condition of no tailwater. Plate 4.1 gives a typical illustration of the flow pattern observed. The expansion was found to be linear and, as discussed previously, the rate of expansion was dependent on the Froude number defined as;

$$F_0 = \frac{U_0}{\sqrt{gy_0}} \quad (4.1)$$

$F_0$  = Froude number

$U_0$  = Initial jet velocity



Table 4.1 Jet Expansion Classification

Set	Tailwater/Nozzle height	Comments
1	$y_t/y_o = 0$	No Tailwater
2	$0 < y_t/y_o \leq 0.3$	
3	$0.3 < y_t/y_o \leq 0.6$	Non-monotonic
4	$0.6 < y_t/y_o \leq 1.0$	Linear but $\hat{z} \neq z_o/2$
5	$1.0 \leq y_t/y_o$	Linear and $\hat{z} = z_o/2$
6	$y_t/y_o \approx 1.0$	Lake model with metal plate
7	$y_t/y_o \approx 1.0$	Lake model with sand bed but no scour



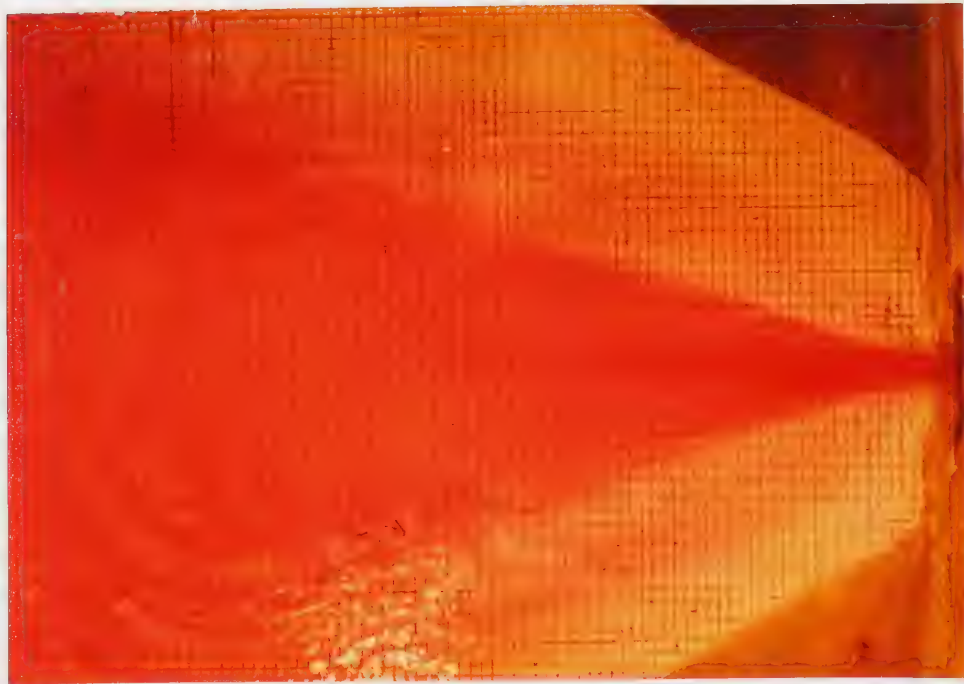


Plate 4.1 - Run 1g

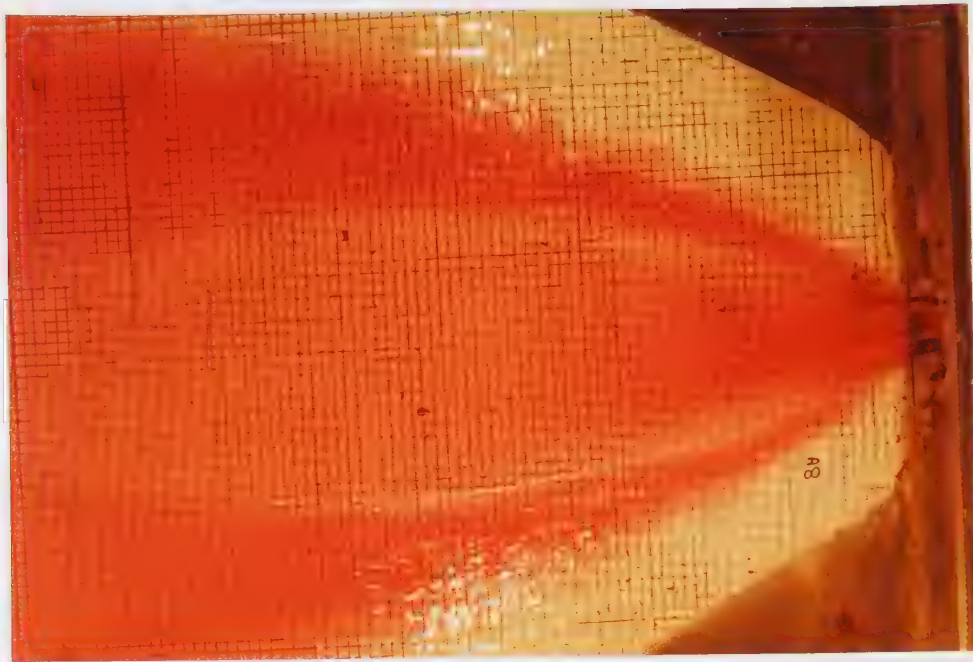


Plate 4.2 - Run 2a



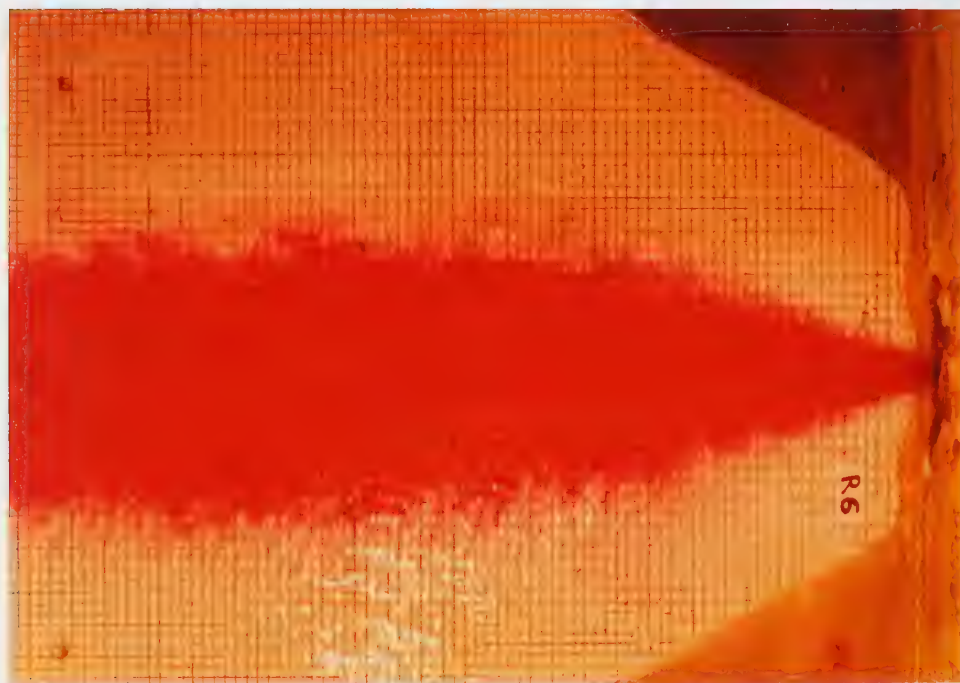


Plate 4.3 - Run 3a



Plate 4.4 - Run 3g





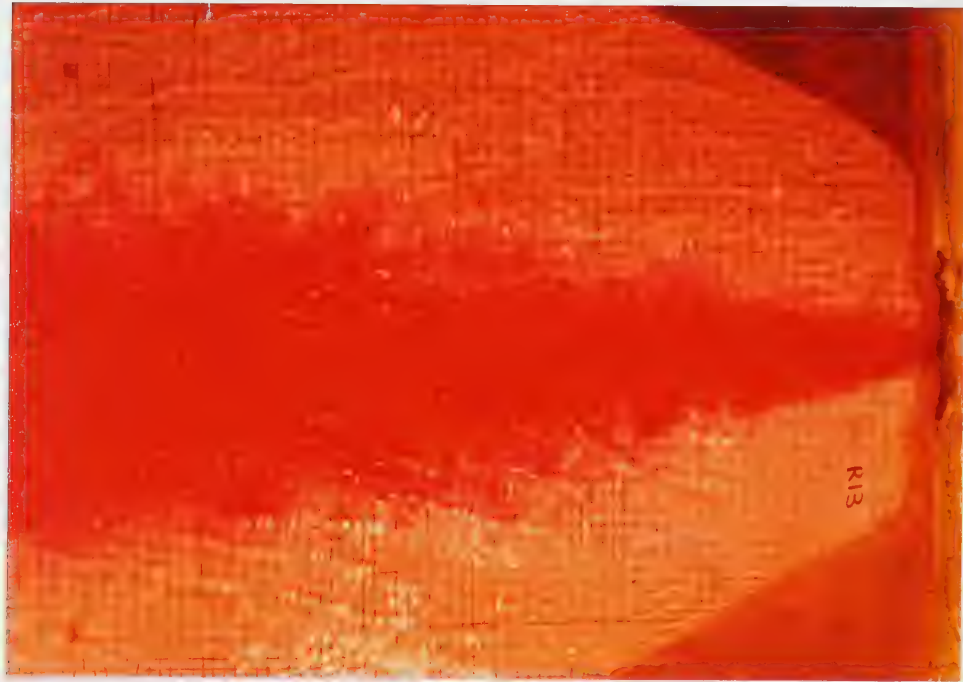


Plate 4.5 - Run 4g

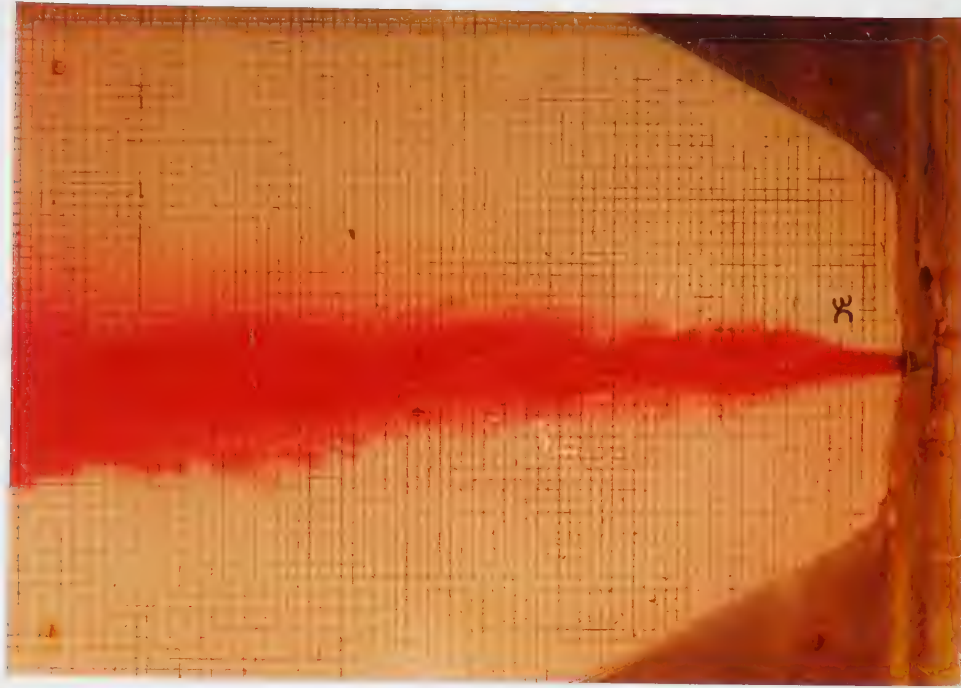


Plate 4.6 - Run 4o



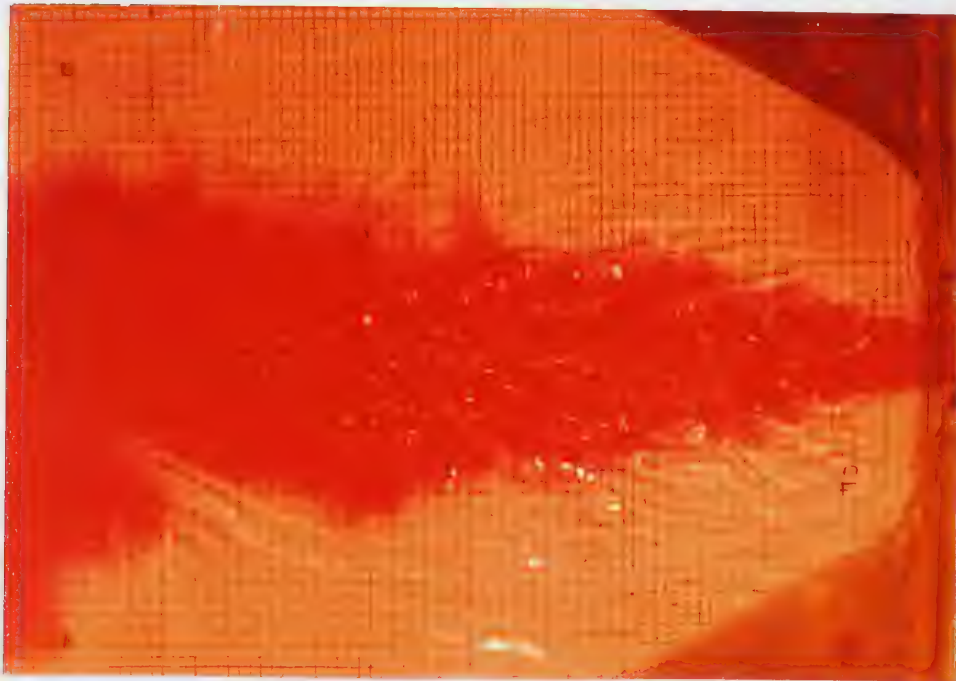


Plate 4.7 - Run 5m



Plate 4.8 - Run 5r





Plate 4.9 - Run 5ax



Plate 4.10 - Run 6h





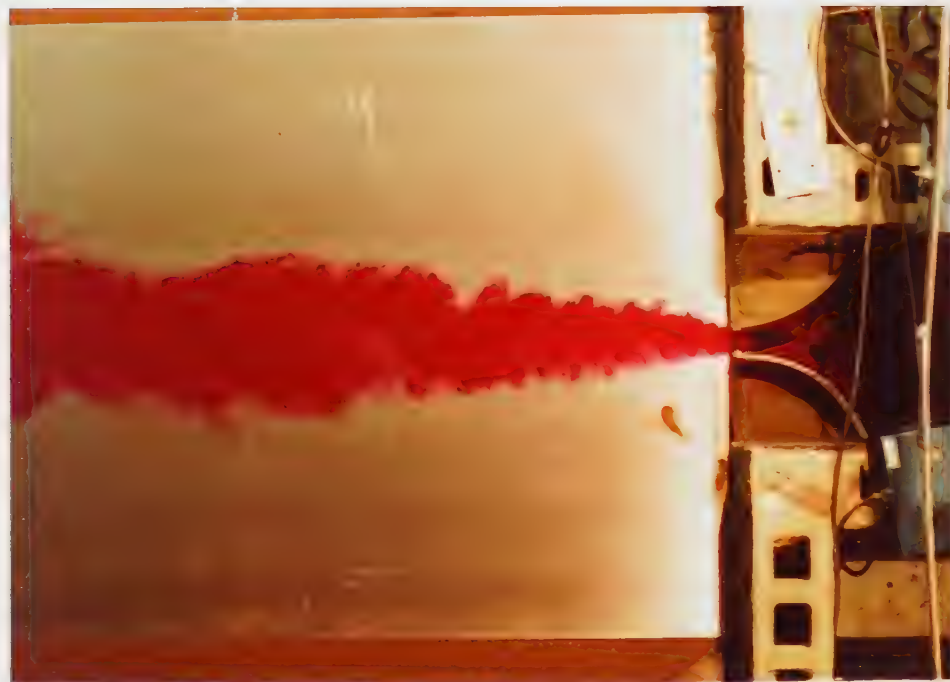


Plate 4.11 - Run 60



Plate 4.12 - Run 7g





$y_0$  = nozzle height

$g$  = acceleration due gravity

The no tailwater condition was not investigated in any great depth and the detailed relationship between the Froude number and the rate of expansion was not obtained. However from Figure 4.3 the trend was obvious. higher Froude numbers have a slower jet expansion, which also agrees with the findings of Rouse (1949) and agrees with general judgement.

## Set 2

Only one run was within this set and it may be an oddity. However from Plates 4.2 and 4.3 it can be seen that that set 2 could be the limiting case of set 3. The observation appears to be a valid result and until proven otherwise must be treated as such.

## Set 3

The results obtained from this set were very interesting, in that the jet did not expand in a monotonic manner. In this range the tailwater was approximately half the nozzle depth and the top portion of the jet tended to plunge into the tailwater creating a 'bulge'. After the initial expansion the jet contracted again. The reason for this contraction was



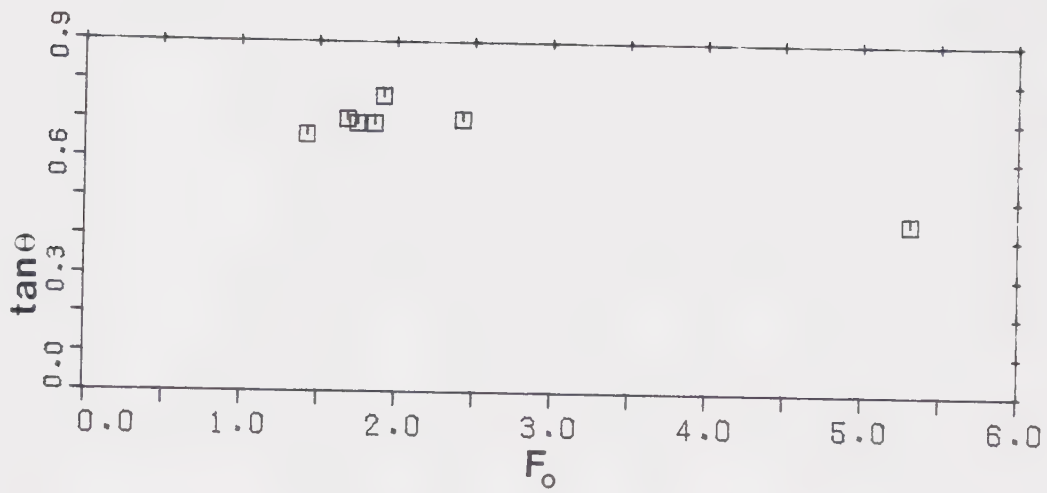


Figure 4.3 - Variation of  $\tan \theta$  with Froude number for  
bluff nozzles and no tailwater



not obvious but may have been due to the forward momentum of the lower portion of the jet and possible side flow into the jet due to the reduced pressure in the high velocity region immediately before the contraction. Figure 4.4 shows a possible representation of the jet. The length of the "bulge" appeared to be dependent on the Froude number  $F_0$ , as can be seen in Plates 4.3 and 4.4. In Plate 4.3 the Froude number was approximately one and one-half that of the jet shown in Plate 4.4, the position of maximum contraction does not appear in Plate 4.3 and obviously occurred further downstream. The flow pattern was obviously very complex and much further research would be required to understand the flow in this range completely.

#### Set 4

In Set 4 the study showed that the jet expanded linearly. However there was an abrupt initial expansion and therefore the line of the nominal jet boundary did not pass through the ends of the nozzle (ie  $\hat{z} \neq z_0/2$ ). A study (Figure 4.5) of the variation of the ratio  $\hat{z}$  to  $1/2z_0$  showed considerable scatter, although a trend was obvious and a straight line could be, for a first approximation, drawn through the data.



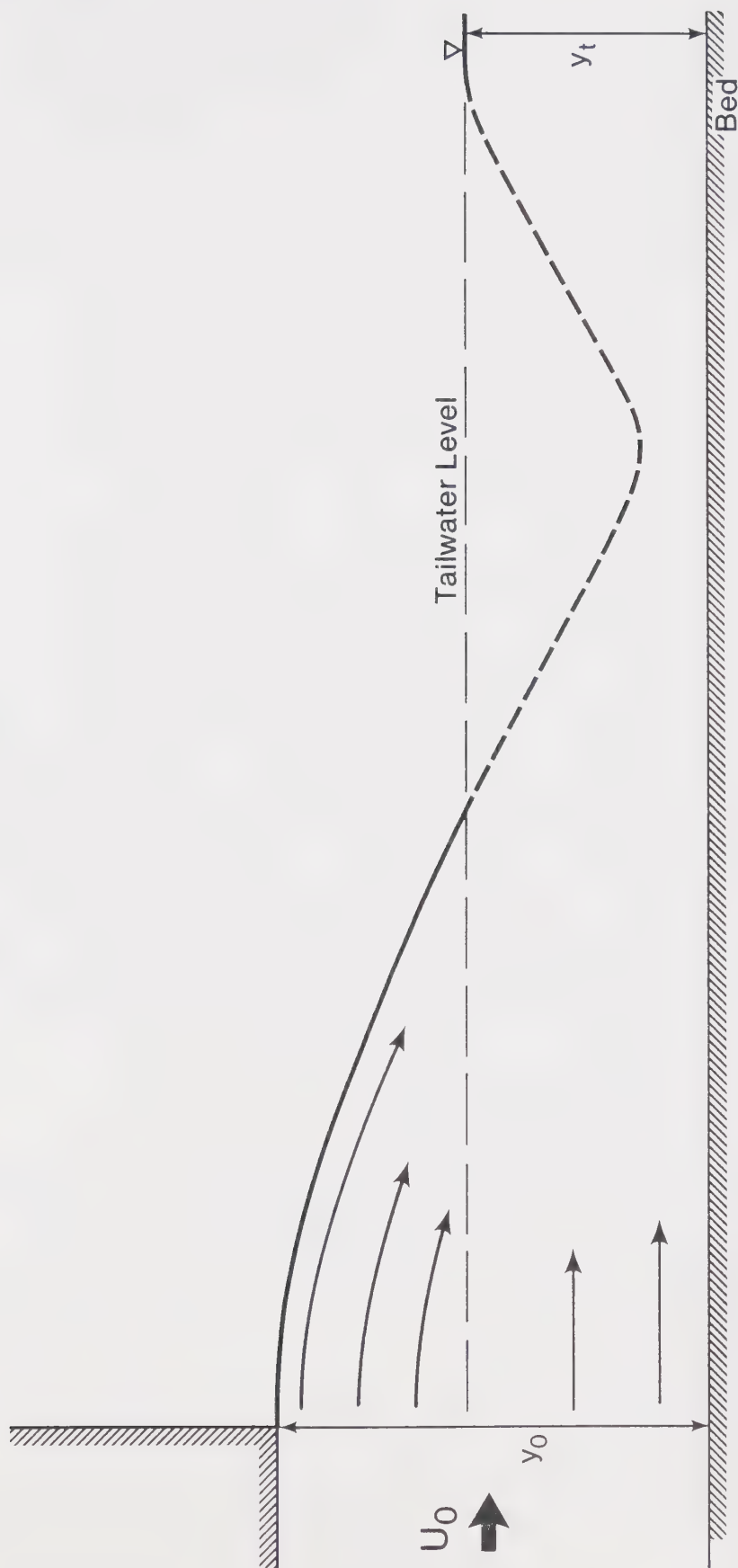


Figure 4.4. Possible streamlines for a plunging jet





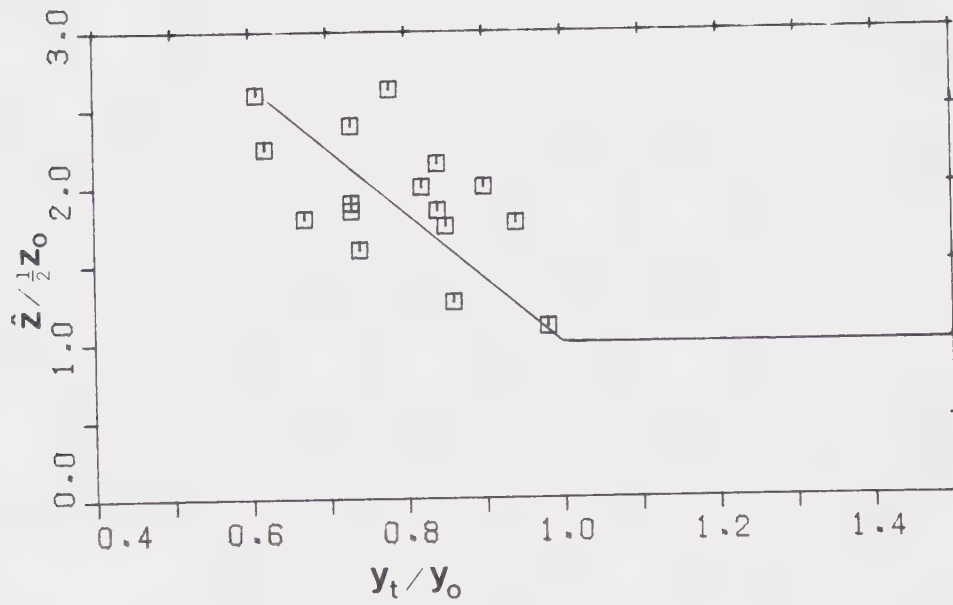


Figure 4.5 - Variation of  $\hat{z}$  for bluff wall jets with very shallow tailwaters



## Set 5

All the tailwater to nozzle height ratios ( $y_t/y_o$ ) greater or equal than one were represented by one set. In this set, the jet expanded linearly and the jet boundary passed (approximately) through the nozzle ends (ie  $\hat{z}=1/2z_o$ ).

Photographic evidence from Newman et al.(1972) and Pani (1972) has shown that, for deep submergence, the jet has an expansion virtual origin slightly in front of the nozzle, this was also observed in Plate 4.9. Unfortunately neither Pani nor Newman et al. conducted any analysis of their photographs nor did they provide any indication of the scale for their work. From the present study this difference in virtual origins appears to be negligible and for practical purposes may be discounted.

## Sets 6 and 7

As noted earlier, sets 6 and 7 were covered by set 5. Both sets were from the lake model and the tailwater to nozzle height ratio was unity. Set 6 gave an expansion angle ( $\tan\theta$ ) varying from 0.14 to a maximum of 0.235 and an average of 0.184. Set 7 gave an average value for  $\tan\theta$  of 0.20, with a variation from 0.14 to 0.26. The slightly larger value of  $\tan\theta$  in set 7 was



due to the additional roughness of the sand bed.

### Correlation of the Transverse Expansion

When all the data available on the variation of  $\tan\theta$  with the tailwater was plotted (Figure 4.6) together in a dimensionless form, they were found to lie, for  $y_t/y_o > 0.6$ , on a single curve. It was noted that the expansion angle ( $\tan\theta$ ) was independent of the jet velocity, because the results from the lake model lay well within the data scatter. For ratios of  $y_t/y_o$  less than 0.6 the curve was undefined due to the non-linearity noted in the paragraph on set 3 and the dependency on the Froude number discussed previously. Figure 4.6 presents the variation of the jet expansion angle for different tailwater to nozzle height ratios and Appendix A contains the data and plots obtained from the photographic study.

### Summary

From experimental observations using a dye injection and photographic technique, it was found that for bluff nozzles the jet expansion in the transverse direction was dependent on the tailwater depth. It was found that the nozzle height could be used as a non-dimensionalising parameter and if used, then a single curve was obtained for the variation of the expansion angle. It was also found that



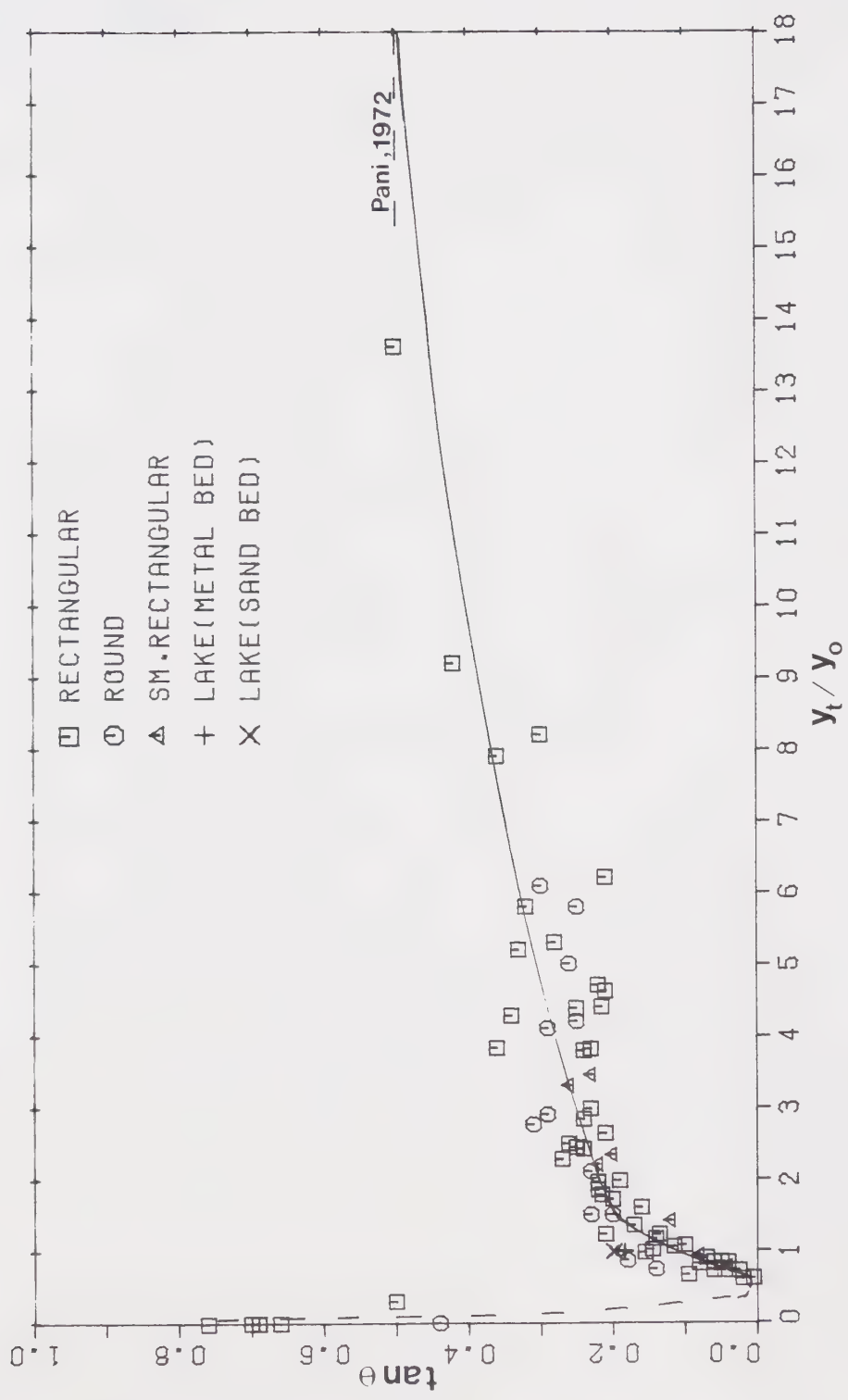


Figure 4.6 - Expansion of bluff wall jets in the transverse direction with varying tailwater depths





the jet could be classified in five sets, each with distinct physical characteristics and that for tailwater to nozzle height ratios less than 0.6 the Froude number became another important parameter.



## B. PART II VELOCITY AND SHEAR STRESS ANALYSIS

### Introduction

The results of velocity measurements taken along the centreline plane, normal to the bed and in the transverse plane of maximum centreline velocity are presented. From these observations, the velocity profiles are shown to be similar and relationships for the maximum velocity decay, growth of length scales, surface velocity and variation in the length of the potential core are established. When possible the empirical relationships are compared with theoretically established laws. Also the results from shear stress measurements are presented in suitable forms.

### Review of Existing Work

The earliest experimental investigations into three dimensional turbulent wall jets were carried out by Viets and Sforza (1966) and Sforza and Herbst (1970). However the first detailed investigations of bluff wall jets were performed by Newman et al. (1972) and Pani (1972), followed by Chandrasekhara Swamy and Bandyopadhyay (1975). The most complete study was performed by Pani (1972) and for this reason, and because his experimental arrangement was very similar to that of the present study, the results obtained



by Pani will generally be used as the asymptotic values for the present relationships. A note will be made of the values assigned to the asymptotic case when they occur in the following sections.

## Experiments

A total of twelve runs were made in the jet tank described in chapter 3. For each run, a different tailwater and initial jet velocity was used. The velocity measurements were made by using the Prandtl-type pitot static tube discussed in chapter 3. The shear stress measurements were obtained by resting the Prandtl type pitot static tube on the bed and using the calibration chart shown in Fig 3.5. The first ten runs were made with the rectangular nozzle of dimensions shown in Fig 4.2(b), while runs 11 and 12 were made with the 2.54cm diameter round nozzle, shown in Fig 4.2(a).

In runs 1 to 6 only measurements of the vertical centreline velocity profiles were obtained but in runs 7 to 12, the vertical centreline velocity profile and the transverse velocity profile, along the plane of maximum centreline velocity was measured. Also for runs 7 to 12, the centreline shear stress and the transverse shear stress values were obtained.

The tailwater was varied between 2.77cm (ie a tailwater to nozzle depth ratio of 1.11) to a maximum of 11.1cm (a



tailwater to nozzle depth ratio of 4.44). The initial jet velocity varied from 61.9cm/s to 100cm/s for runs 1 to 10, while for the runs with round nozzle, the initial jet velocity was of the order of 190cm/s. The significant details for each run are given in Table 4.2.

### Typical Vertical Velocity Profiles

As discussed in chapter 2, it is possible to describe the tailwater condition as three separate types, shallow, moderate submergence and deep submergence. Each tailwater type has its own distinct characteristics. Shallow tailwaters have a short potential core and pass directly from the potential core region into the "uniform flow" transition zone. Moderate tailwaters pass from the potential core region into a radial type decay region before entering the "uniform flow" transition. While deep tailwaters never really enter the transition into uniform flow. Figure 4.7 (a),(b),(c) shows typical velocity profiles from each of the three tailwater types. In Fig 4.7  $x$  is the distance in centimetres measured downstream from the nozzle,  $y$  is the distance measured from the bed and  $u$  is the forward horizontal velocity. In each profile, it can be seen that the maximum velocity decays the further downstream the jet travels and that the surface velocity approaches the maximum velocity for the section further downstream. Fig 4.7(a)





Table 4.2 Details of Experiments

Run	Shape	$U_o$ cm/s	$y_t$ cm	$y_t / y_o$	R
1	Rect.	95.0	2.77	1.11	23,109
2	Rect.	92.0	3.78	1.51	22,379
3	Rect.	98.0	4.05	1.65	23,838
4	Rect.	100.0	3.2	1.28	24,325
5	Rect.	84.0	4.63	1.85	20,433
6	Rect.	84.5	3.1	1.24	20,555
7	Rect.	61.9	11.1	4.44	15,057
8	Rect.	79.2	7.86	3.14	19,266
9	Rect.	80.8	4.35	1.74	19,655
10	Rect.	85.1	3.35	1.34	20,700
11	Round	187.3	7.0	2.76	32,432
12	Round	191.2	1.94	1.94	33,107



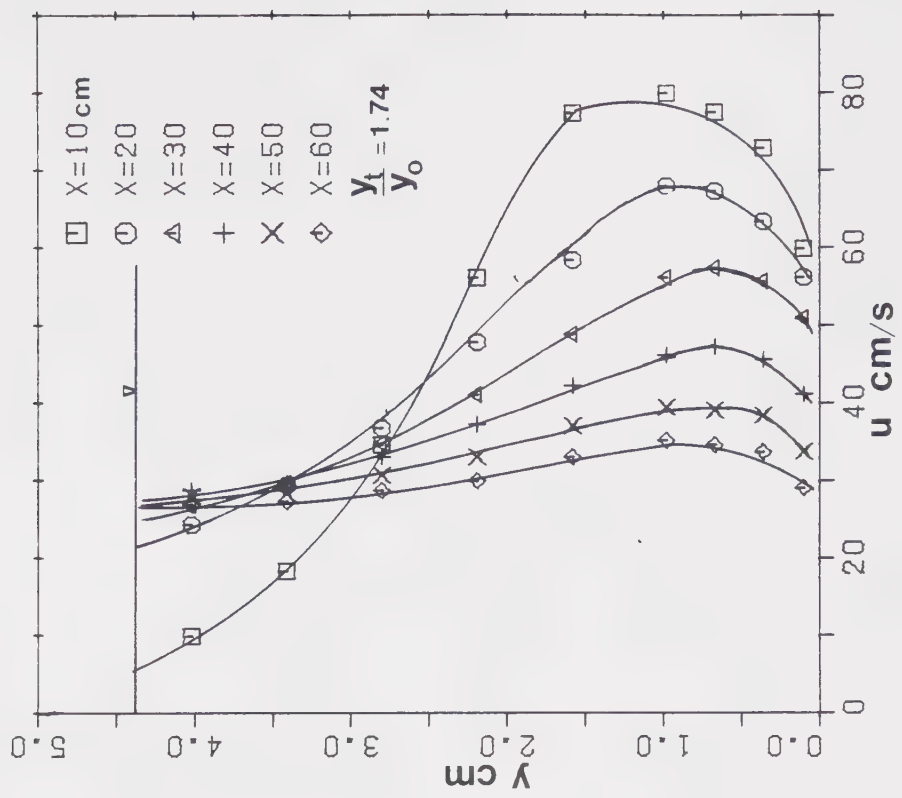
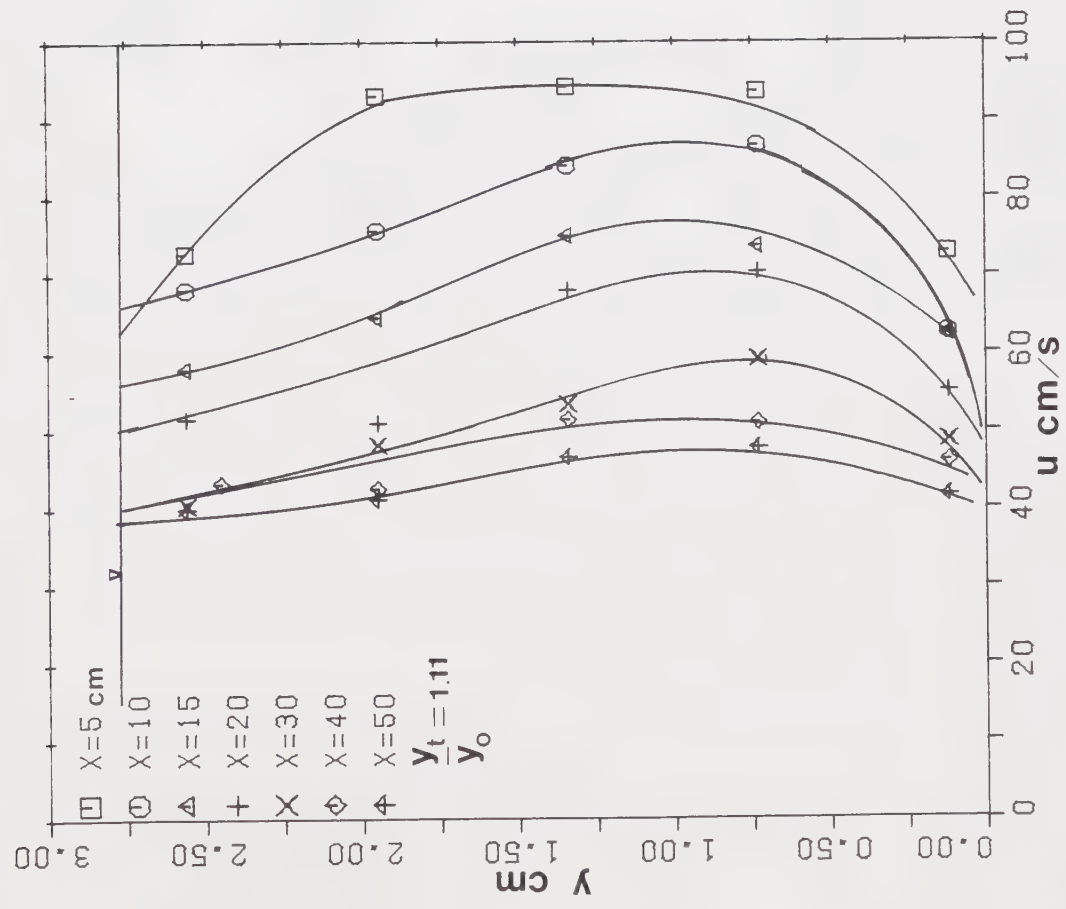
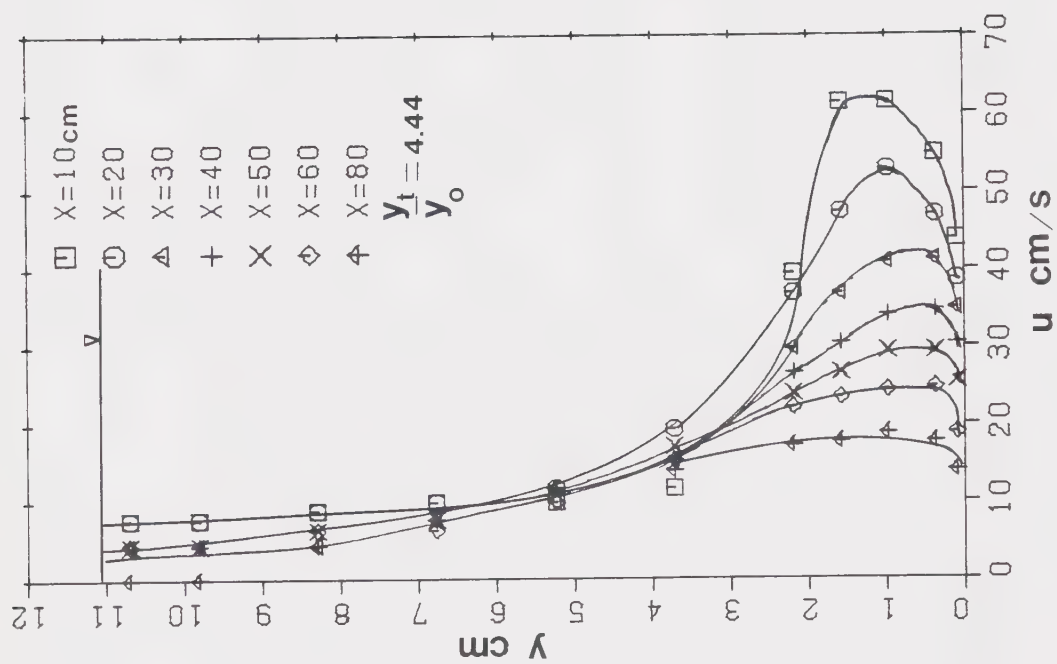


Figure 4.7 - Typical vertical velocity profiles for the rectangular bluff nozzle with different tailwater depths







gives a very clear illustration of the vertical velocity profile becoming almost uniform but still having a large forward velocity.

### Similarity of Vertical Velocity Profile

It has been common among investigators of jets issuing into an infinite ambient fluid, to reduce the velocity profiles into a similar form by using the half length as a characteristic length scale. However when investigating the problem of a finite tailwater it was found that the velocity, in the vertical plane, often never reached a value of half the local maximum velocity. This obviously leads to a need to find another suitable scale and after a process of trial and error, it was found that the length,  $b$ , when the velocity becomes 85% of the maximum velocity could be used satisfactorily as the characteristic length. When this scale was used to non-dimensionalise the vertical distance,  $y$ , and the maximum velocity,  $u_{mo}$ , at that section was used to non-dimensionalise the velocity, it was found that for each run the velocity profiles became similar after a downstream distance of approximately twelve times the nozzle height. Fig 4.8(a) gives a definition sketch for the scales used in non-dimensionalising the velocity profiles and Figure 4.9 shows three typical reduced vertical velocity profiles. Furthermore when all the reduced profiles were plotted together on one plot, it was found that they all collapse





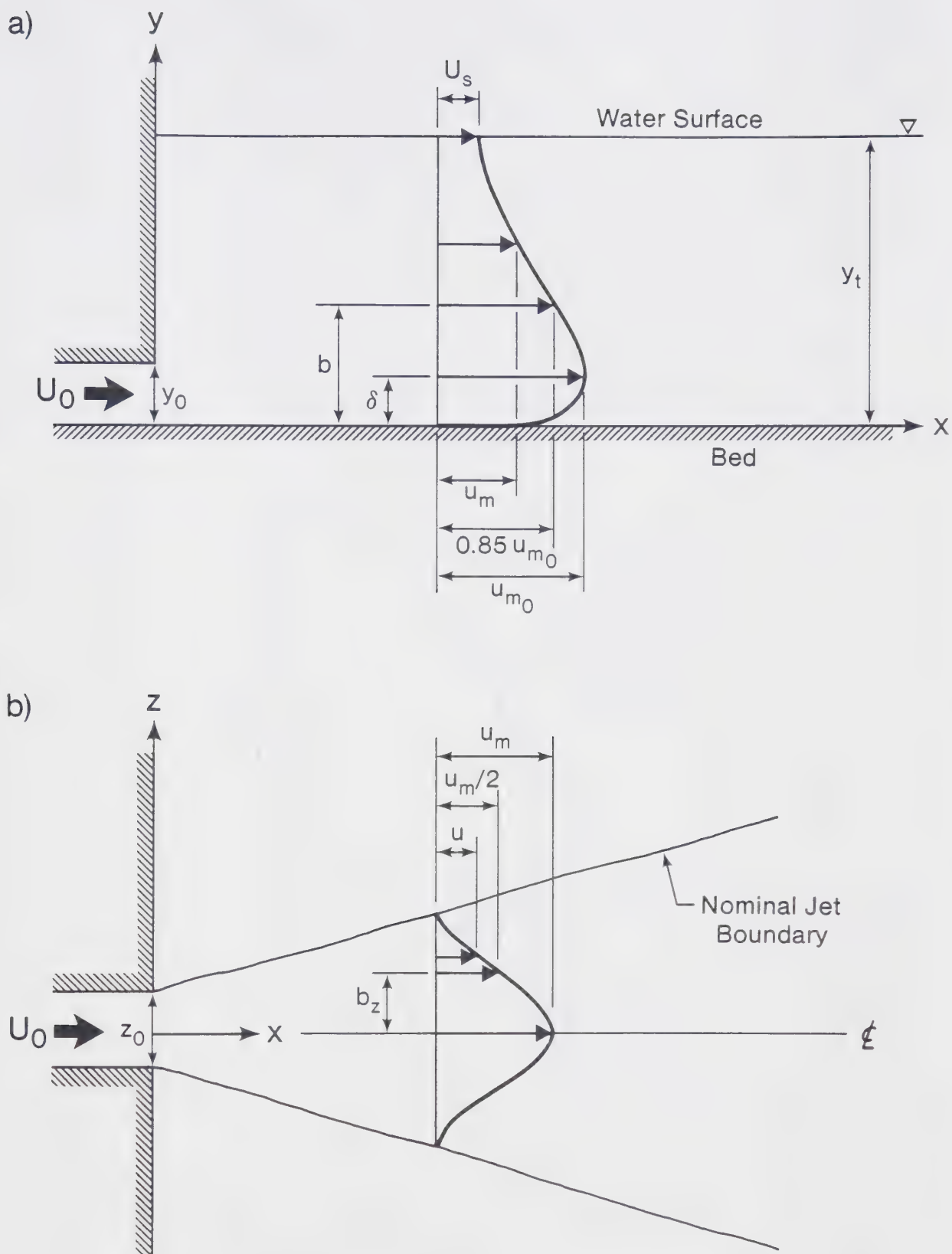


Figure 4.8. Definition sketch for scales a) vertical b) transverse



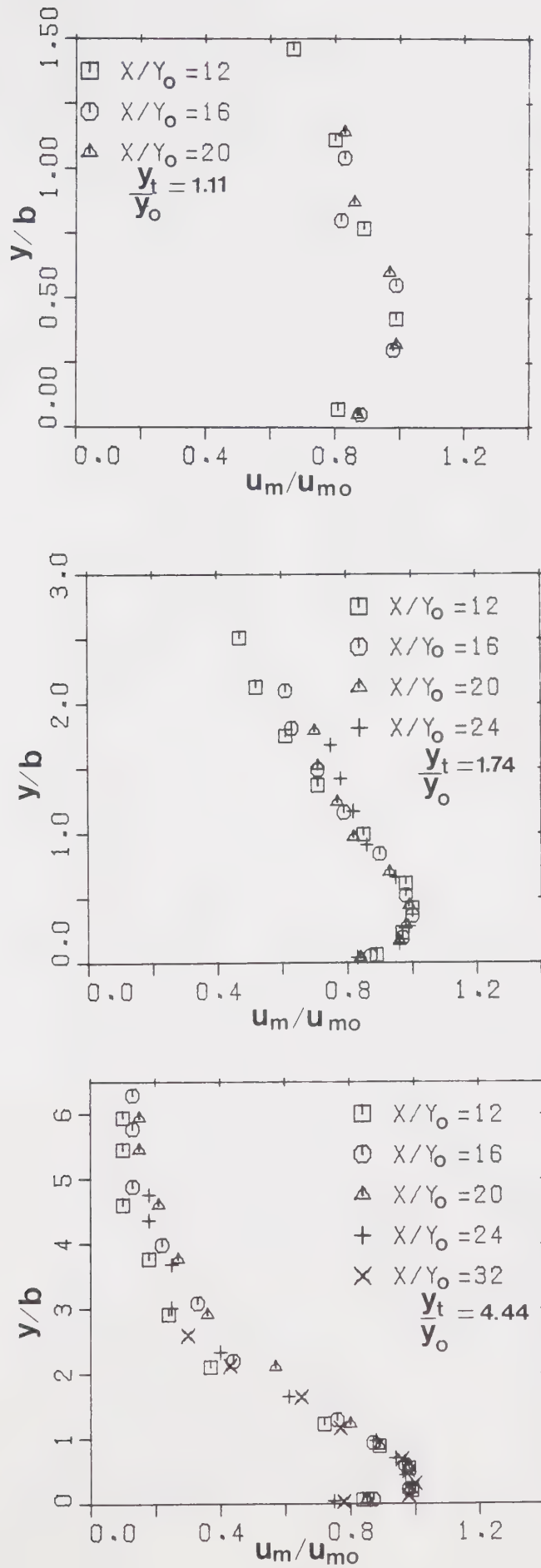


Figure 4.9 - Typical reduced vertical velocity profiles  
for the rectangular bluff nozzle



onto a single curve. The similarity is very good in the region close to the maximum velocity but some scatter occurs further away from the bed. This scatter was not unexpected considering the length scale used but the general trend of the curve, shown in Figure 4.10, is clear. From Fig 4.10 it can be seen that the similarity profile lies above the curve of the plane turbulent wall jet on a smooth wall (the classical wall jet). This is due to the greater acceleration of the jet at distances away from the wall, discussed previously in chapter 1. It is interesting to note, that for deeper tailwater (runs 7 and 11) the data lie closer to the C.W.J. curve than the data for shallow tailwater (runs 4, 6, 10).

### Surface Velocity

During the course of the observations, it was noticed that the surface of the tailwater was accelerated as the jet expanded into the whole depth. Plotting the ratio of the surface velocity to the local maximum velocity against the ratio of the tailwater depth to the nozzle height, shown in Figure 4.11, indicated that for each run there was considerable scatter but that generally it could be said that the ratio  $U_s/u_{mo}$  decreases for larger  $y_t/y_o$  ratios. No definitive curve through the points is possible but the trend indicated reinforces that which intuitively should be expected. However, study of the velocity profiles indicated



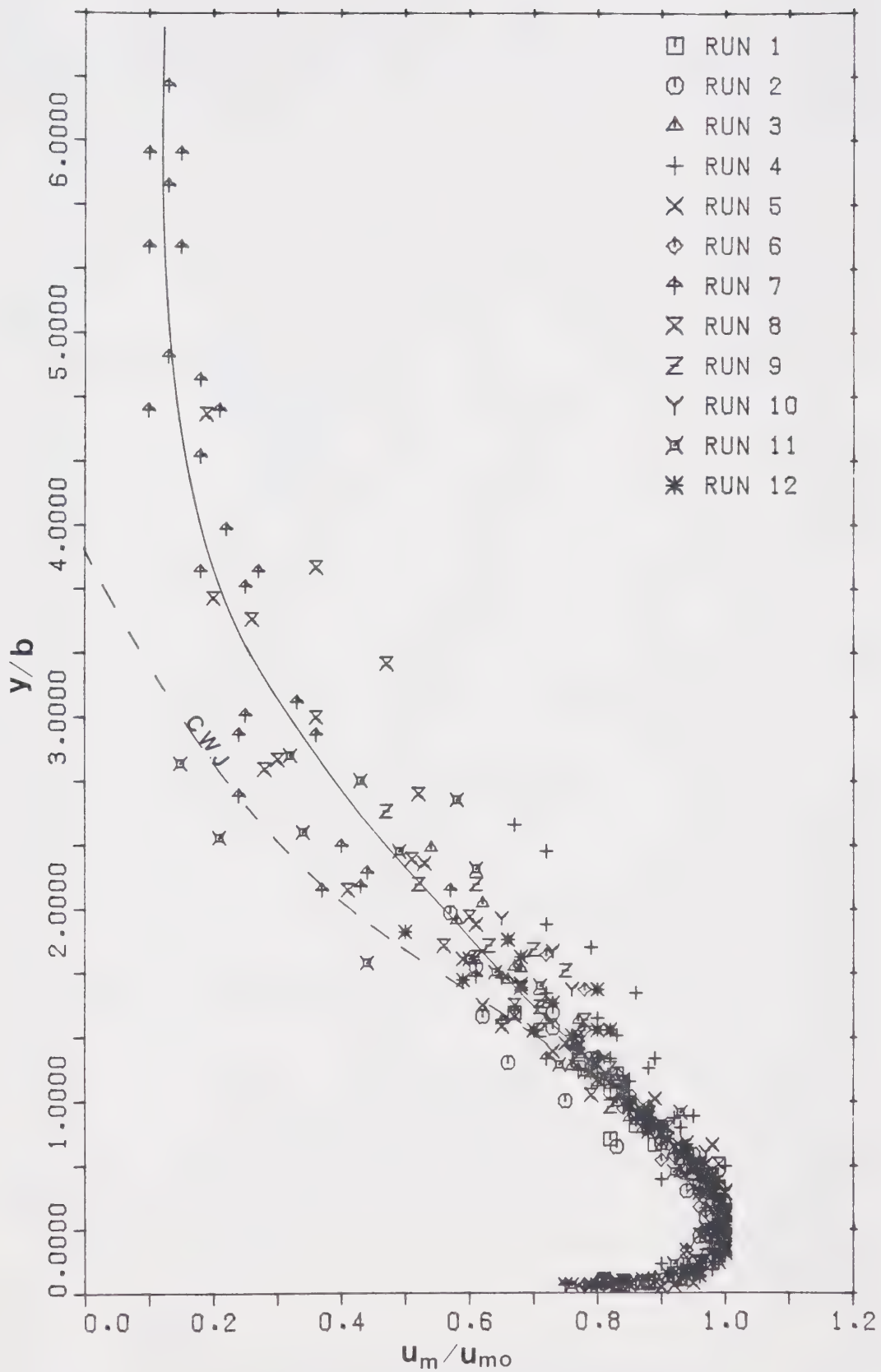


Figure 4.10 - Dimensionless vertical velocity profile  
for the bluff wall jet with finite tailwater depth





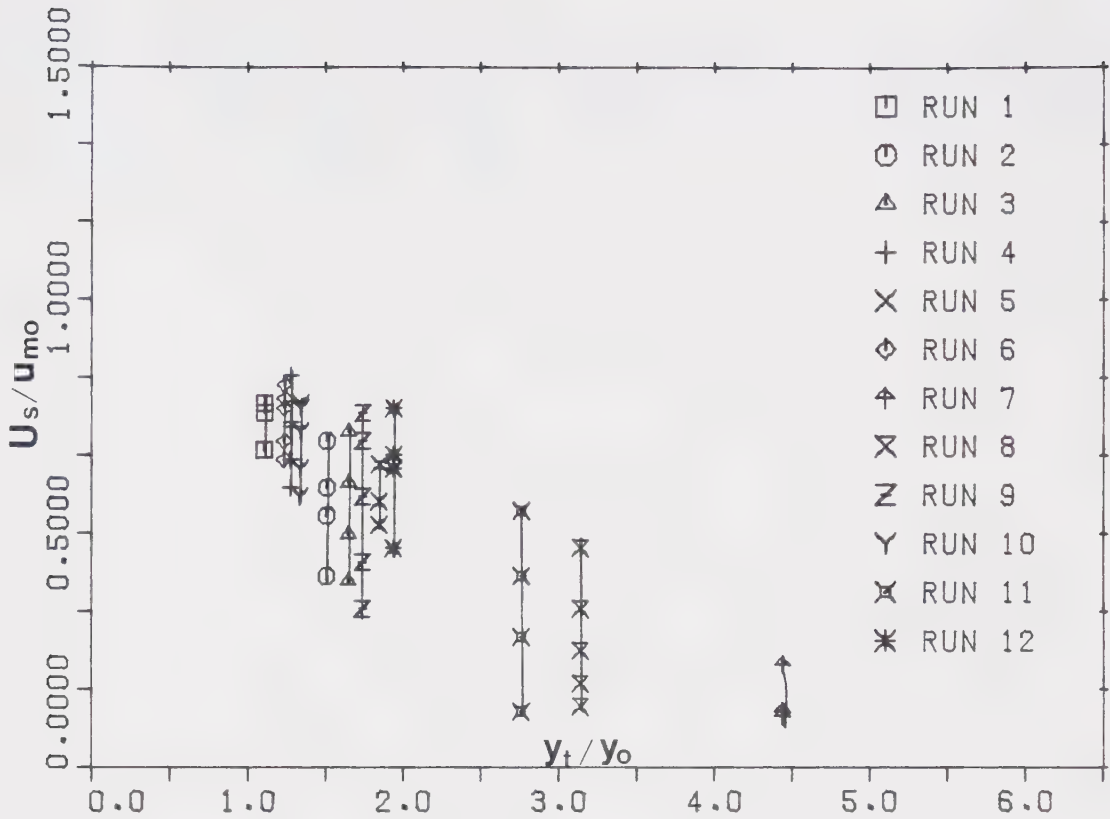


Figure 4.11 - Variation of centreline surface velocity

with tailwater depth for bluff nozzles

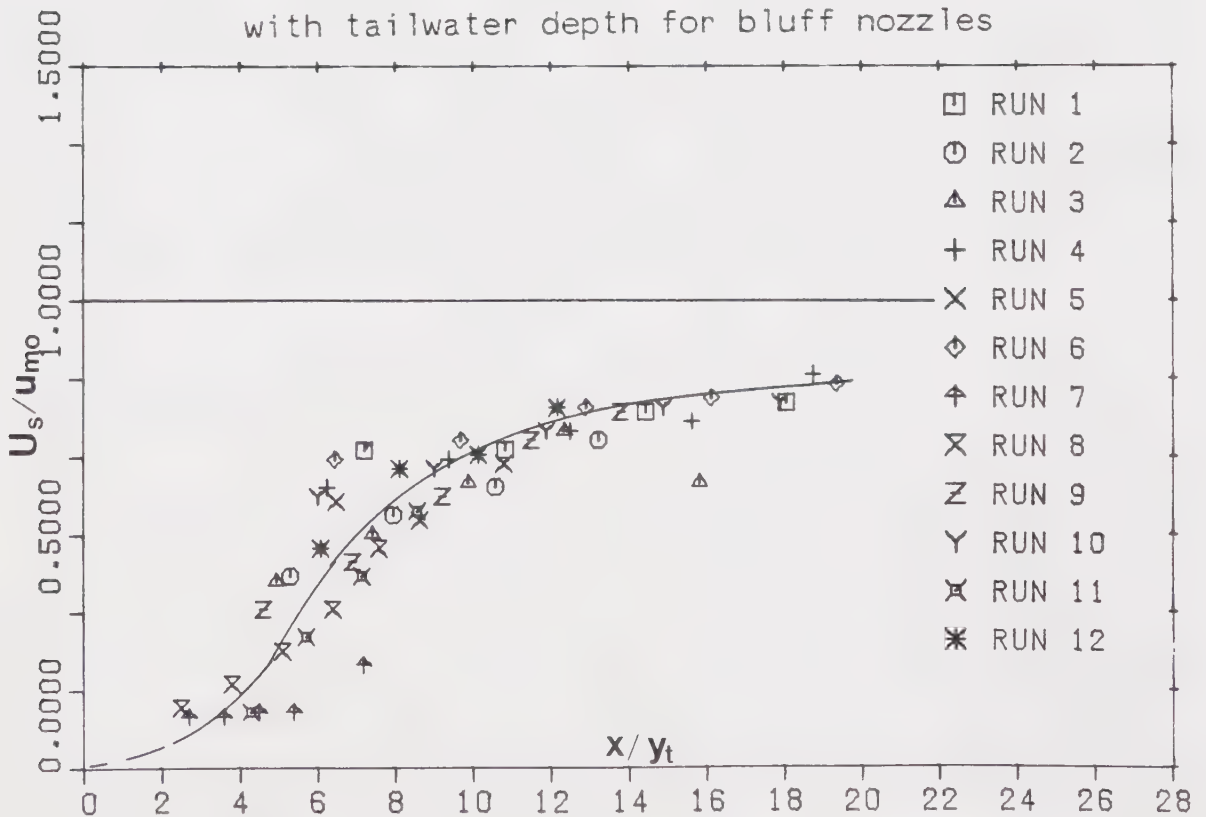


Figure 4.12 - Variation of centreline surface velocity

with tailwater and longitudinal distance



that the surface velocity,  $U_s$ , was dependent not only on the tailwater depth but also on the distance,  $x$ , downstream of the nozzle. It appeared that

$$\frac{U_s}{u_{m0}} = f_2 \left( \frac{x}{y_t} \right) \quad (4.2)$$

where  $f_2$  = a functional relationship.

When the above relationship was plotted, Figure 4.12, a correlation became evident and a single curve could be drawn through the values obtained from all the runs. For values of  $x/y_t$  less than approximately 3 the curve becomes undefined, this is because as the tailwater decreases the jet expansion into the tailwater, in the vertical plane, becomes greater and the surface acceleration is increased for a region close to the nozzle. Indeed for a  $y_t/y_o$  ratio approaching unity the expansion of the jet into the total tailwater depth becomes almost instantaneous.

### Velocity Decay

The maximum velocity at any section is the relevant velocity scale and it is important to be able to predict the maximum velocity at any position. Pani (1972) has shown that when  $\sqrt{A}$ , where  $A$  is the cross-sectional area of the nozzle, is used as the length scale all the maximum velocity decay curves for bluff nozzles collapse onto a single curve.



Theory also predicts that the maximum velocity is inversely proportional to the distance measured from the virtual origin. The virtual origin is a fictitious point at which the flow velocity approaches infinity in order that the conservation of momentum can be maintained from a point source.

In the present study when the decay of the maximum velocity was plotted, it was found that the length of the potential core varied with the tailwater depth. It was therefore necessary to shift the origin in the longitudinal direction to where the potential core vanished, ie where the velocity first begins to decay, Figure 4.13. When the velocity decay was plotted in a non-dimensional form, using the shifted origin, some interesting results were obtained. Although the observations exhibited some variation, it was found that the results for shallower tailwaters were located above the adjusted deeply submerged curve, thereby indicating that the velocity decay is less for shallow tailwaters. However for tailwater to nozzle depth ratios greater than approximately two the curve given by Pani (1972) is of adequately good fit. The various velocity decay curves are shown in Figure 4.14.

As noted earlier, the maximum velocity was predicted by theory in chapter 2 to be inversely proportional to the longitudinal distance but that the proportionality should change with the tailwater. Eq 2.38 stated



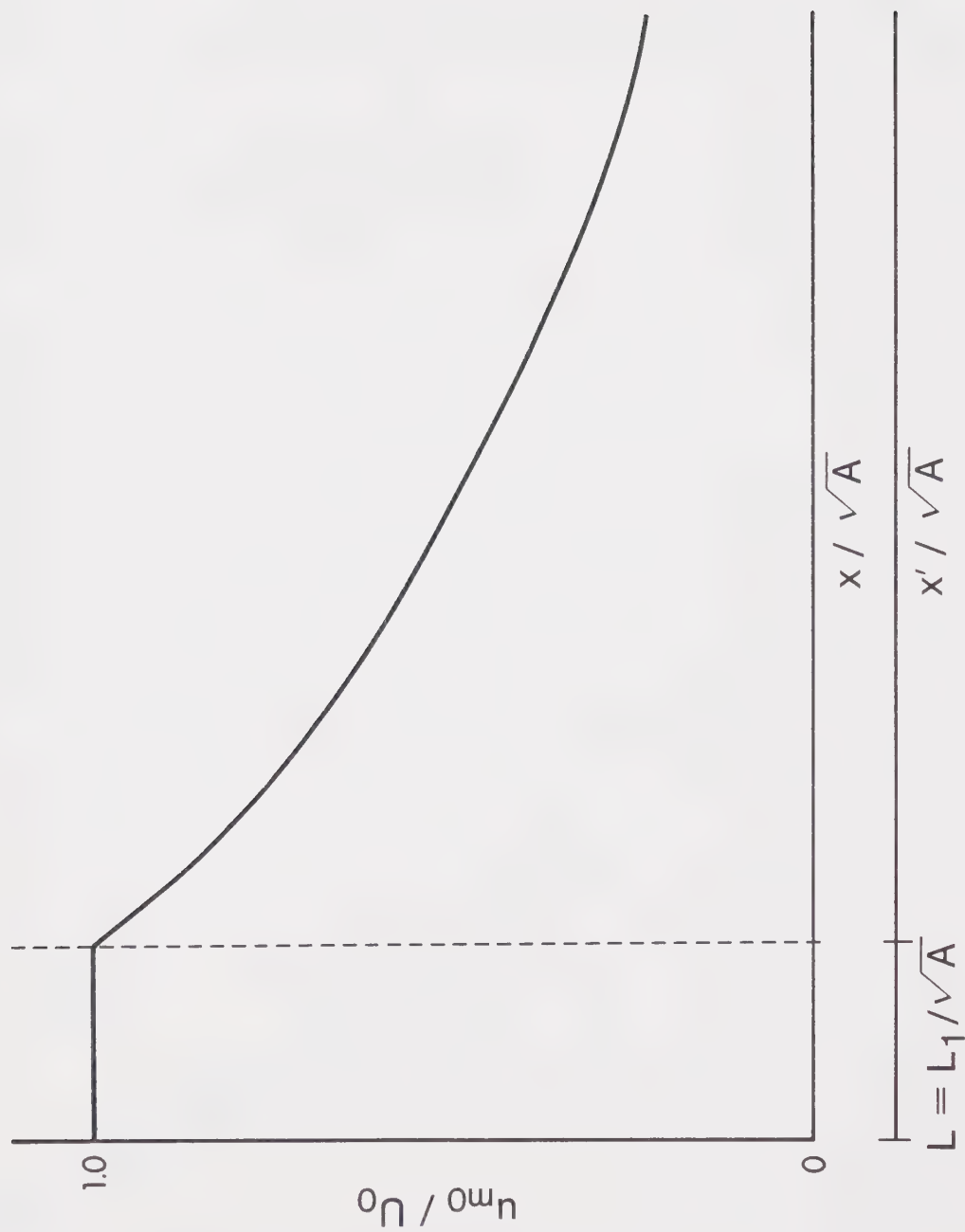
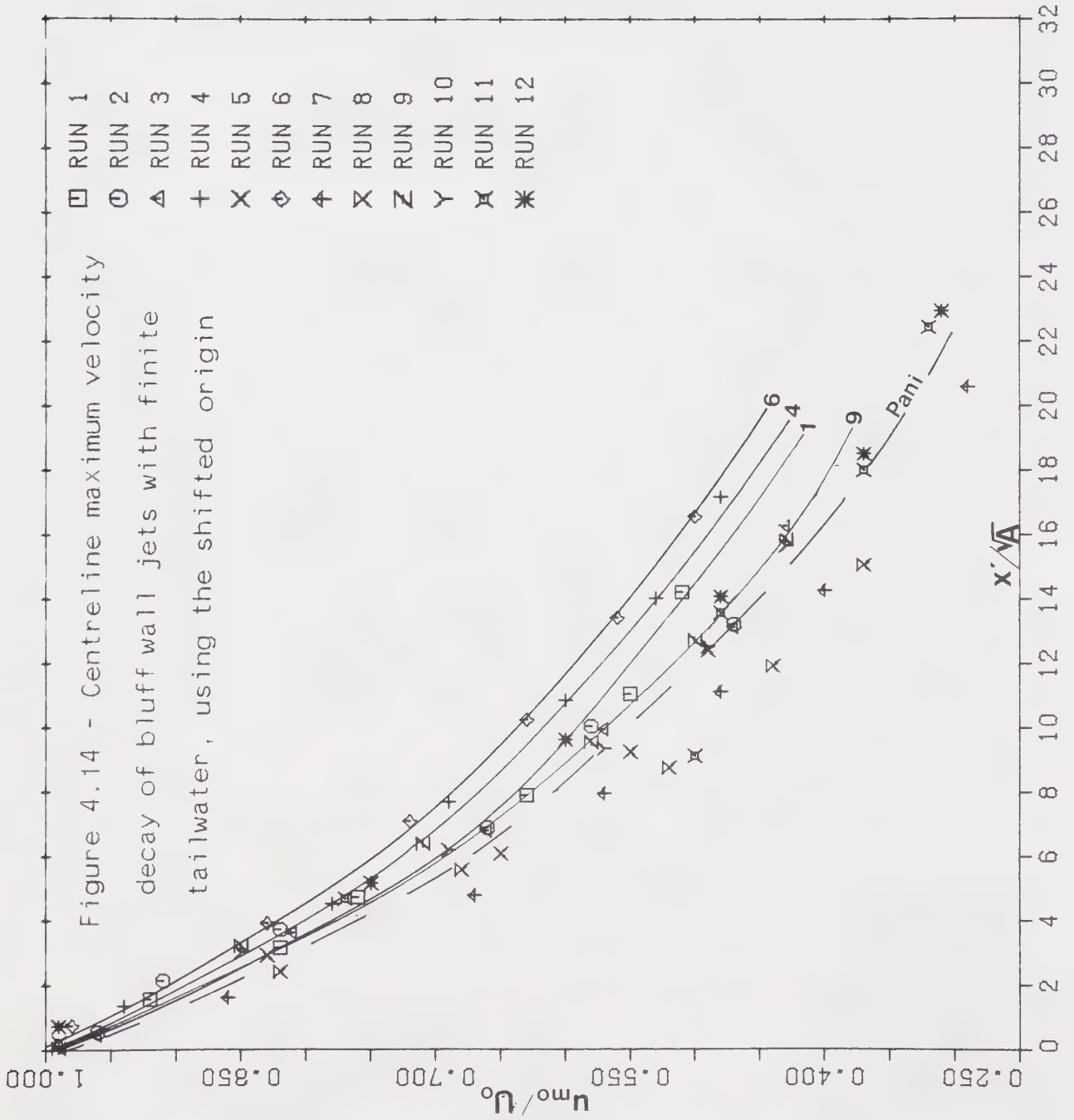


Figure 4.13. Definition sketch for velocity decay with shifted origin.









$$\frac{u_{mo}}{U_o} = \frac{C}{(\bar{x}/\sqrt{A})} \quad C = f_3\left(\frac{y_t}{y_o}\right)$$

defining  $x^*$  as the distance from the nozzle ( $x=0$ ) to the virtual origin, Eq 2.38 could be rewritten as

$$\frac{u_{mo}}{U_o} = \frac{C}{(x-x^*)/\sqrt{A}} \quad (4.3)$$

The asymptotic values given for Eq 4.3 are  $C=8.4$  and  $x^*/\sqrt{A} \approx 2.0$  (Pani, 1972). When  $U_o/u_{mo}$  vs  $x$  was plotted for each run (Appendix B) the curves were found to be linear. Correlating the calculated values for  $C$  and the distance to the virtual origin,  $x^*$ , with the variation of tailwater in non-dimensional forms produced very distinct trends, Figure 4.15 (a), (b), to which curves could be fitted easily. Both curves differ sharply from the asymptotic value for  $y_t/y_o$  ratios less than about two.

#### Length of potential core

As has been stated above and in chapter 1, as the tailwater decreased so did the length of the potential core. If the length of the core is denoted by the symbol  $L_1$ , then the dimensionless length,  $L$ , may be defined as

$$L = \frac{L_1}{\sqrt{A}} \quad (4.4)$$



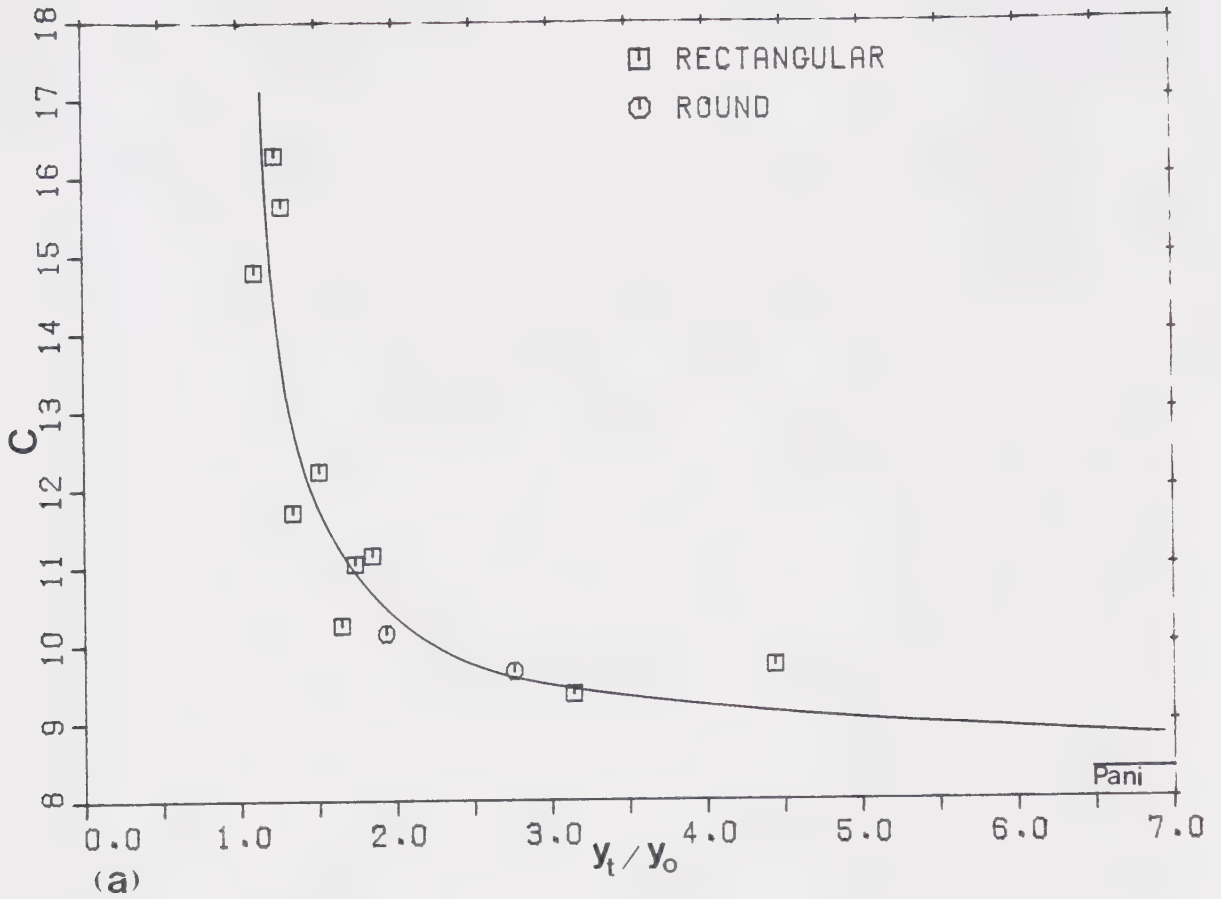
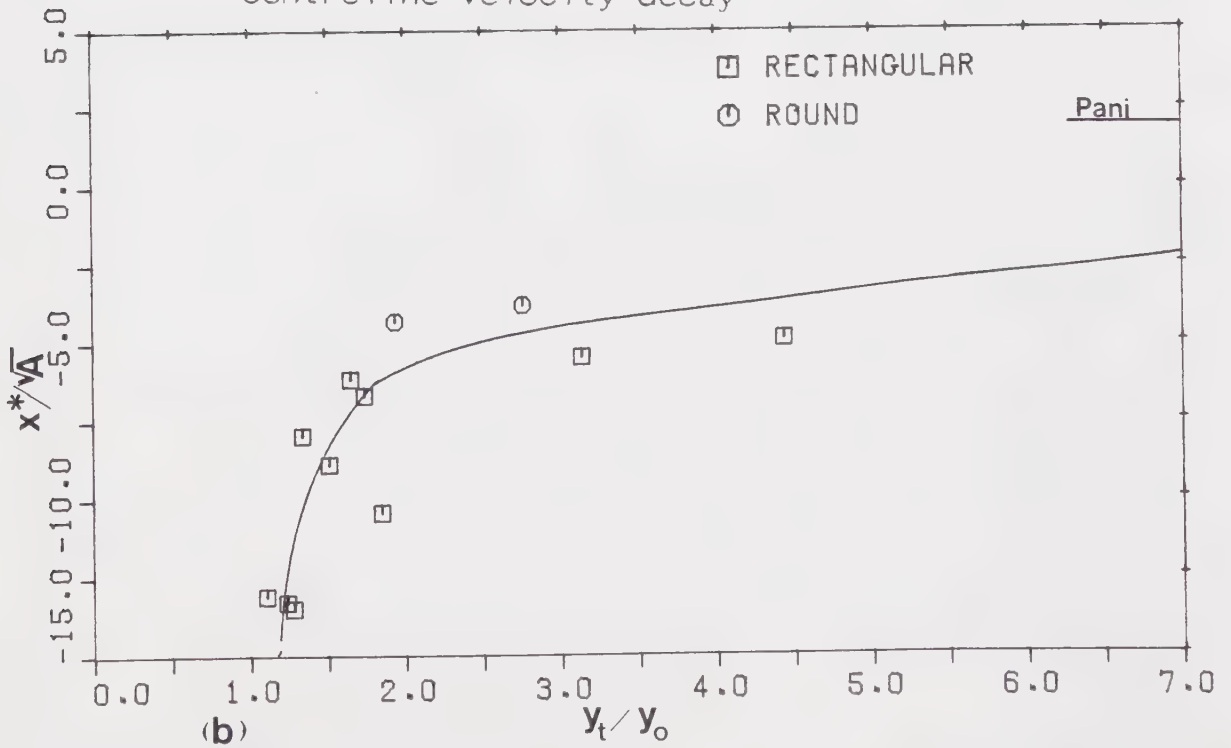


Figure 4.15 - Variation of a)  $C$  and b)  $x^*$ , for the centreline velocity decay





Pani (1972) found the non-dimensional length to be equal to 5.8. When the dimensionless lengths observed in the present study were compared with the variation of the tailwater to nozzle depth ratio (Figure 4.16), a single curve described the data extremely well.

### Vertical Length Scale

The theory in chapter 2 predicted that the length scales in both vertical and transverse directions should grow linearly in their respective directions, but that the growth of the scales will also depend on the tailwater depth. In the vertical plane an inconsistency immediately becomes obvious because of the finite tailwater, after a certain distance downstream from the nozzle, according to theory, the vertical length scale will be greater than the tailwater. This obviously is an impossibility and therefore it should be expected that the linearity of the growth of the length scale will break down before this condition occurs. This deviation from theory occurs when the jet enters a stage, termed in chapter 1, as the "uniform" flow transition zone.

For each run the growth of the length scale,  $b$ , was plotted against the longitudinal distance (in a suitable dimensionless form) and although the number of experimental





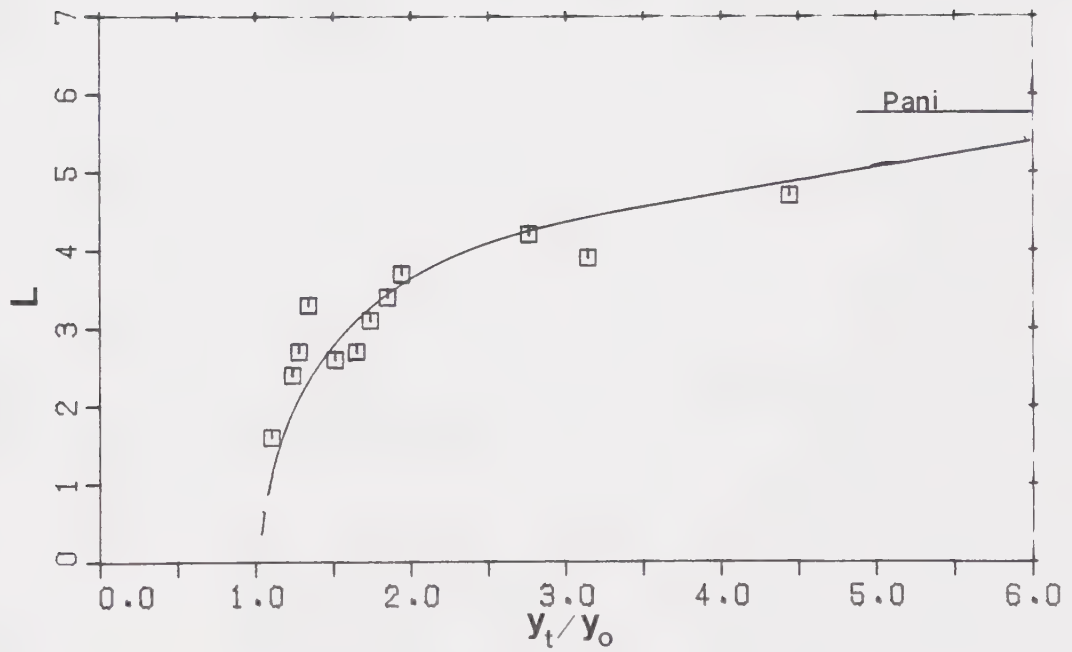


Figure 4.16 - Growth of non-dimensional potential core length with increasing tailwater



points for each graph was somewhat limited, it was possible to represent most plots by a straight line. Pani (1972) gives the equation of the growth of the vertical length scale as

$$\frac{b_y}{y_0} = 0.90 + 0.045 \frac{x}{y_0} \quad (4.5)$$

however the definition of the length scale,  $b$ , used in the present study is approximately  $0.588b_y$  and therefore Eq 4.5 becomes

$$\frac{b}{y_0} = 0.53 + 0.026 \frac{x}{y_0} \quad (4.6)$$

The general case of Eq 4.6, for when the tailwater becomes a finite depth can be represented as

$$\frac{b}{y_0} = \frac{\hat{b}}{y_0} + \frac{db}{dx} \frac{x}{y_0} \quad (4.7)$$

where  $\frac{db}{dx}$ =gradient of the linear growth in the length scale  
 $\hat{b}$ =the intersect on the  $y$  axis, when  $x=0$ , of the growth in the length scale and is related to the position of the virtual origin for  $b$ .

From the plots discussed above and given in Appendix B, it was possible to find a value of  $db/dx$  and  $\hat{b}/y_0$  for each



run. When these were plotted versus the tailwater to nozzle depth ratio,  $y_t/y_o$ , they exhibited a very clear trend that was easily described by a single curve (Figure 4.17 (a) and (b)). It is interesting to note how the curves differ markedly from the asymptotic values for  $y_t/y_o$  less than about two. This deviation agrees well with the observed increase in expansion, in the direction normal to the bed, of the jet discussed in chapter 1 and the shortening of the potential core. These observations can be explained by the occurrence of greater turbulent mixing near the nozzle for shallower tailwaters. It is also of interest that the virtual origin for the vertical length scale moves from being behind the nozzle to in front of the outlet.

## Transverse Velocity

### Typical velocity profile

It was shown in part I that the expansion of the jet in the transverse plane is severely affected by the tailwater conditions. However there appears to be no reason why the velocity distribution within the jet should be affected and, from observations made, this was found to be the case. The transverse velocity profile was measured at a height  $\delta$  from the bed for runs 7 to 12.  $\delta$  is the distance at which the maximum jet velocity occurs at the section in question, see Fig 4.8(b) for a



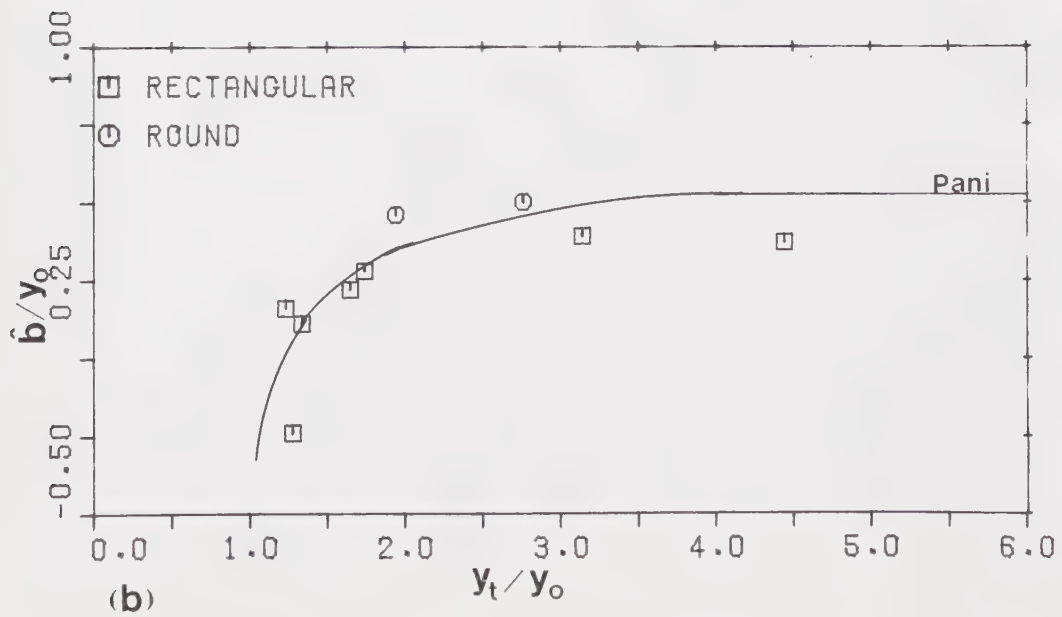
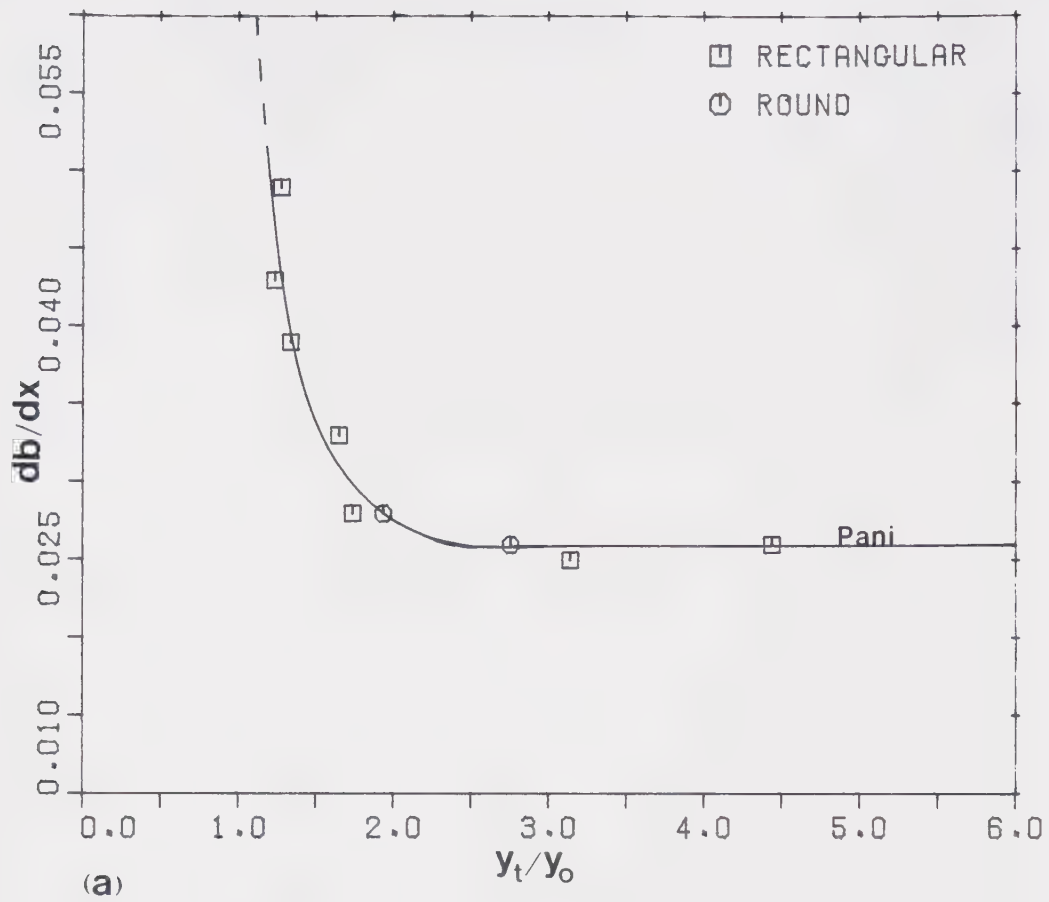


Figure 4.17 - Vertical length scale parameters a)Change in  $db/dx$  b)Change in  $\hat{b}/y_0$





definition sketch. The velocity profiles appeared to be of a very similar form to those obtained from studies on infinite tailwaters and a typical profile obtained in the present observations is shown in Figure 4.18. Exploratory velocity readings indicated that the jet was, within experimental error, symmetrical and therefore only measurements of one half were taken.

#### Dimensionless transverse velocity

Using the half length,  $b$ , defined as in chapter 2 and shown in the definition sketch Fig 4.8(b), as the length scale and using the maximum local velocity as the velocity scale, it was possible to reduce the transverse velocity profiles for each run into a single curve, providing the distance was approximately greater than eight times the nozzle height (Figure 4.19). Furthermore when the data points for every run were plotted together, it was found that they collapsed onto a single curve (Figure 4.20). This curve can be described quite well by the error function, which has been shown by analysis to describe the diffusion of laminar flow and has been found satisfactory in turbulent flow. The equation can be written as

$$\frac{u}{u_{m0}} = e^{-0.693(z/b_z)^2} \quad (4.8)$$



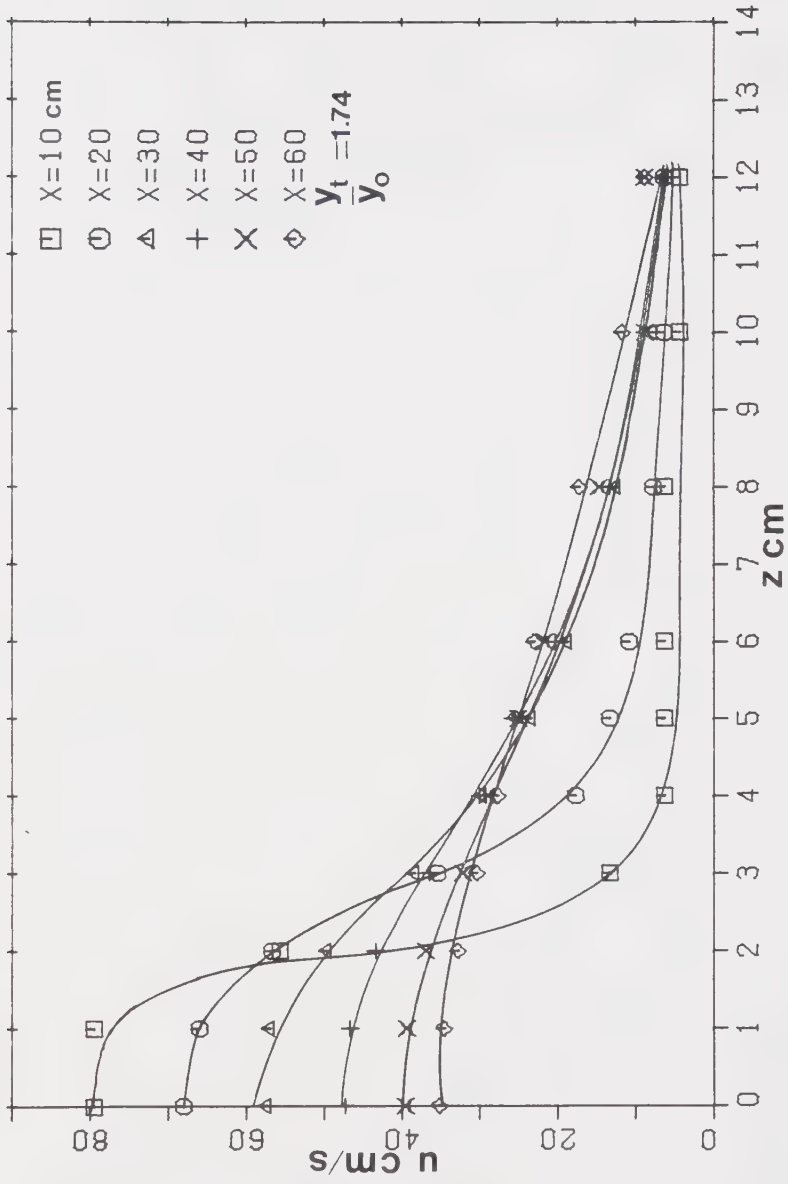


Figure 4.18 - Typical bluff wall jet transverse velocity profile



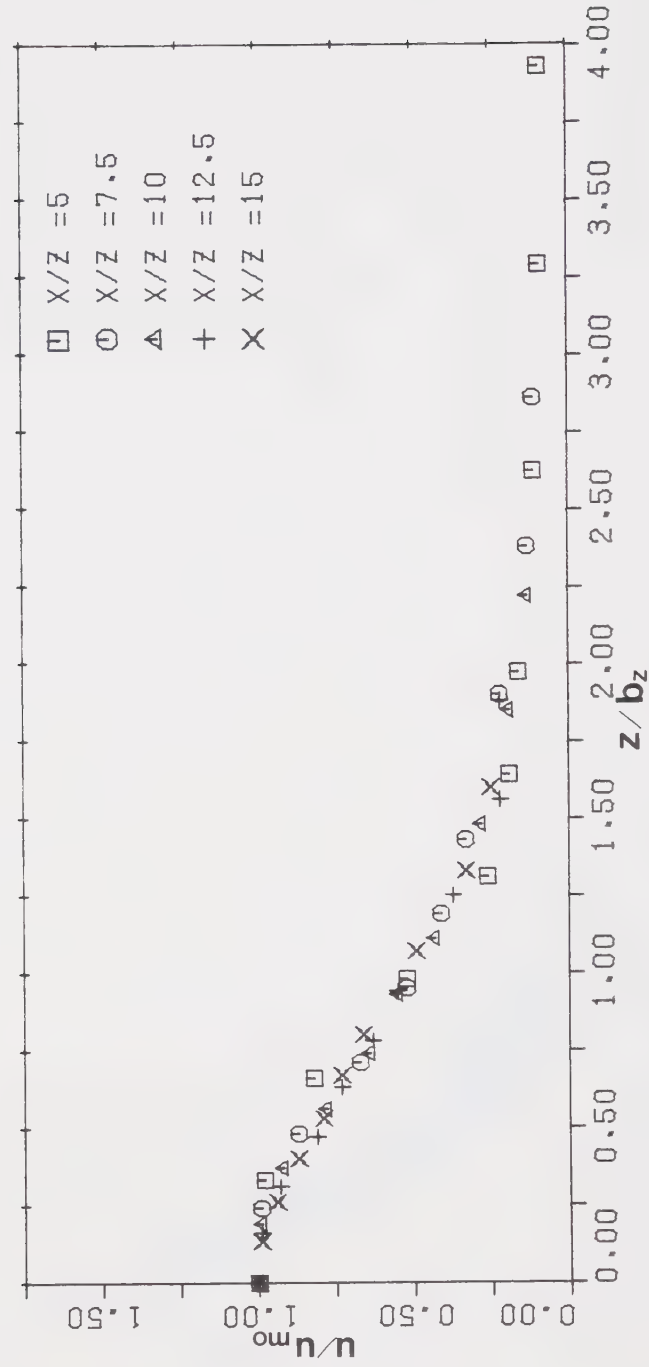


Figure 4.19 - Typical reduced transverse velocity  
profile for a bluff wall jet with finite tailwater  
depth



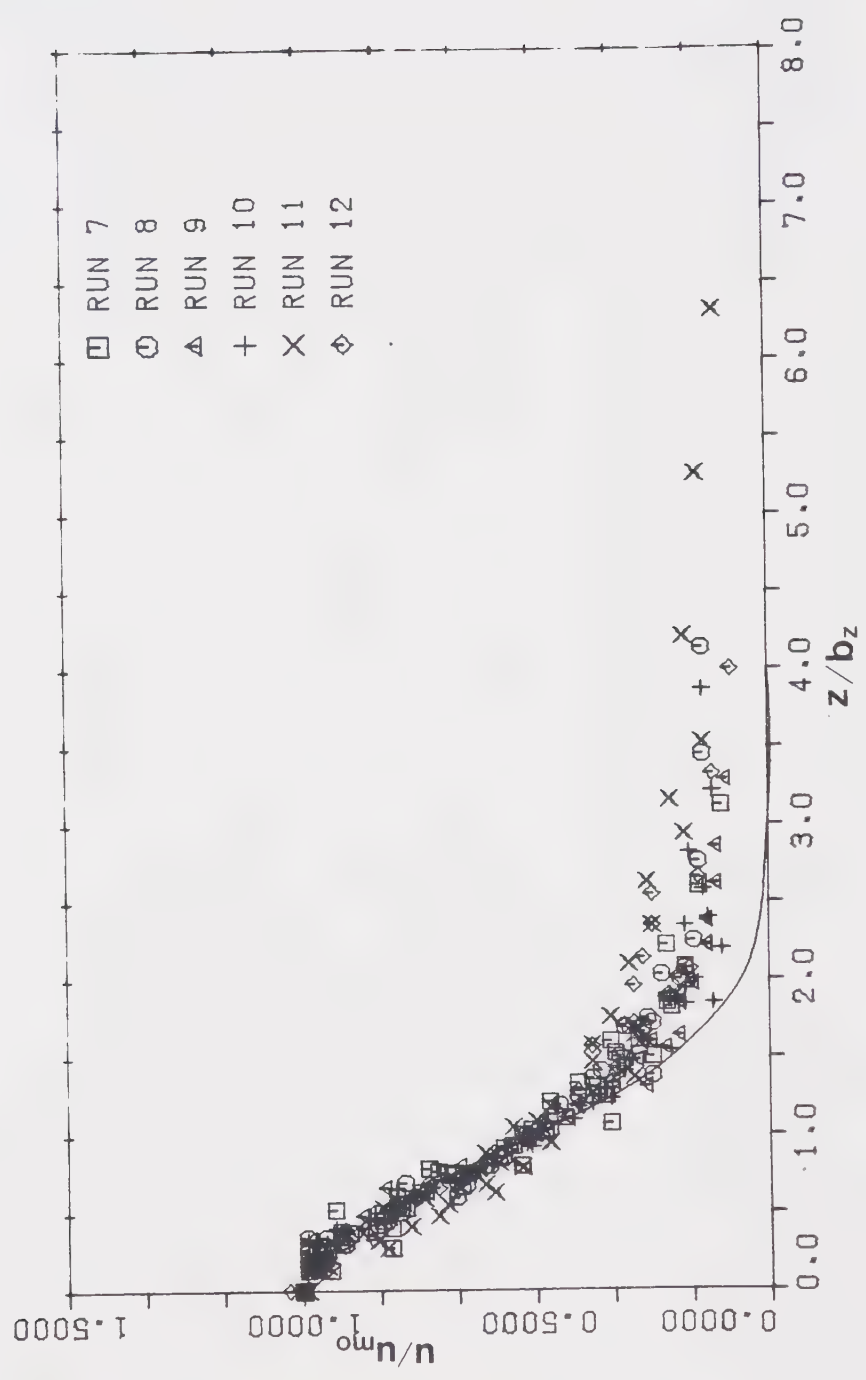


Figure 4.20 - Dimensionless transverse velocity profile  
for bluff wall jets with finite tailwater





It can be seen from Fig 4.20 that the data lie above the error function curve as the distance away from the jet centreline increases. This may be due to the inaccuracies caused by the velocity measuring apparatus, that was relatively insensitive to low velocities, as discussed in chapter 3. However it should be pointed out that this trait has also been observed by some other investigators (Pani, 1972 ; Newman et al., 1972 ; Chandrasekhara Swamy and Bandyopadhyay, 1975). It may be that this trend is the true profile in the transverse direction but measurements made with a sensitive instrument, capable of measuring the low velocities occurring at the edge of the jet , should be used to confirm these results. However the use of the error function curve to describe the transverse velocity profile is acceptable, providing it is recognised that the true profile may be just above the tailend of the curve. It should be noted that the value of the maximum velocity, used for the velocity scale, is equivalent to  $u_{mo}$  and the method of obtaining the value of  $u_{mo}$  , for any given longitudinal distance, has been discussed in detail in section on "Velocity Decay".

Length scale  $b_z$



Pani (1972) has shown that there is considerable difficulty in obtaining a general equation for the line representing the growth of the transverse length scale,  $b_z$ , for the case of an infinite tailwater but he did obtain an equation that fits the data reasonably well

$$\frac{b_z}{z_0} = 0.2 \frac{x}{z_0} - 1.25 \quad (4.9)$$

where  $z_0$  = width of the nozzle

For a varying tailwater Eq 4.9 can be written in a more general form

$$\frac{b_z}{z_0} = \frac{db_z}{dx} \frac{x}{z_0} + \frac{\hat{b}_z}{z_0} \quad (4.10)$$

where  $\hat{b}_z$  = the intersect of the  $z$  axis when  $x=0$

When  $b_z$  versus  $x$  was plotted in a non-dimensional form (Appendix B), the growth was found to be linear and the values for  $db_z/dx$  and  $\hat{b}_z/z_0$  were calculated for each run. Unfortunately there were only a few values for both the parameters. However the change in  $db_z/dx$  should be related to the expansion of the jet, investigated in part I. Using a factor of 2.50, as discussed in Part I, to reduce the curve given in Fig 4.6, it was found that the values of  $db_z/dx$  obtained lay above the curve but within the range of values shown in Fig 4.6. When a



value of 2.25 was used to reduce the curve, the data lay about it and are shown in Figure 4.21(a). For the variation of  $\hat{b}_z/z$  there was no additional information to enable the development of an accurate curve.

Therefore the line shown in Figure 4.21(b) is only a possibility for its true location but until more information becomes available it can be used as a first estimate.

### Centreline Bed Shear Stress

It was shown in chapter 2 that the bed shear stress,  $\tau_o$ , was a function of the Reynolds number. This factor brings added complications into any analysis and therefore the results presented here can only be regarded as a preliminary investigation of shear stress. The measurements made of the shear stress are presented in Appendix B. For runs 7 to 10 the Reynolds number is of the same order of magnitude and can therefore be regarded as a constant. Defining the local skin friction coefficient as

$$C_F = \frac{\tau_{mo}}{1/2 \rho u_{mo}^2} \quad (4.11)$$

and the coefficient of skin friction as

$$C_F' = \frac{\tau_{mo}}{1/2 \rho U_o^2} \quad (4.12)$$



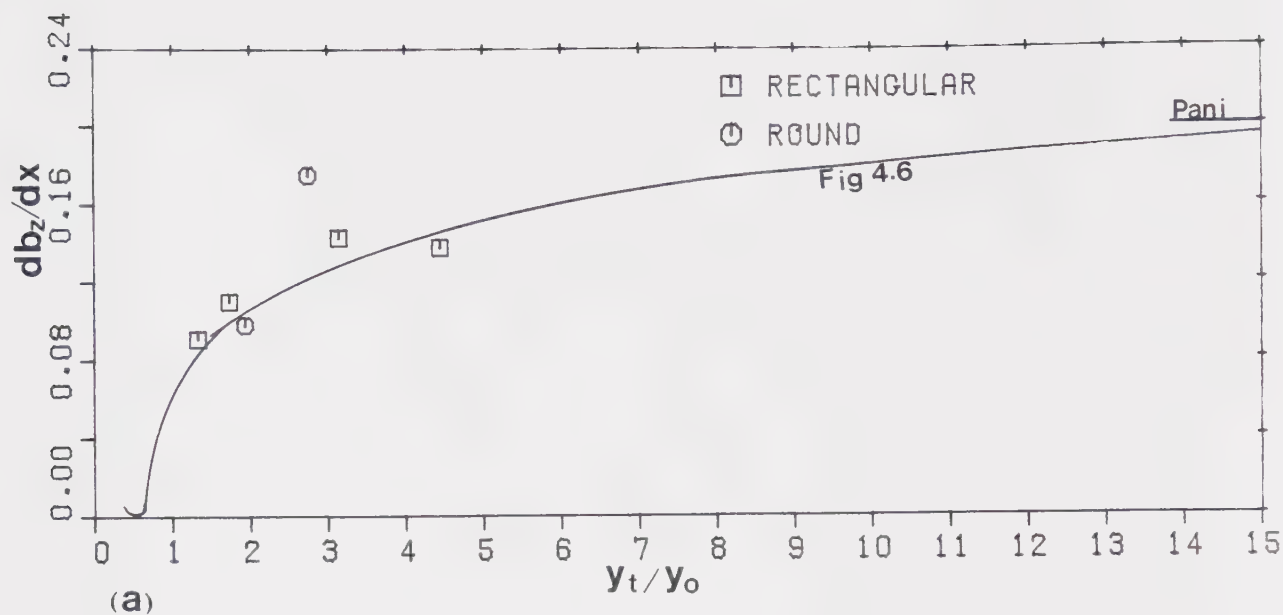
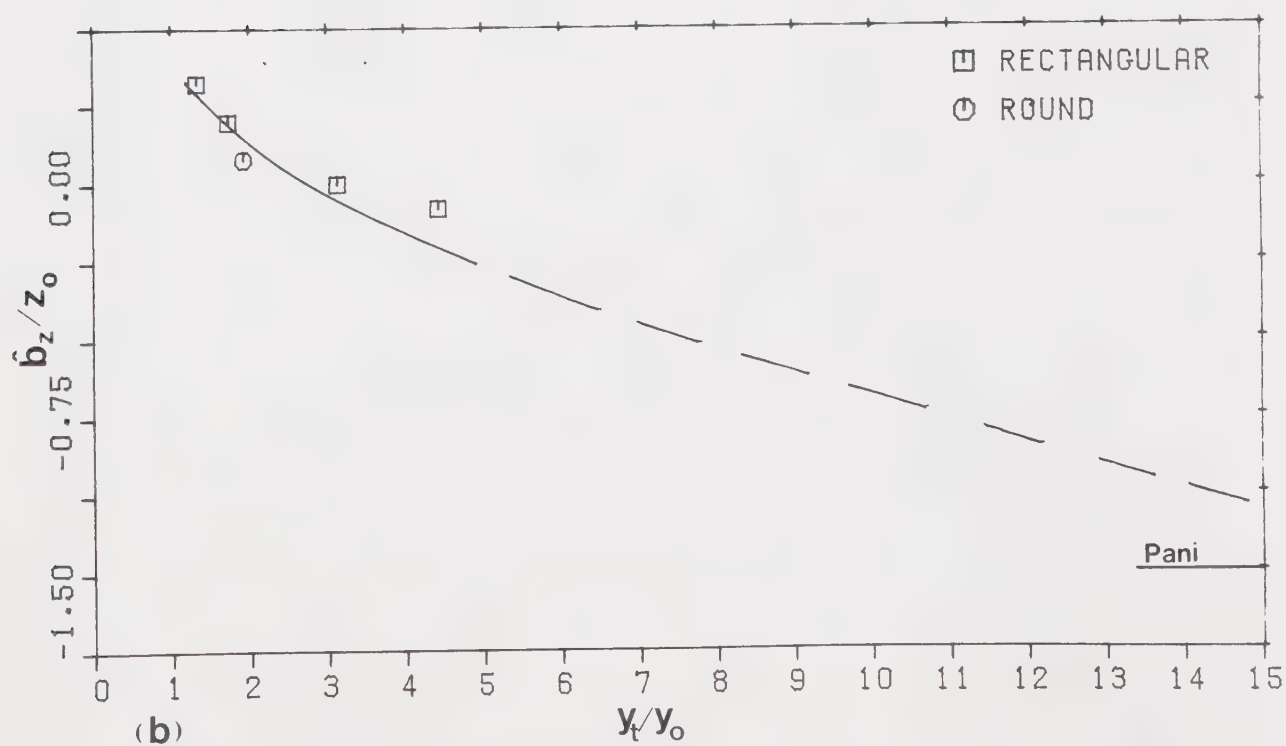


Figure 4.21 - Change in transverse length scale

parameters a) Variation of  $db_z/dx$  b) Variation of  $\hat{b}_z/z_0$ 





Some interesting observations can be made by plotting the coefficients in a suitable form. From Figure 4.22(a) it can be seen that for lower tailwater runs (6,10), the variation in the local coefficient,  $C_F$ , is not as significant as for the deeper runs (7,8). It is also interesting to note that close to the nozzle the coefficient is higher for the low tailwaters, indicating a greater shear stress and therefore greater turbulence, which agrees with the observation of a shorter potential core. Figure 4.22(b) shows a more convenient plot as it avoids the necessity of finding the local maximum velocity. This plot shows that the centreline bed shear stress decays more slowly as the tailwater is reduced, this again agrees with the results of the investigation into the velocity decay. The results obtained from runs 7 to 10 lie well above the curve given by Pani(1972) but this is due to the much larger Reynolds numbers used in Pani's work. The Reynolds numbers in runs 11 and 12 are of similar order to those of Pani(1972) and it can be seen on Fig 4.22(b) that the coefficients of skin friction are in the same range as those obtained by Pani, however the shear stress decay is still less than the infinite tailwater case.

Dimensional predictions indicate that the shear stress should be inversely proportional to the square of the



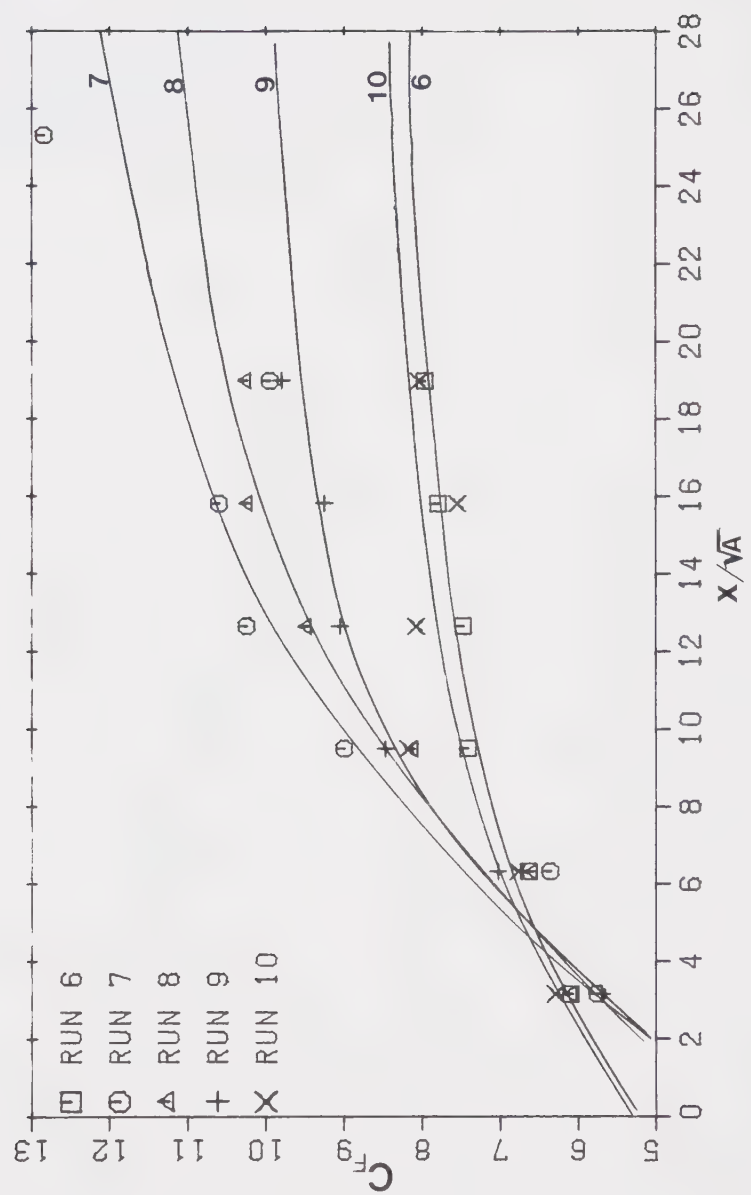
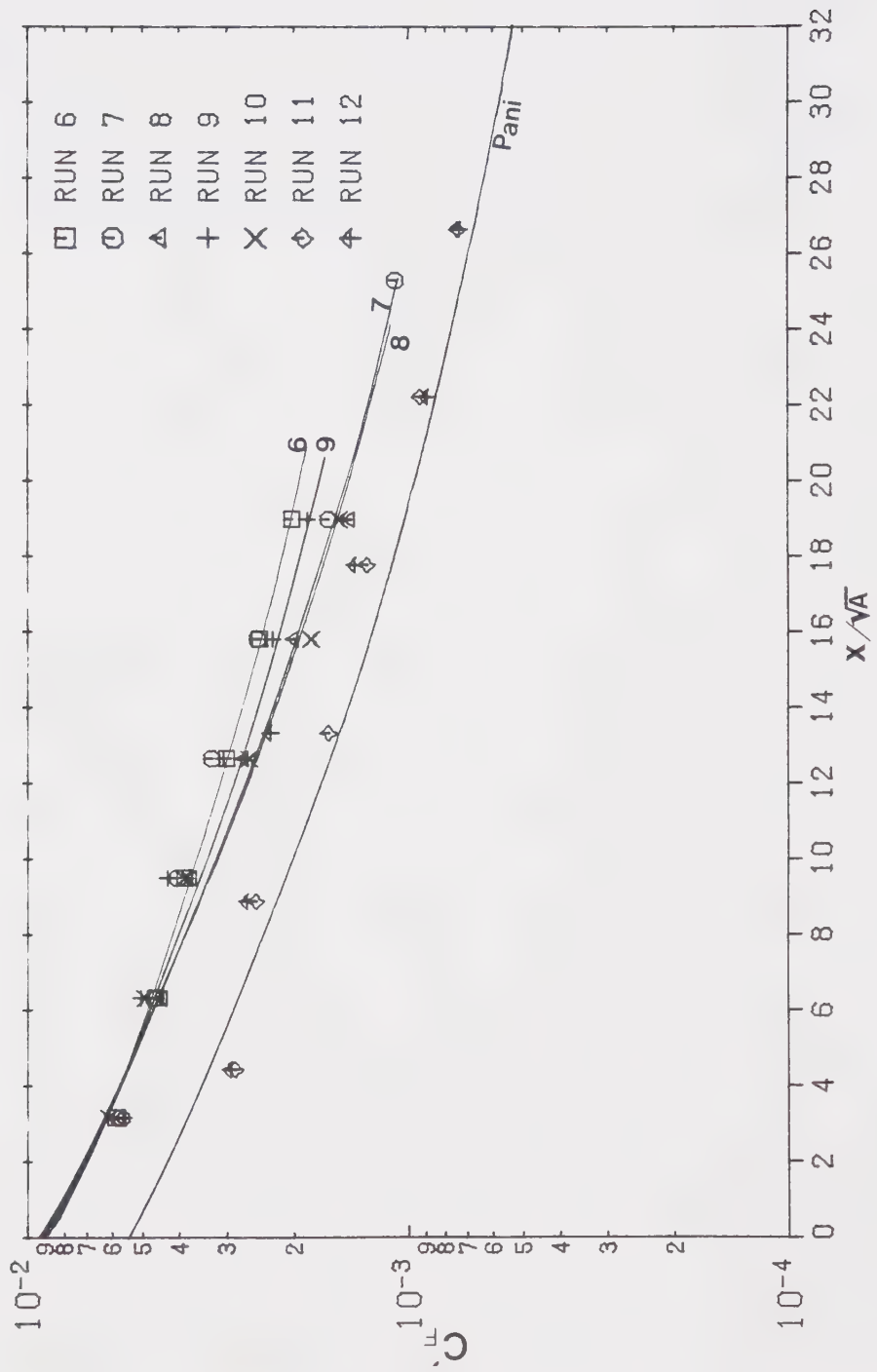


Figure 4.22 - a)Variation of  $C_F$  with longitudinal downstream distance





b) Variation of  $C_F$  with longitudinal downstream distance



longitudinal distance. In an attempt to predict the variation of shear stress decay along the centreline with different tailwater depths, the ratio of the initial shear stress to the local shear stress ( $\tau_{0,0}/\tau_{mo}$ ) was plotted against the square of the distance ( $x^2$ ). Although these relationships were linear, as predicted, when attempts (similar to those for the velocity decay) were made to relate the variations in slope and virtual origin to the change in tailwater depth no correlation was apparent. The results of the attempt are presented in Appendix B.

### Transverse Shear Stress

An elementary study of the transverse shear stress was made but some useful results can be obtained from the measurements. When the shear stress profiles were plotted they appeared very similar to the velocity profiles discussed earlier. Defining the half length,  $b^*$ , as the distance from the central axis to where the shear stress is reduced by half and using the maximum local shear stress as the shear stress scale, it was possible to reduce all the measured profiles onto one dimensionless curve. Therefore the shear stress profiles can be said to be similar. As before, with the similar transverse velocities, the error function defined by Eq 4.8 but now rewritten as

$$\frac{\tau_0}{\tau_{mo}} = e^{-0.693(z/b^*)^2} \quad (4.13)$$





describes the curve well. In this case the data lie only slightly above the error function curve for distances removed from the central axis. Figure 4.23(a) and (b) show a typical transverse shear stress profile, while Figure 4.24 shows the collapsed similar profile.

Length scale  $b^*$

Approaching the length scale in a similar manner to the analysis adopted for the velocity length scale,  $b^*$  was plotted against  $x$  in a convenient non-dimensional form. Although the number of points for each graph was very limited, it could be said that the plots appeared linear. Writing the equation of the line as

$$\frac{b^*}{z_0} = \frac{\hat{b}^*}{z_0} + \frac{db^*}{dx} \frac{x}{z_0} \quad (4.14)$$

where  $\frac{db^*}{dx}$  = gradient

$\hat{b}^*$  = intersect of line on the  $z$  axis

It was possible to obtain estimates for the values of  $db^*/dx$  and  $\hat{b}^*/z_0$  for each run. Pani (1972) gave the approximate values for infinite tailwater as  $db^*/dx = 0.09$  and  $\hat{b}^* = 0$ . When the data is correlated with the tailwater to nozzle height ratio the trends become apparent. For



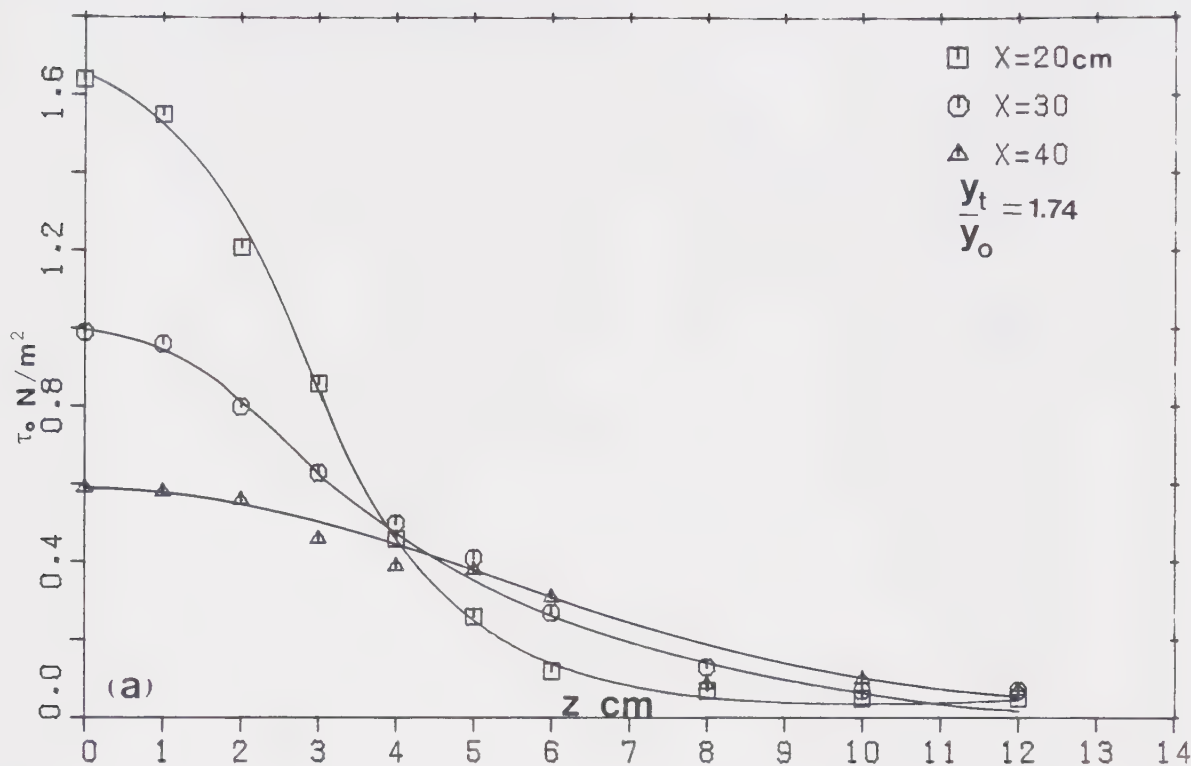
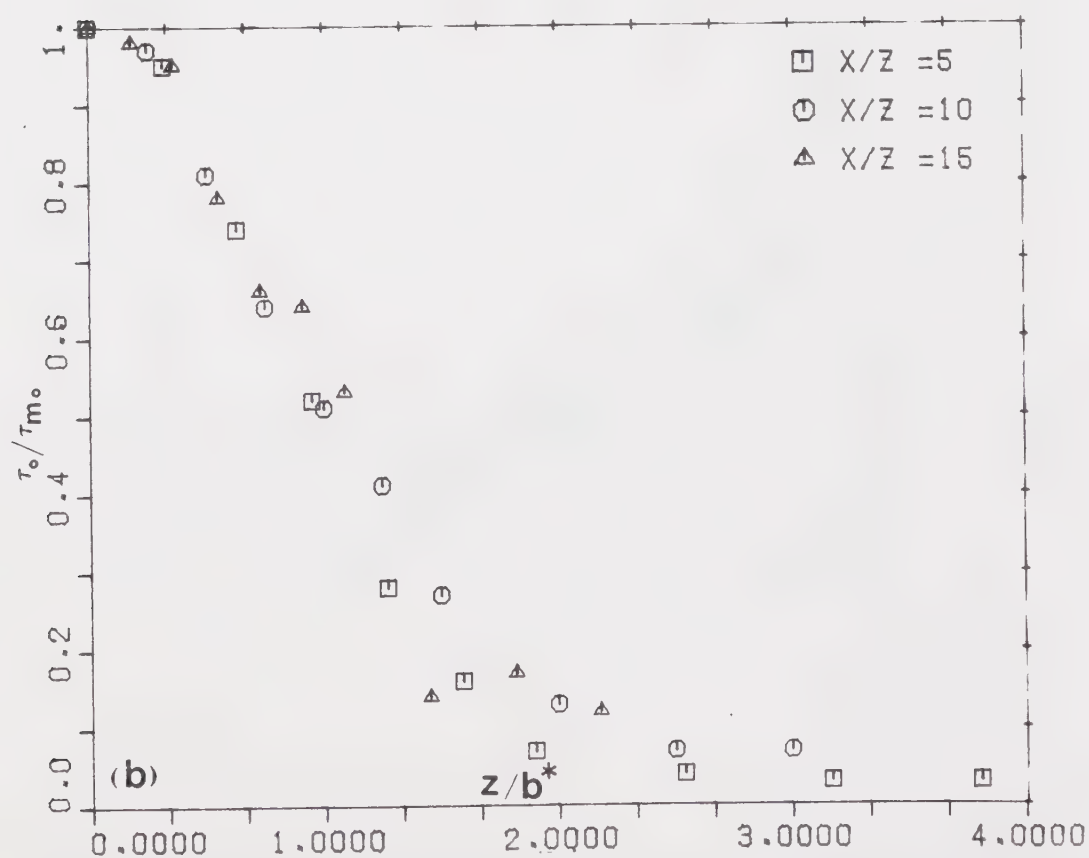


Figure 4.23 - a) Typical transverse shear stress profile for a bluff wall jet with finite tailwater depth



b) Typical reduced transverse shear stress profile



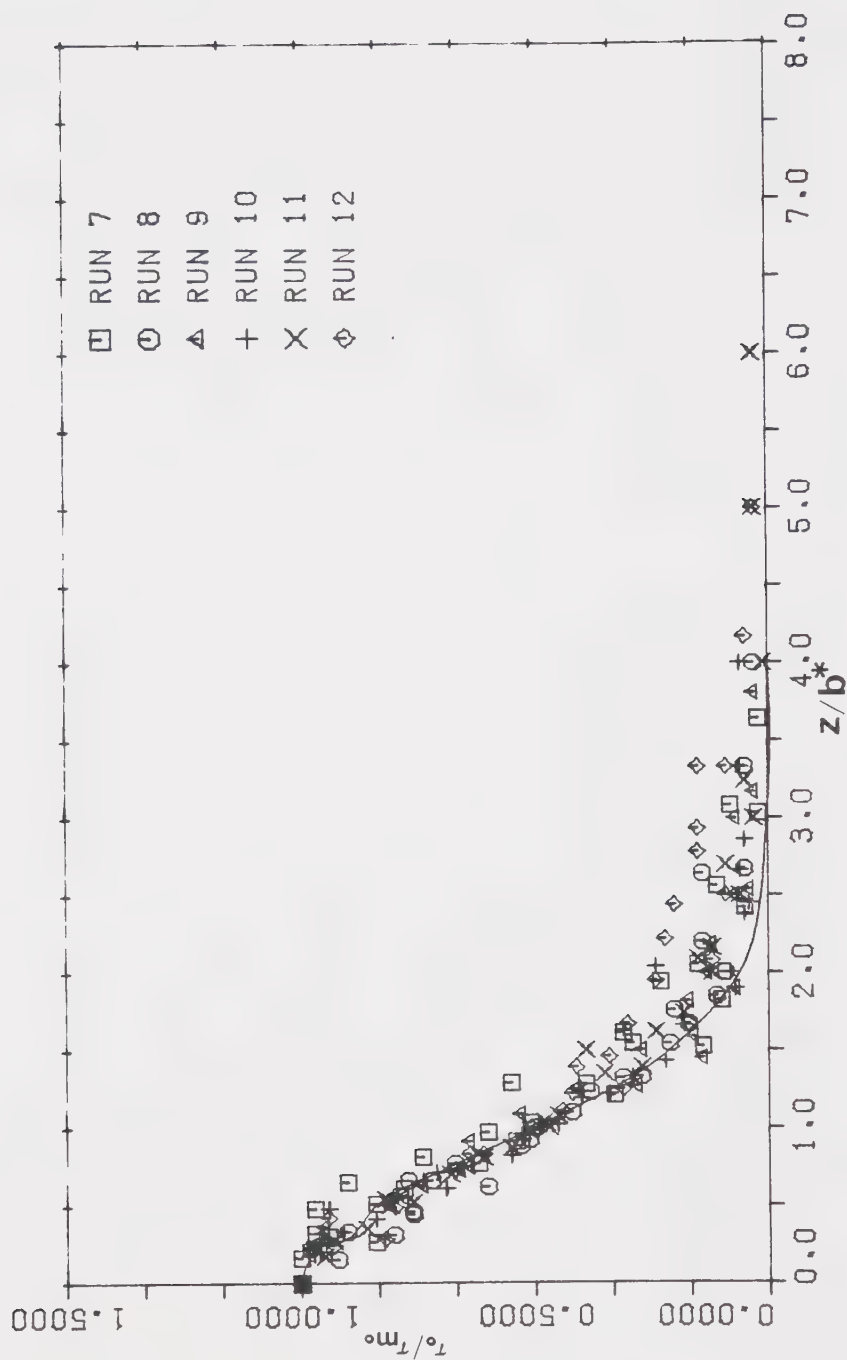


Figure 4.24 - Transverse shear stress similarity



the variation of the gradient, the correlation to the change in tailwater is quite good and a single curve can be drawn with some confidence. Unfortunately the variation of  $b^*/z_0$  with the tailwater is not so well defined, although a trend is obvious and a curve can be drawn that will serve as a useful first estimate. Figure 4.25(a) and (b) show the two relationships. As discussed earlier the variation of the shear stress length scale,  $\tau_{mo}$ , has not been successfully found.

## Summary

From experimental observations of bluff wall jets, it has been found that both the vertical and transverse velocity profiles are similar. It was also found that the transverse velocity profile agreed fairly closely with the error function curve. The length of the potential core was affected by the tailwater depth and the variation was plotted in a convenient form. If adjustment was made for the potential core length, it was found that the centreline velocity decayed at a slower rate for shallower tailwaters. The maximum velocity decay was found to be inversely proportional to the distance measured from the virtual origin. The change in the velocity decay rate and the change in the position of the virtual origin due to the change in tailwater depth was presented in a convenient form. The length scales for both the vertical and the transverse





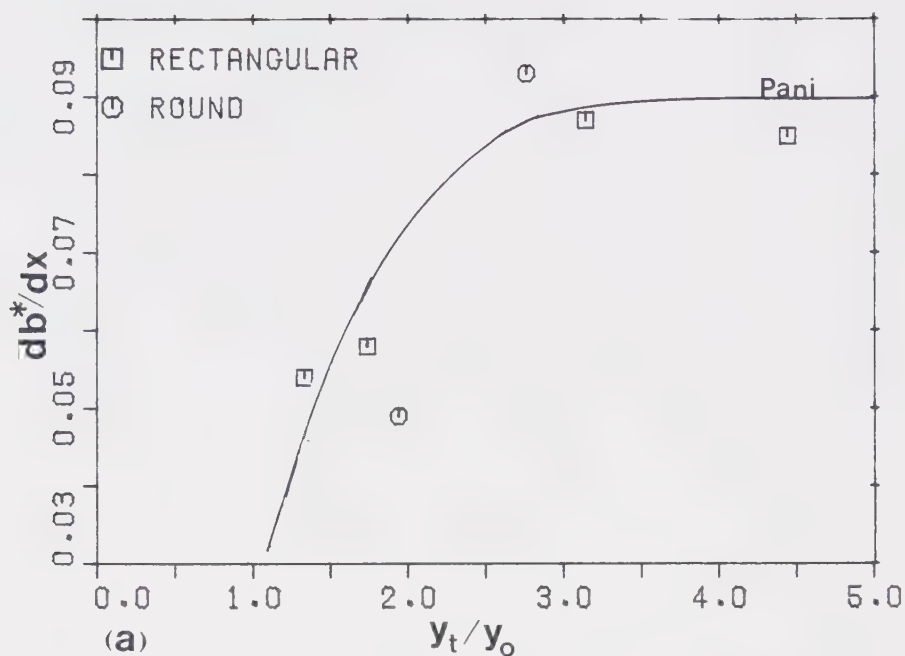
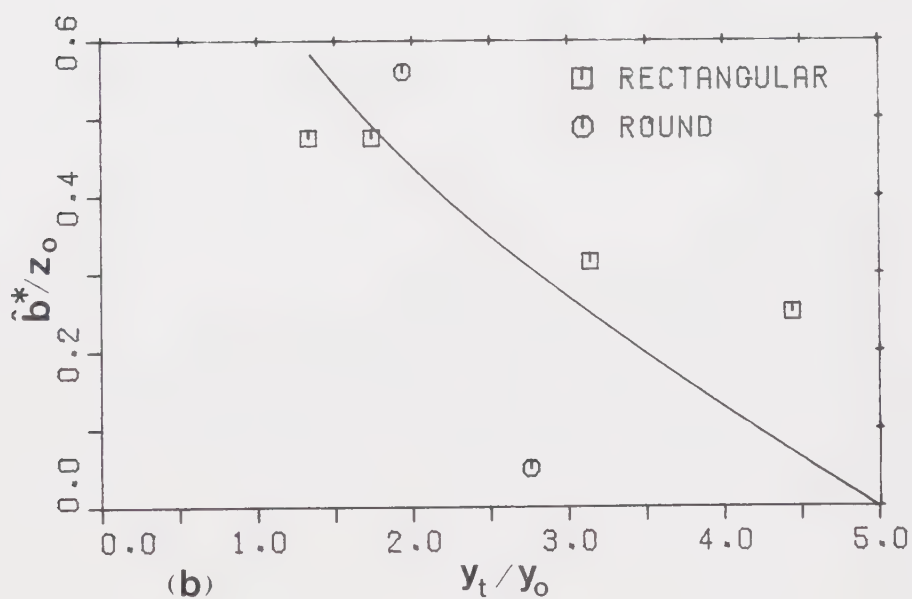


Figure 4.25 - a) Variation of transverse shear stress length scale gradient b) Variation of transverse shear stress of length scale intercept





velocity profiles were found to be linear and dependent on the tailwater. The equations of both lines were correlated to the tailwater depth. A preliminary investigation of the shear stress indicated that the centreline shear stress decay was reduced as the tailwater depth became smaller and that the transverse shear stress profile was similar. The shear stress length scale in the transverse direction was shown to be linear and that the equation of the line was dependent on the tailwater depth.



## C. PART III EROSION STUDIES

### Introduction

This section presents the results of a preliminary study made investigating the effects on the three dimensional wall jet with a finite tailwater when the bed is allowed to scour. The shape of the scour hole is investigated and shown to be similar.

### Review of Existing Work

Rajaratnam and Berry (1977) carried out studies of the erosion caused by circular turbulent wall jets on the beds of loose sand and polystyrene particles. The experiments were conducted in both air and water, and had an infinite tailwater. Rajaratnam and Diebel (1981) extended this work to turbulent circular wall jets with low tailwater and/or narrow channel width. The results obtained indicated that the erosion in air behaved somewhat differently than the erosion in water. It was also shown that the scour hole could be collapsed onto a single curve provided the correct scales were used, however the observations indicated that the deposition ridge needed different scales in order to obtain similarity. Rajaratnam and Berry (1977) defined two states of scour, the evolution and the asymptotic states but that in both states the scours were similar and that the



length scales were the maximum depth of scour and the longitudinal distance to the point of maximum scour. Rajaratnam and Macdougall (1981) investigated the erosion caused by plane turbulent water wall jets with minimum tailwater and were also able to show that the scour hole profiles was similar. In all the studies mentioned the particle size mean diameter was of the order of 1mm.

## Experiments

A series of nine runs were made in the lake model described in chapter 3. Each experiment was allowed to run for a considerable length of time, at least 18hrs and occasionally for 56hrs in order to ensure that the asymptotic state was reached. The tailwater depth remained constant for all the runs, at a depth of 3.1cm but the outlet velocity was varied from 8.88cm/s to a maximum of 40.4cm/s. The important flow parameters are given in table 4.3.

A photographic study was made of the jet expansion and the centreline scour hole profile was measured.

## Results and Analysis

### Photographic observations





Table 4.3 Important Flow Parameters

Run	$U_o$ cm/s	$y_t$ cm	$y_o$ cm	$z_o$ cm	$F_o$	$Re = U_o y_o / \nu$
S2	23.2	3.1	3.47	5.0	0.40	9,440
S3	18.8	3.1	3.38	5.0	0.33	7,550
S4	8.88	3.1	3.38	5.0	0.15	3,566
S5	33.2	3.1	3.51	5.0	0.57	13,588
S6	15.9	3.1	3.41	5.0	0.275	6,414
S7	18.0	3.1	3.38	5.0	0.31	7,229
S8	28.7	3.1	3.53	5.0	0.49	11,527
S9	40.4	3.1	3.59	5.0	0.68	16,721



From the photographs obtained it was possible to measure the jet expansion. Qualitatively it may be said that when the jet enters the scour hole a great deal of turbulence occurs and the jet loses momentum. The jet then spills out over and around the region of the deposition of scoured material and appears, in most cases, to expand linearly. Plates 4.13 and 4.14 show two runs, one of very little scour and the other with considerable scour. It may be possible that the expansion of the jet, after leaving the scour hole, could be analysed as a slender wall jet with a shallow tailwater but because there appears to be no information available on the jet expansion for slender wall jets with a shallow tailwater and because the observations presented here are limited, no attempt is made at predicting the expansion (refer to Appendix C for plots and details of data).

### Scour hole study

Referring to Figure 4.26 for the definition of the symbols used, the centreline asymptotic scour hole profile was measured and the results presented in Figure 4.27. The asymptotic or end state is virtually a steady state, although there are occasional bursts of turbulence within the scour hole. From Fig 4.27 it can be seen that the scour holes appear to be of a similar





Plate 4.14 - Run S8



Plate 4.13 - Run S4



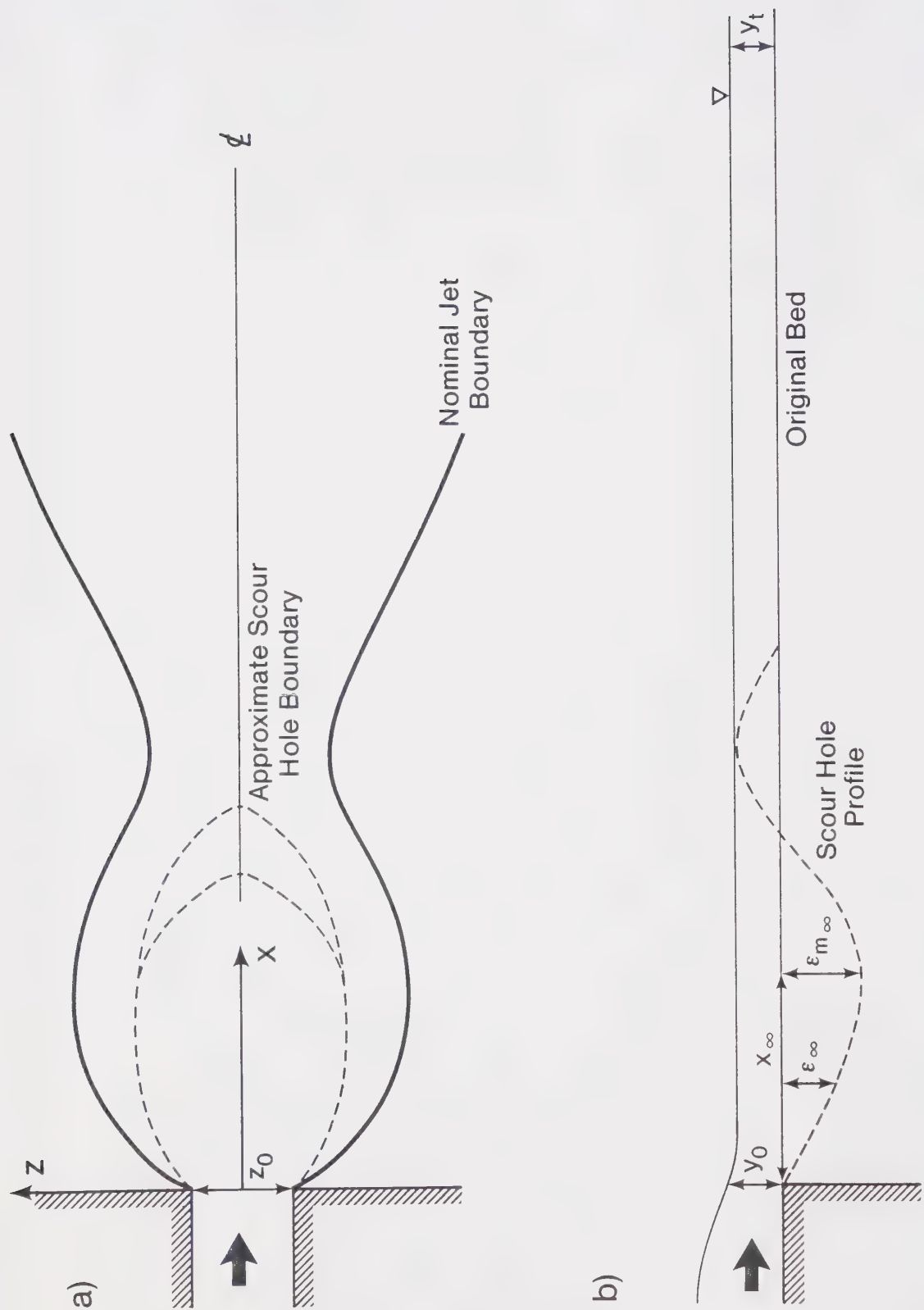


Figure 4.26. Definition sketch a) plan b) section





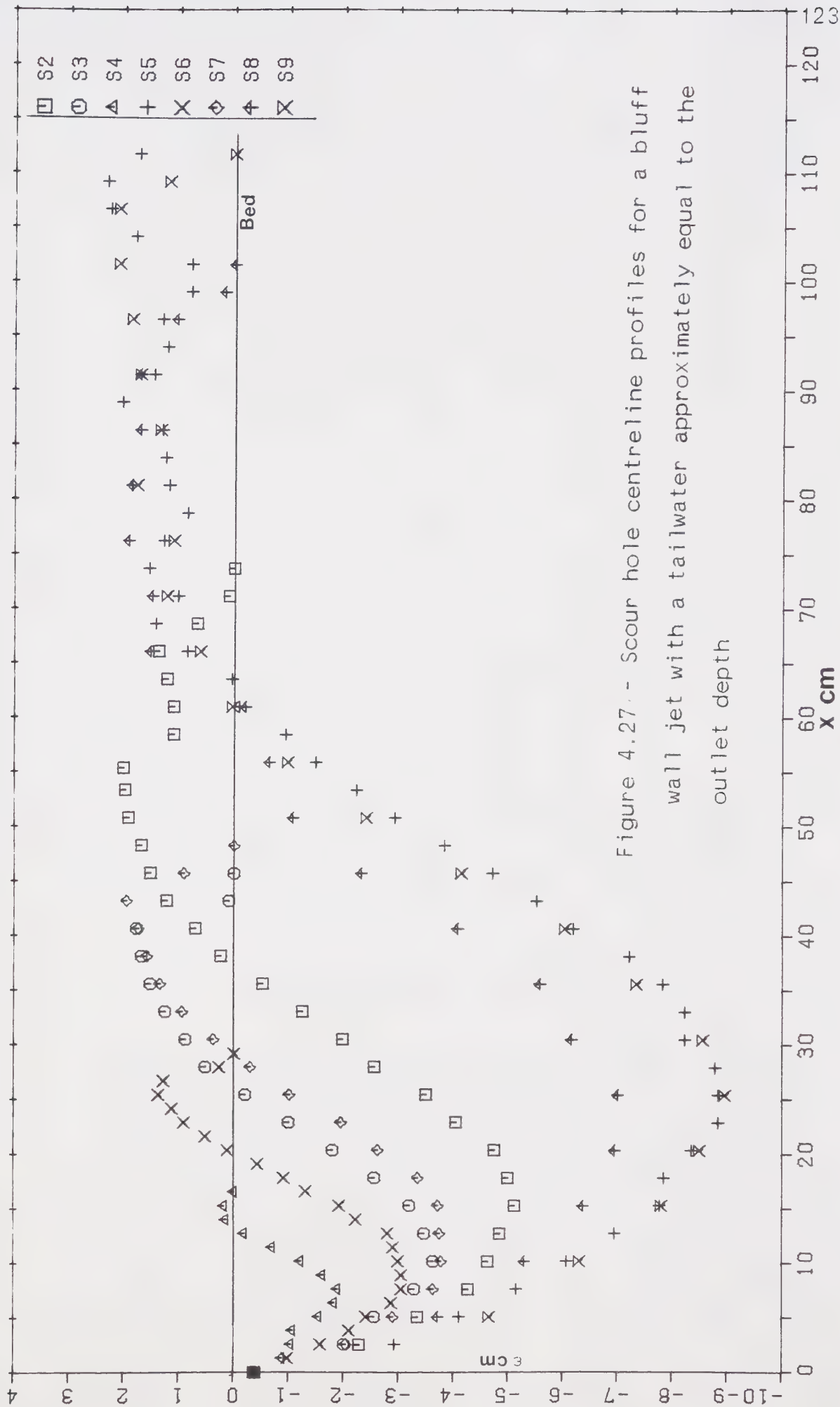


Figure 4.27 - Scour hole centreline profiles for a bluff wall jet with a tailwater approximately equal to the outlet depth



shape. Using the maximum eroded depth,  $\epsilon_{m\infty}$ , as the depth length scale and the distance to the point of maximum erosion,  $x_{\infty}$ , as the longitudinal length scale, it was found that the scour hole profiles collapse onto a single curve, Figure 4.28. It will be noticed that run S4 does not fit the collapsed curve very well. Run S4 only had a Reynolds number of 3,565, which was the lowest for all the runs, and it may be that the jet was not fully turbulent but in the transition range. As can be seen from Fig 4.28 the deposition ridge behind the scour hole did not become similar using the stated length scales. This was not unexpected because this fact had been noticed by other investigators. Due to the preliminary nature of the present study, no attempt was made to find convenient scales for the ridge.

Following the analysis presented by Rajaratnam and Berry (1977) for the variation of the length scales; Considering  $\epsilon_{m\infty}$ , it could be written

$$\epsilon_{m\infty} = f \left[ U_0, y_0, y_t, \rho, D, g, \Delta\rho, \nu, B, z_0 \right] \quad (4.15)$$

where  $\Delta\rho$  is the difference between the mass density of the bed material and that of the fluid,  $g$  is the acceleration due to gravity,  $\nu$  is the kinematic viscosity,  $B$  is the width of the lake model and  $D$  is the mean diameter of bed material. For the present study  $D=0.11\text{mm}$  and the specific gravity of the sand was 2.65.



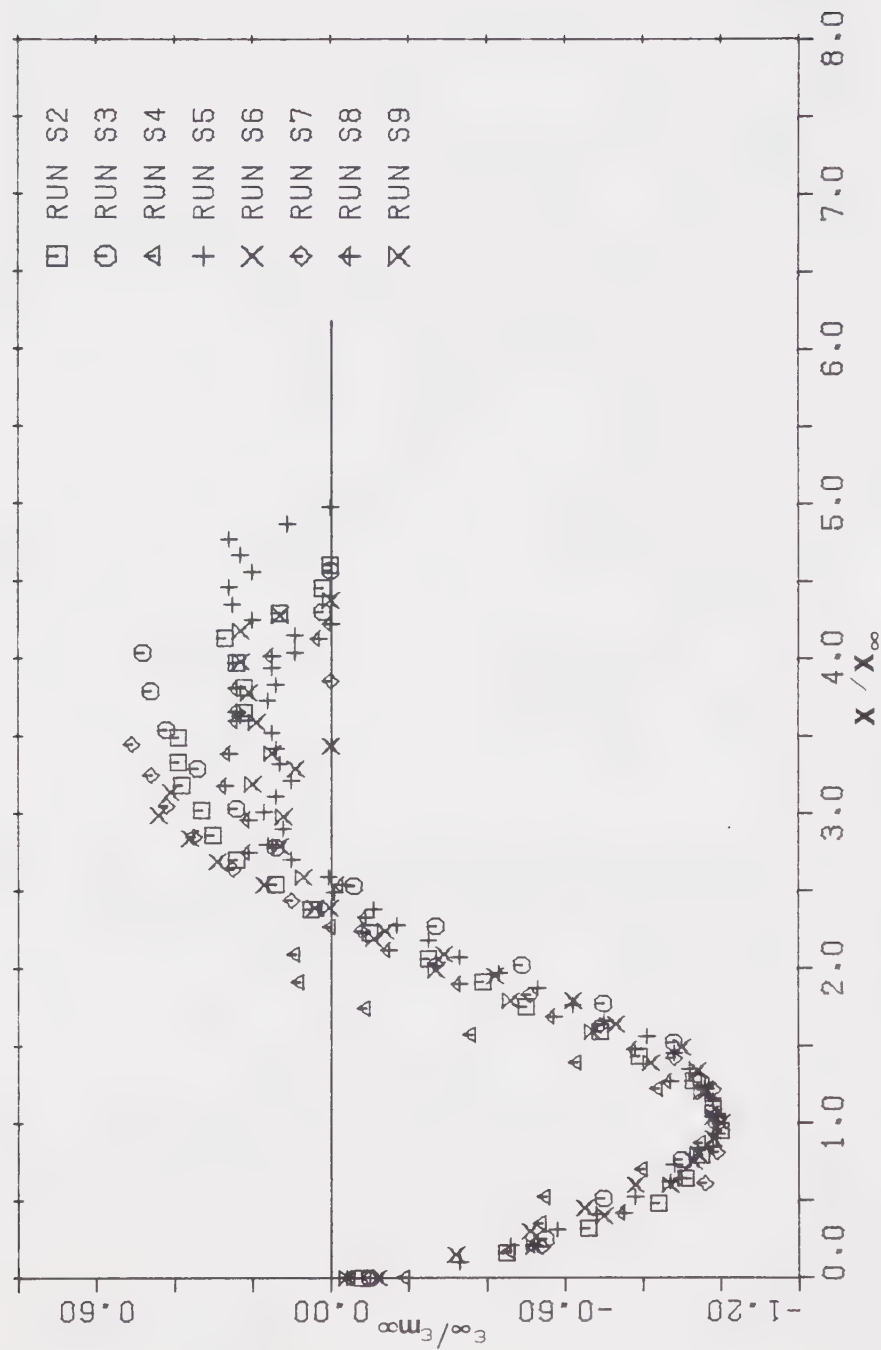


Figure 4.28 - Dimensionless scour hole centreline profile for a bluff wall jet with a tailwater approximately equal to the outlet depth



Using Buckingham's Pi theorem Eq 4.15 reduces to

$$\frac{\epsilon_{m\infty}}{y_0} = f_1 \left[ \frac{U_0}{gD\Delta\rho/\rho}, \frac{U_0 y_0}{\nu}, \frac{y_0}{D}, \frac{y_0}{y_t}, \frac{y_0}{B}, \frac{y_0}{z_0} \right] \quad (4.16)$$

for sufficiently large Reynolds numbers,  $\frac{U_0 y_0}{\nu}$ , the effects of viscosity can be ignored. The tailwater depth is approximately equal to the outlet depth and the nozzle is bluff, therefore  $y_0/z_0$  and  $y_0/y_t$  can be dropped from Eq.4.16. Also the width  $B$  is very large compared to the outlet depth and defining the densimetric Froude number,  $F_d$ , as  $U_0/\sqrt{gD\Delta\rho/\rho}$ , then Eq 4.16 reduces to

$$\frac{\epsilon_{m\infty}}{y_0} = f_3 \left[ F_d, \frac{y_0}{D} \right] \quad (4.17)$$

it has been found by the other investigators that Eq 4.17 can be simplified, providing that  $y_0/D$  is large, to

$$\frac{\epsilon_{m\infty}}{y_0} = f_4 \left( F_d \right) \quad (4.18)$$

The longitudinal length scale,  $x_\infty$ , can be predicted in a similar manner

$$\frac{x_\infty}{y_0} = f_5 \left( F_d \right) \quad (4.19)$$





When the two equations 4.18 and 4.19 were plotted it was found, Figure 4.29(a) and (b), that the points described reasonably well a straight line. The variation of  $\frac{L}{D}$  can be adequately described by the line given by Rajaratnam and Diebel (1981) for a finite tailwater but unconstrained width. However the longitudinal scale has more scatter and lies below the curve obtained by Rajaratnam and Diebel (1981), although it is possible to draw a straight line through the observed data.

## Summary

It was shown that the expansion of the jet was severely affected by the presence of a scour hole. The scour hole centreline profiles were shown to be similar and that the length scales correlated well with the densimetric Froude number.



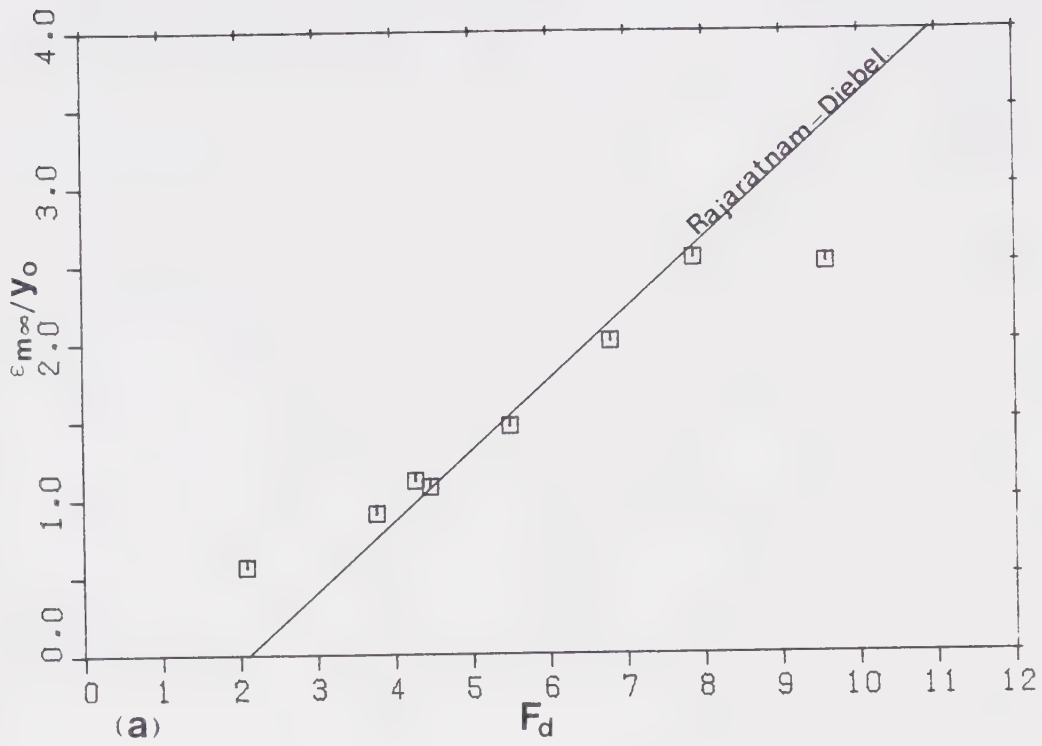
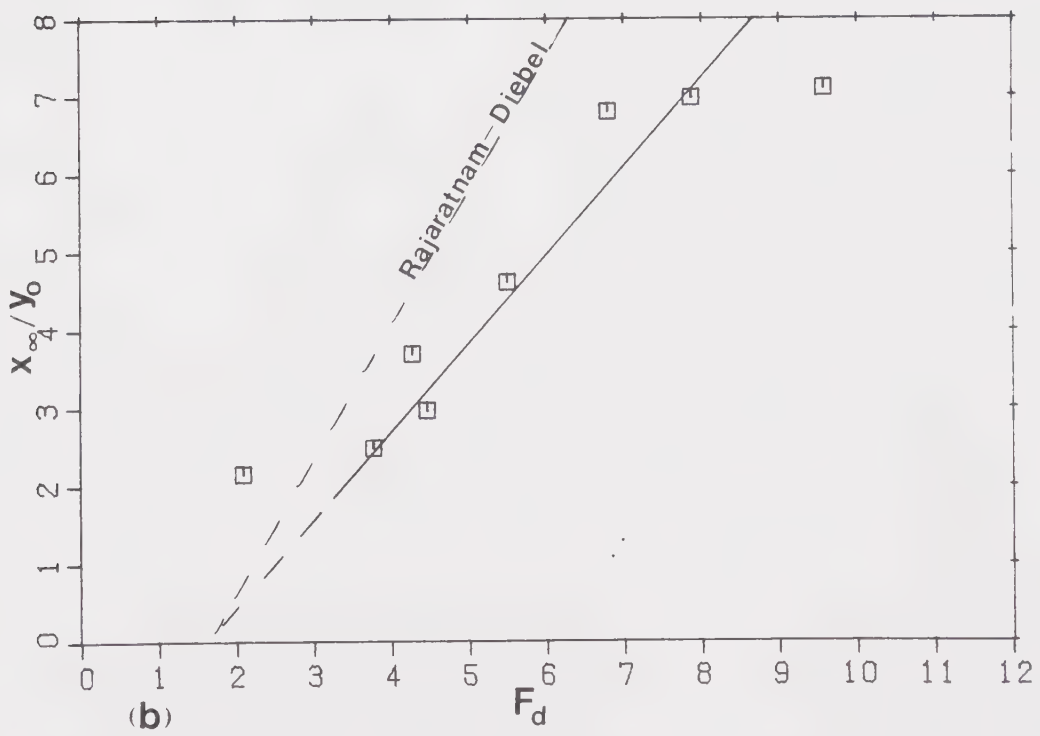


Figure 4.29 - Variation of the scour hole centreline profile length scales a)  $\epsilon_{m\infty}$  b)  $x_{\infty}$





## V. CONCLUSIONS AND RECOMMENDATIONS FOR FURTHER STUDY

### A. Conclusions

Using theoretical considerations, it was concluded that the theory of three dimensional turbulent bluff wall jets with infinite tailwater depth could be applied to bluff wall jets with limited tailwaters under certain circumstances. The theory did not apply when the tailwater was less than approximately one and one third times the outlet height. For tailwaters greater than one and one third times the outlet height but less than approximately four times the nozzle height the theory applied for a limited streamwise distance.

From experimental studies made of the flow, it was found that the jet expansion was dependent on the tailwater depth. For very shallow or no tailwater conditions the jet expansion was also dependent on the Froude number but when the tailwater to nozzle height ratio was greater than 0.6 the variation with the Froude number became insignificant. The vertical and transverse velocity profiles were similar in the fully developed flow and the variation of the respective length scales were functions of the tailwater depth. The surface velocity was dependent on both the tailwater depth and the downstream distance from the nozzle. It was also found that the potential core of the jet was shortened by reducing the tailwater, it was also observed that the expansion of the jet in the vertical plane was



increased as the tailwater depth diminished. The use of  $A$  to non-dimensionalise the longitudinal direction enabled the decay of the maximum velocity to be correlated in a suitable form, utilising the virtual origin. The maximum velocity decay was found to be reduced for lower tailwater depths. Shear stress measurements along the centreline indicated that the shear stress decayed at a slower rate as the tailwater was reduced. The transverse bed shear stress profiles were found to be similar and that the length scale was linear but a function of the tailwater. Elementary study of the bluff wall jet with erosion showed that the jet expansion was severely altered by the presence of a scour hole but that the scour holes were similar and that the length scales varied linearly with the densimetric Froude number.

## B. Recommendations for Further Study

During the course of this study the lack of knowledge about finite tailwater conditions became very obvious and this study only answers the problems arising from a very limited field of exploration. To understand the flow under varying shallow tailwater conditions the following topics are recommended for future study.

- 1) A detailed investigation of bluff wall jets, for all tailwaters, at distances far from the nozzle.





- 2) Measurements of the transverse velocities and the turbulent characteristics of the flow.
- 3) Detailed investigations into the cases of no tailwater and very low tailwater, including pressure distribution measurements.
- 4) Investigations of the effects on the bluff wall jet due to bed roughness and/or a downstream channel of limited width.
- 5) More experimental observations on the bed shear stress under varying tailwater conditions and bed roughness.
- 6) Investigations into the expansion of the jet and the scour produced by the bluff wall jet issuing tangentially to an erodable bed under varying tailwater depths and channel widths.
- 7) A complete detailed study of the diffusion characteristics of a slender wall jet with variations of tailwater, and the effect of side walls on the slender jet. Especially the case when the tailwater is equal to the outlet depth, which can model the river flow into a lake.
- 8) Investigations into the effect of finite tailwater conditions on the diffusion of the plane jet.
- 9) Arising from 7, investigations of a surface jet entering a body of fluid with a severely limited depth.
- 10) Investigations of the effect on the diffusion of the turbulent jet due to cross currents in the shallow tailwater.
- 11) All of the above but with a jet of different temperature or density than that of the ambient fluid.



## LIST of REFERENCES

- Abramovich, G.N., "The Theory of Turbulent Jets", M.I.T. Press, Mass., 1963. (English Translation)
- Bakke, P., "An Experimental Investigation of a Wall Jet", J.F.Mech., Vol 2, 1957.
- Catalano, G.B., Morton, J.B., and Humphris, R.R., "An Investigation of a Three Dimensional Wall Jet", A.I.A.A. Journal, Vol 15, 1977.
- Chandrasekhara Swamy, N.V., and Bandyopadhyay, P., "Mean and Turbulent Characteristics of Three-Dimensional Wall Jets", J.F. Mech., Vol 71, 1975.
- Glauert, M.B., "The Wall Jet", J.F. Mech., Vol 1, 1956.
- Hollingshead, A.B., and Rajaratnam, N., "A Calibration Chart for the Preston Tube", Journal of Hydr. Research, I.A.H.R., Vol 18, 1980.
- Kellerhals, R., "Factors Controlling the Level of Lake Athabasca", Proc. Peace-Athabasca Delta Symposium, Univ. of Alberta, Edmonton, 1971.



Launder, B.E., and Rodi, W., "The Turbulent Wall Jet", Prog. Aerospace Sci., Vol 19, 1981.

Massey, B.S., "Mechanics of Fluids", Van Nostrand Reinhold Co., 1975.

Merzkich, W., "Flow Visualisation", Academic Press, 1974.

Newman, B.G., Patel, R.P., Savage, S.B., and Tjio, H.K., "Three Dimensional Wall Jet Originating from a Circular Orifice", Aeronautical Quart., Vol 23, 1972.

Pande, B.B.Lal., "A Theoretical and Experimental Study of Heated Surface Discharge into Quiescent Ambients", Ph.D. Thesis, Dept. of Civ. Engg., Univ. of Alberta, Edmonton, Canada, 1975.

Pani, B.S., "Three Dimensional Turbulent Wall Jets", Ph.D. Thesis, Dept. of Civ. Engg., Univ of Alberta, Edmonton, Canada, 1972.

Patel, V.C., "Calibration of the Preston Tube and Limitations of its use in Pressure Gradients", J.F.Mech., Vol 23, 1965.

Pearce, A.F., "Critical Reynolds Number for Fully-Developed



Turbulence in Circular Submerged Water Jets", C.S.I.R.  
Report MEG 475, August 1966.

Preston, J.H., "The Determination of Turbulent Skin Friction  
by means of Pitot Tubes", J. Royal Aero. Soc., Vol 58,  
1954.

Rajaratnam, N., "On the Preston Tube with a Hemispherical  
Nose", Civ. Eng. and P.W. Rev., Vol 66, 1960.

Rajaratnam, N., "The Hydraulic Jump as a Wall Jet", A.S.C.E.  
Journal of Hyd. Div., Vol 91, Sept 1965.

Rajaratnam, N., "Submerged Hydraulic Jump", A.S.C.E. Journal of  
Hyd. Div., Vol 91, 1965.

Rajaratnam, N., "Turbulent Jets", Developements in Water  
Science 5, Elsevier Pub. Co., 1976.

Rajaratnam, N., "Erosion by Plane Turbulent Jets", Journal of  
Hyd. Research, I.A.H.R., 1981. (in press)

Rajaratnam, N., and Beltaos, S., "Erosion by Impinging Circular  
Turbulent Jets", A.S.C.E. Journal of Hyd. Div., Vol 103,  
1977.

Rajaratnam, N., and Berry, B., "Erosion By Circular Turbulent





Wall Jets", Journal of Hyd. Research, I.A.H.R., Vol 15, 1977.

Rajaratnam, N., and Diebel, M., "Erosion below Culvert-Like Structures", Proc. 5th Canadian Hydrotechnical Conf., Fredricton, N.B., Canada, May 1981.

Rajaratnam, N., and Muralidhar, D., "The Prandtl Tube as a Preston Tube", Civ. Eng. and P.W. Rev., 1968.

Rajaratnam, N., and Pani, B.S., "Three Dimensional Turbulent Wall Jets", Technical Rep., Dept. of Civ. Engg., Univ. of Alberta, Edmonton, Aug 1970.

Rajaratnam, N., Pochylko, D.S., and Macdougall, R.K., "Further Studies on the Erosion of Sand Beds by Plane Water Jets", Water Resources Engineering Rept. WRE81, Dept. of Civ. Engg., Univ. of Alberta, Edmonton, Canada, Sept 1981.

Rajaratnam, N., and Subramanya, K., "Flow Immediately below Submerged Sluice Gate", A.S.C.E. Journal of Hyd. Div., Vol 93, July 1967.

Rajaratnam, N., and Subramanya, K., "Hydraulic Jump below abrupt Symmetrical Expansion", A.S.C.E. Journal of Hyd. Div., Vol 94, March 1968.



Rouse, H., "Engineering Hydraulics", Ed., John Wiley and Sons Inc., 1949.

Schlichting, H., "Boundary Layer Theory", McGraw-Hill Book Co., 1968.

Sforza, P.M., and Herbst, G., "A Study of Three Dimensional, Incompressible, Turbulent Wall Jets", A.I.A.A. Journal, Vol 8, Feb 1970.

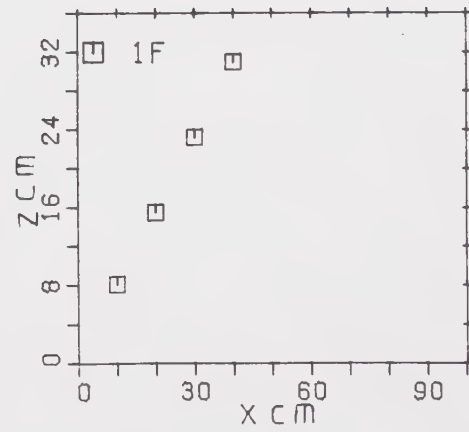
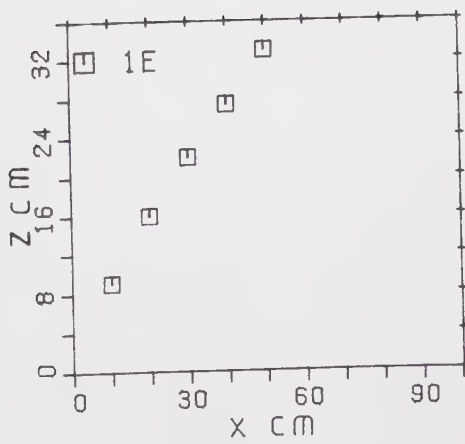
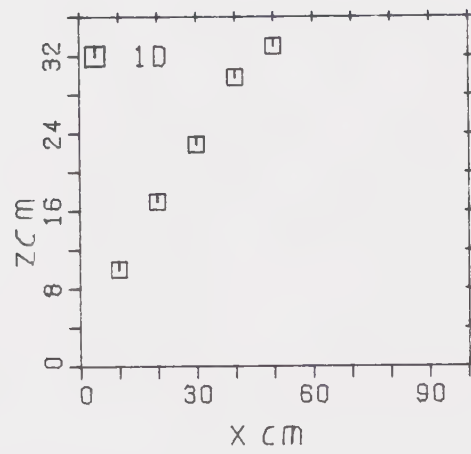
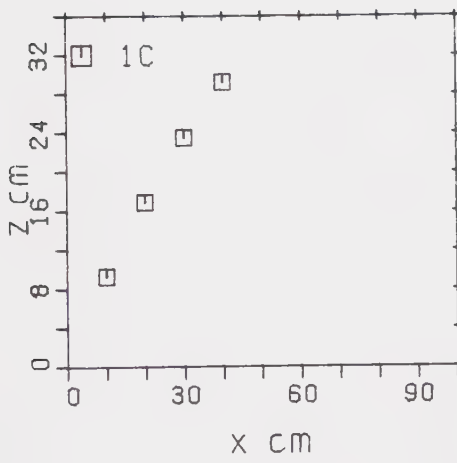
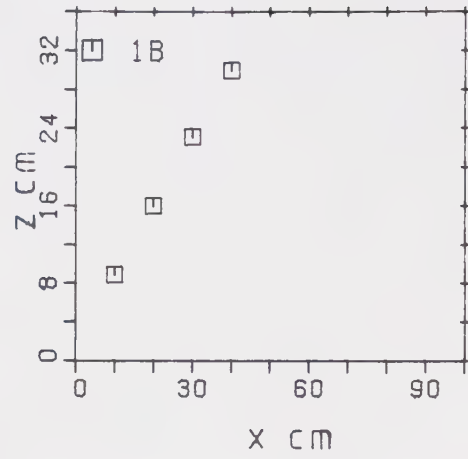
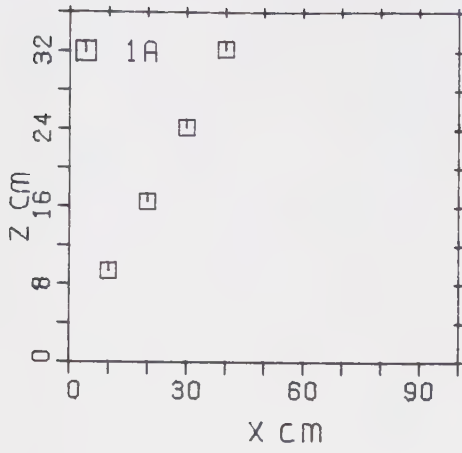
Viets, H., and Sforza, P.M., "An Experimental Investigation of a Turbulent, Incompressible, Three Dimensional Wall Jet", Polytechnic Inst. of Brooklyn, Dept. of Aerospace Engg. and Appl. Mech., PIBAL Report No. 968, April 1966.



## APPENDIX A - Experimental Data on the Transverse Expansion

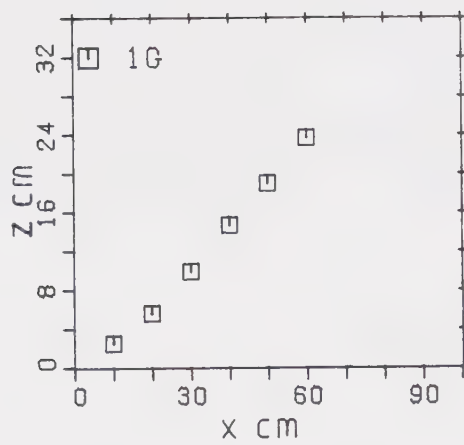


## Set 1

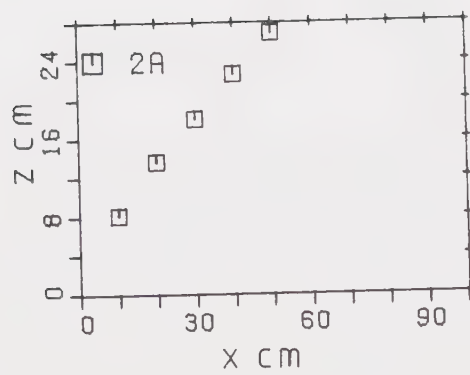








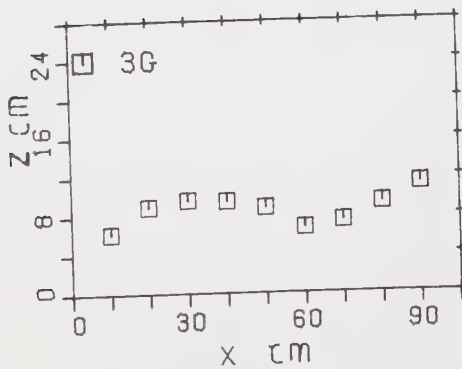
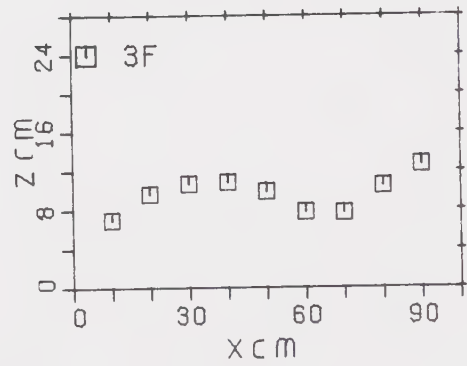
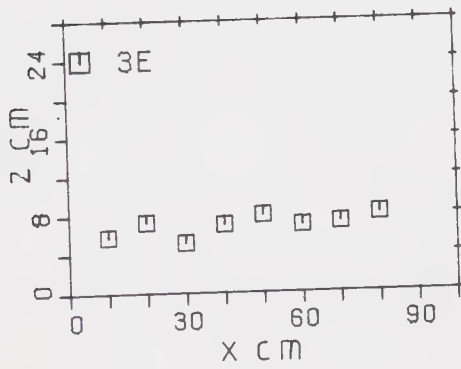
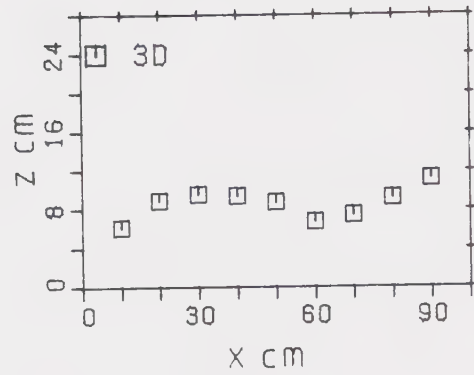
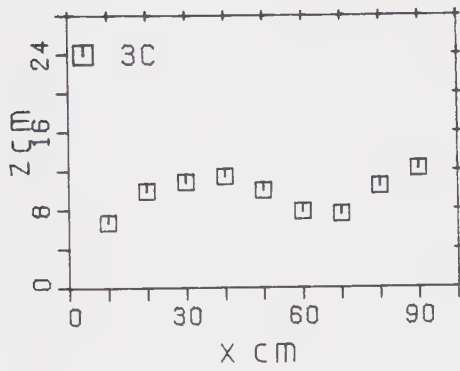
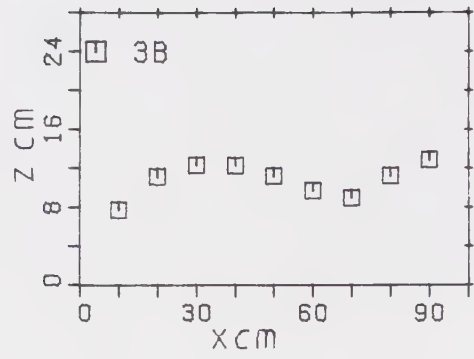
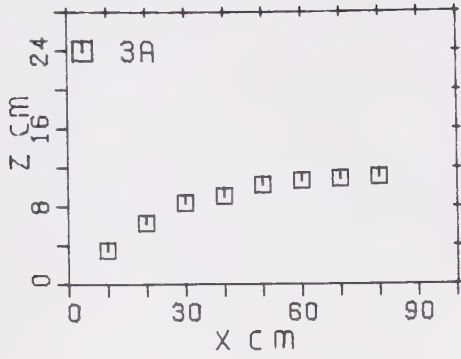
## Set 2





# Set 3

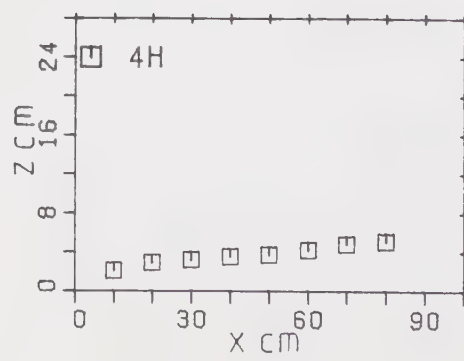
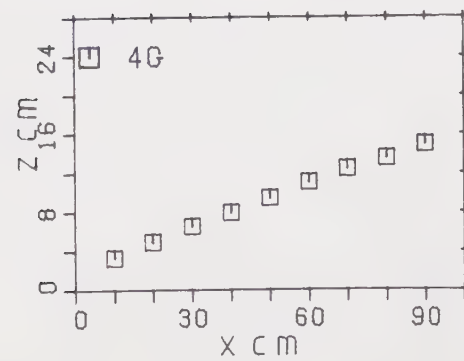
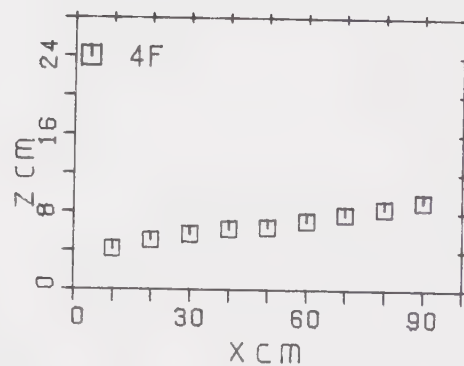
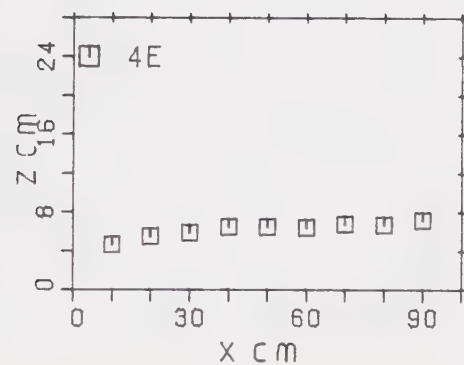
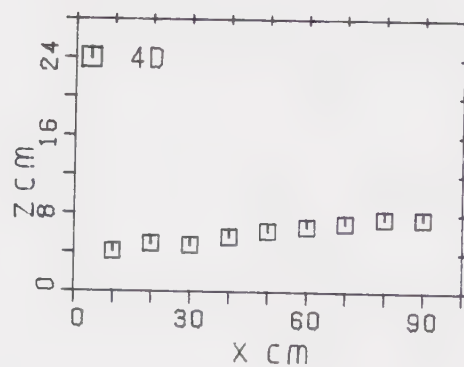
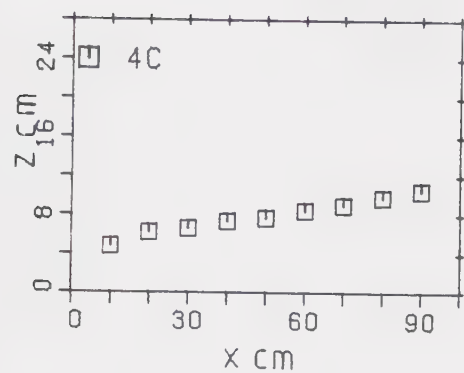
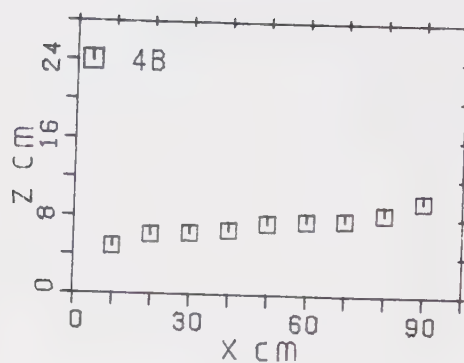
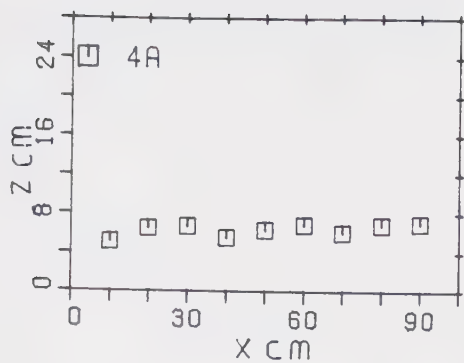
A4



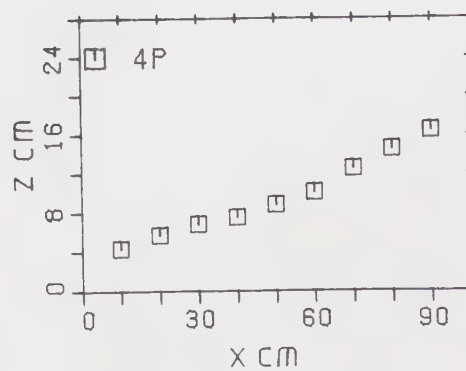
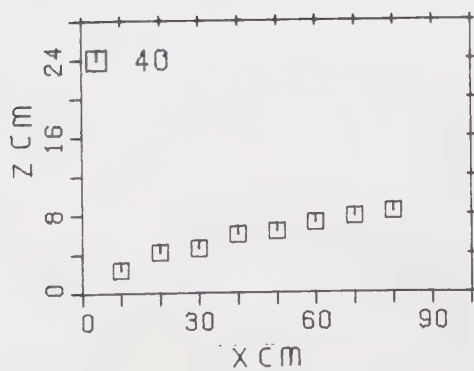
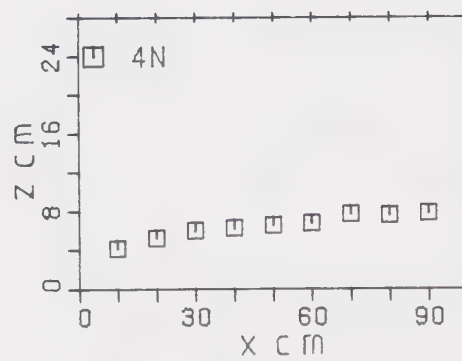
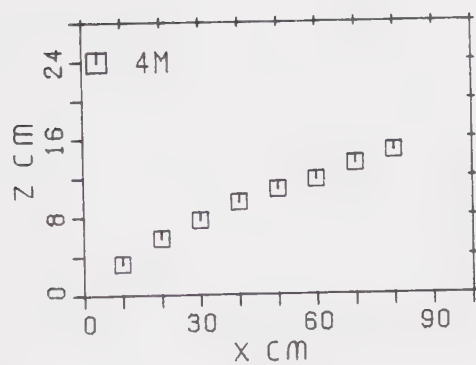
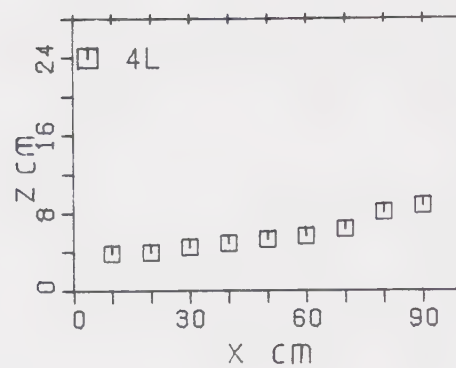
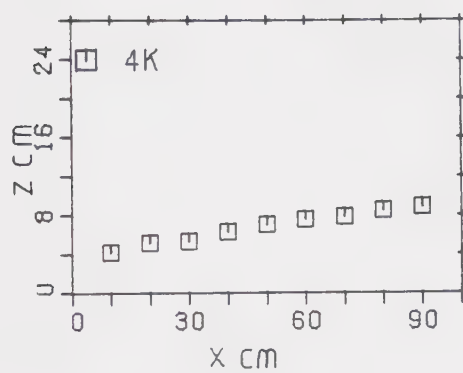
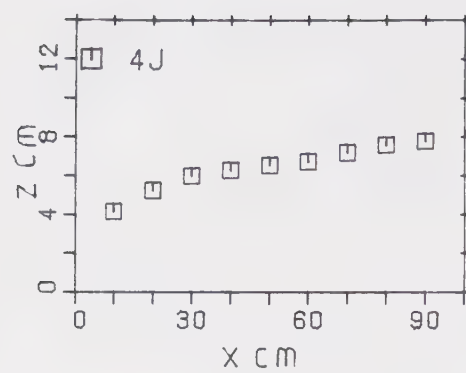
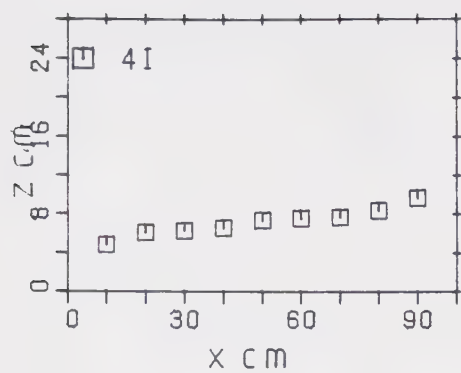


# Set 4

A5





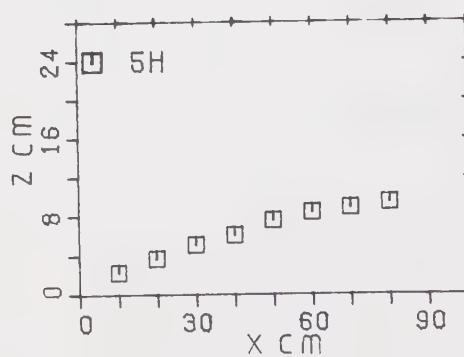
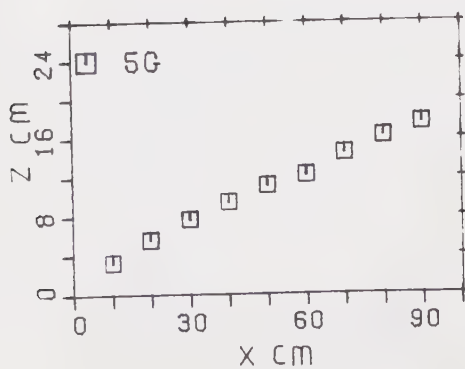
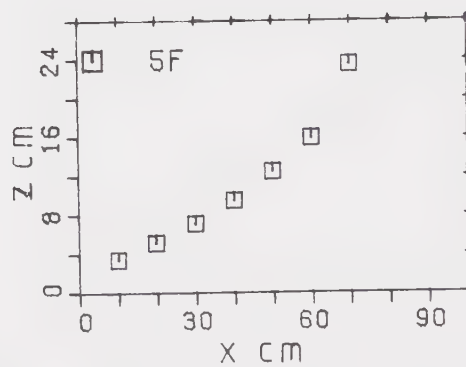
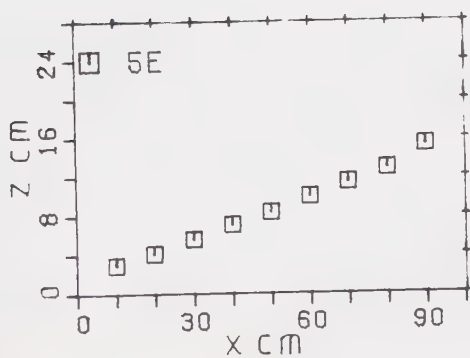
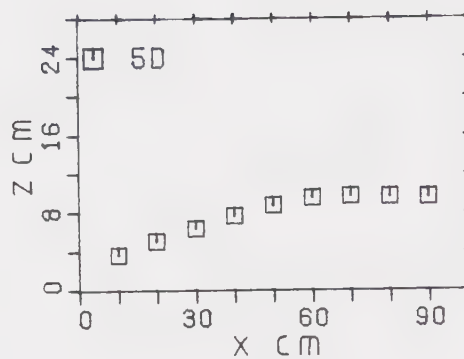
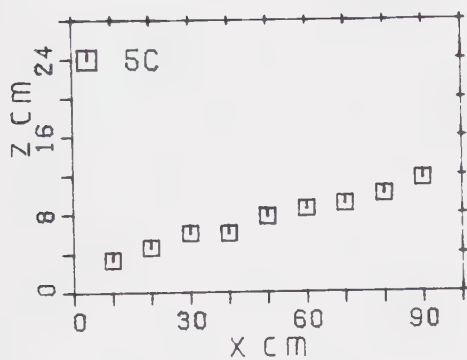
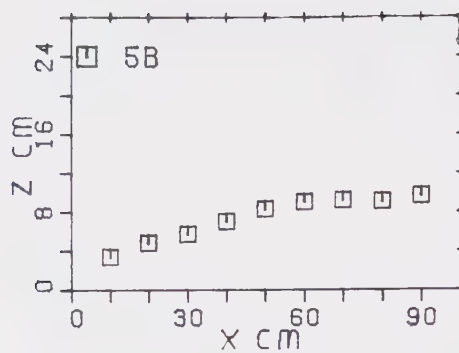
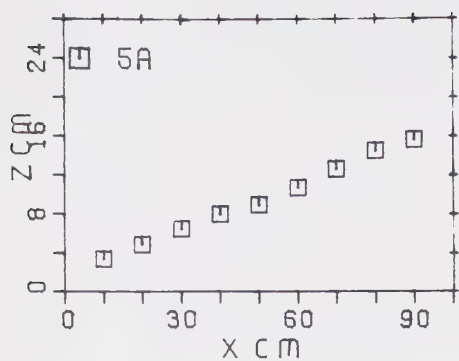




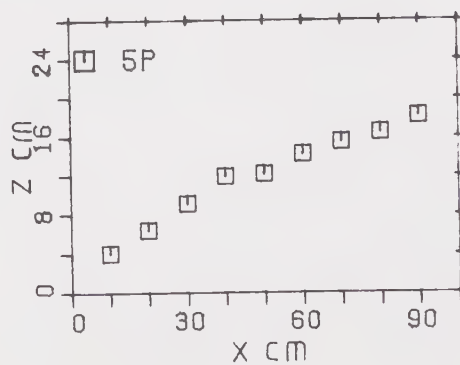
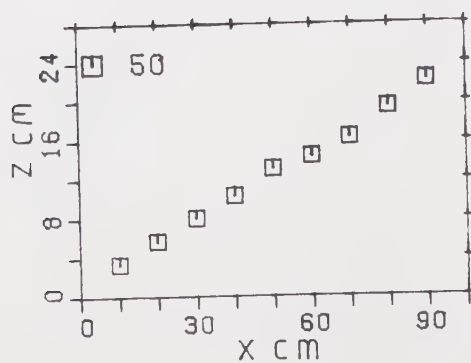
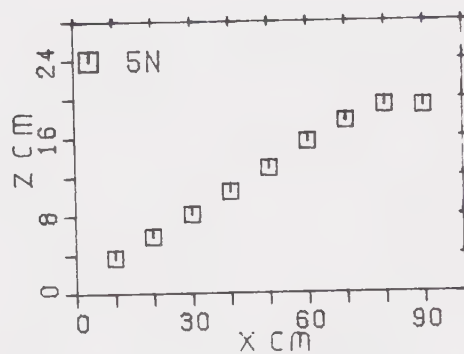
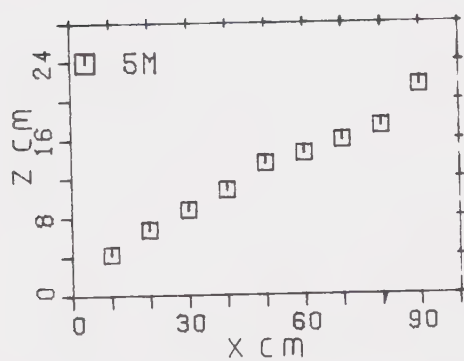
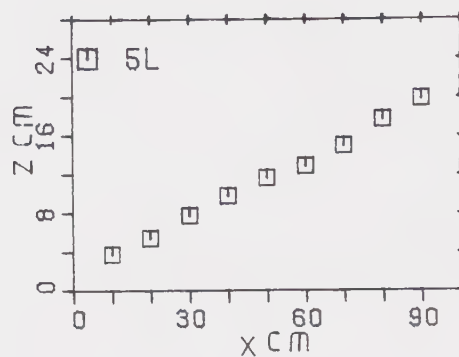
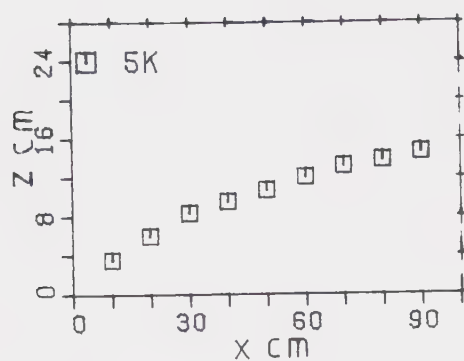
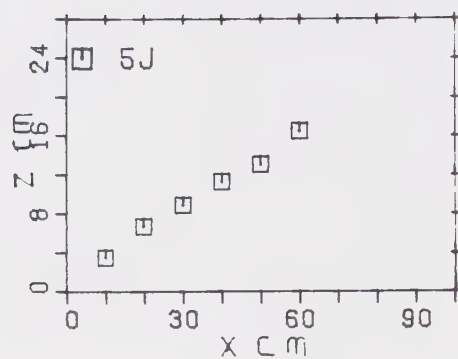
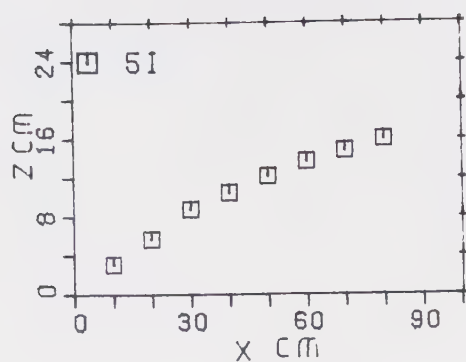


# Set 5

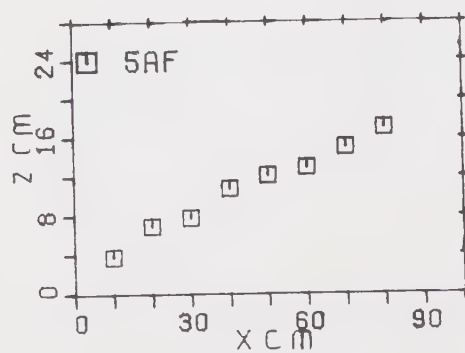
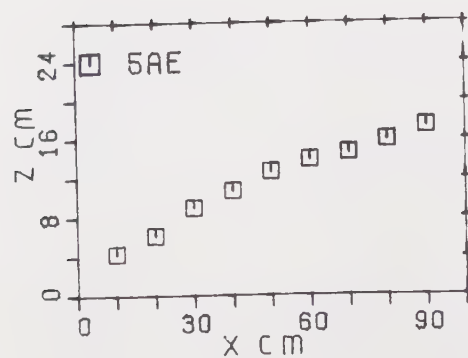
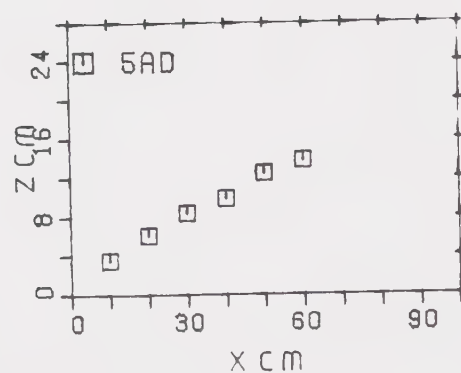
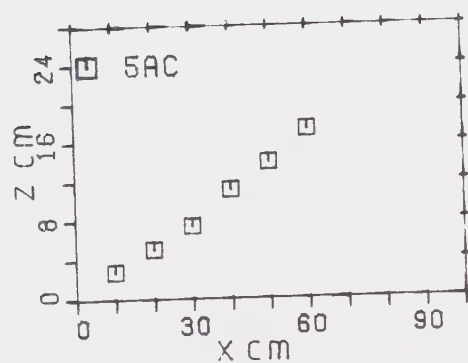
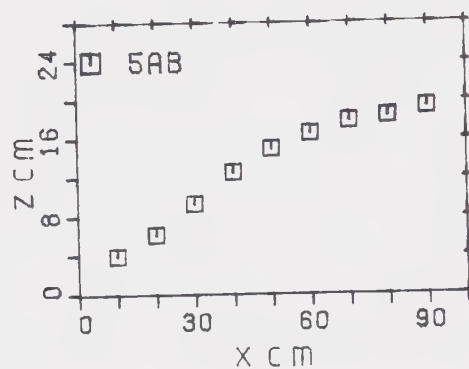
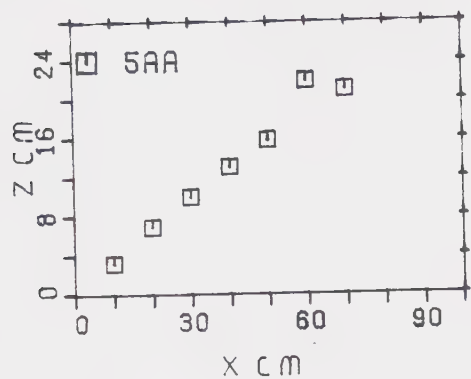
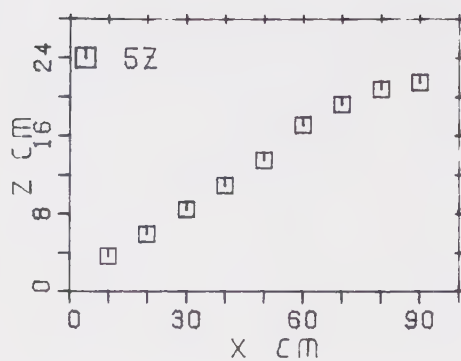
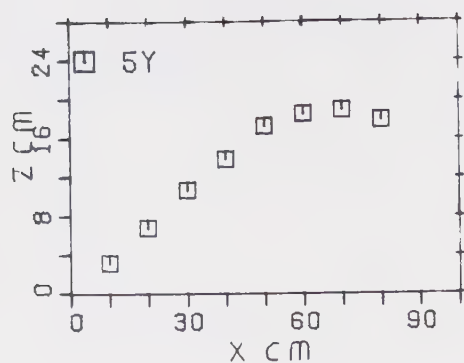
A7



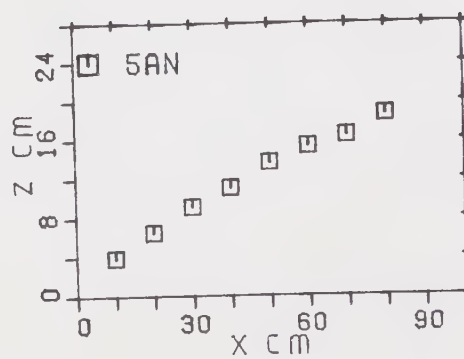
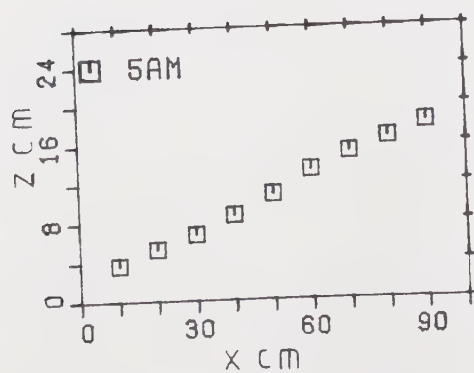
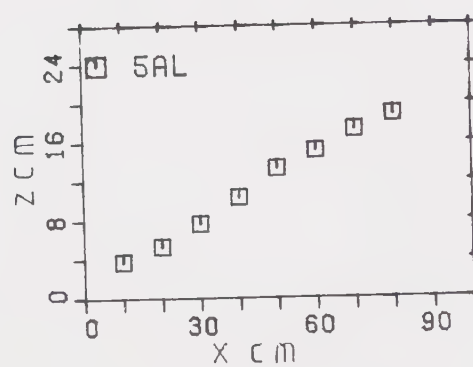
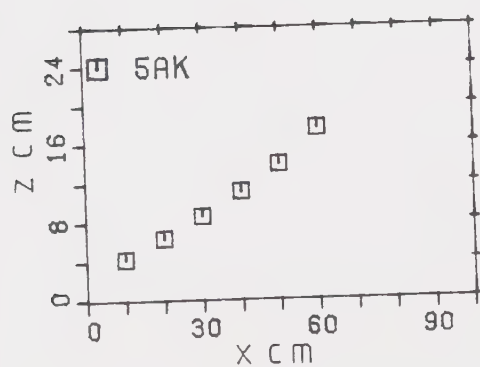
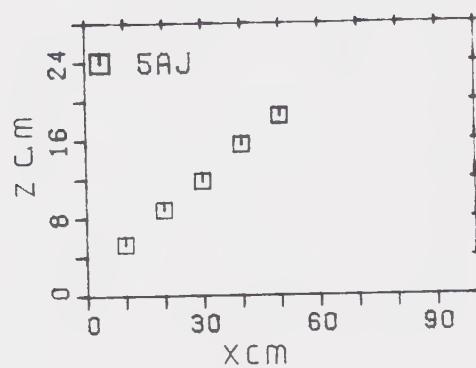
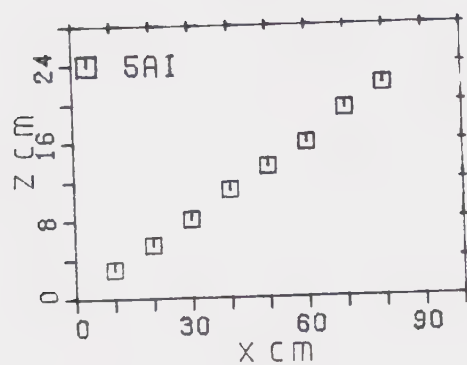
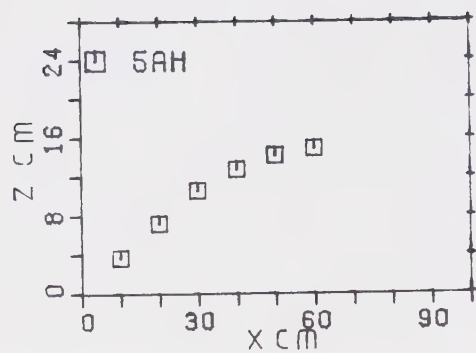
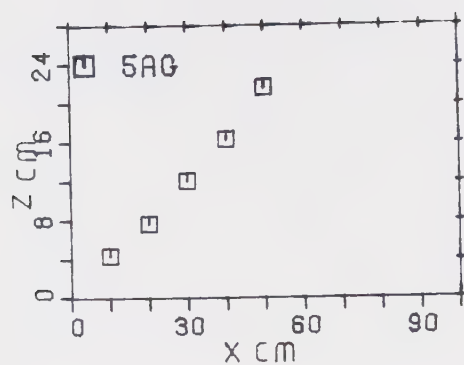






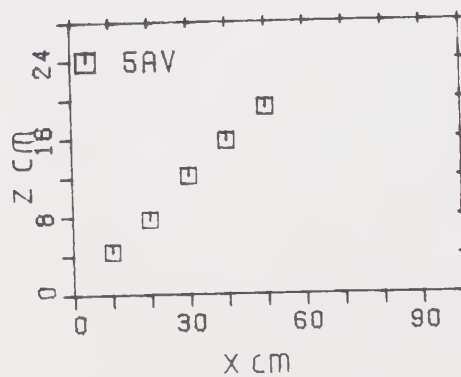
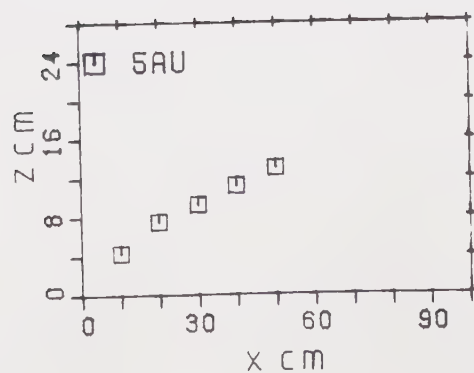
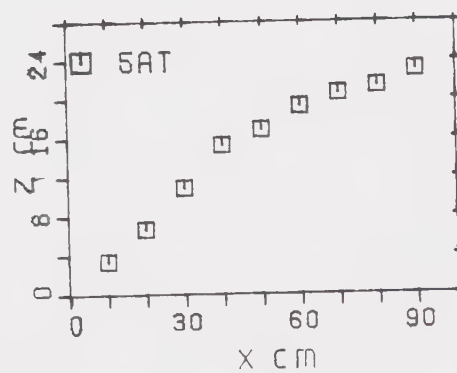
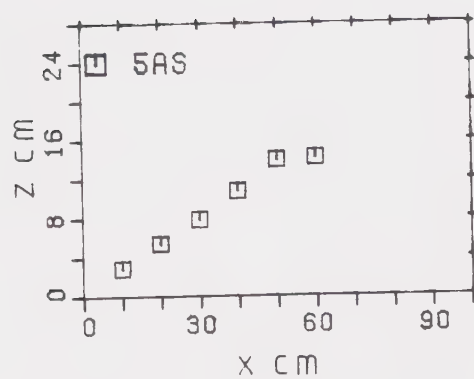
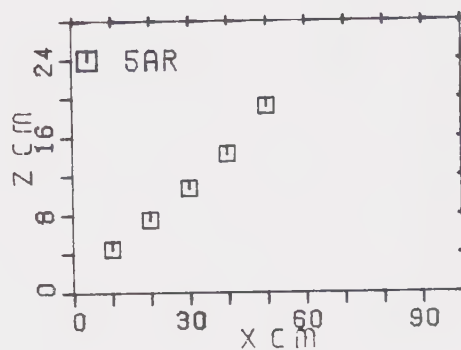
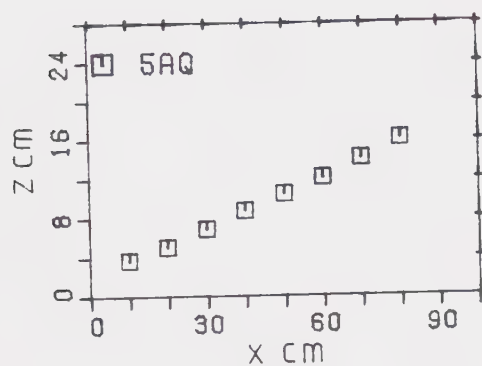
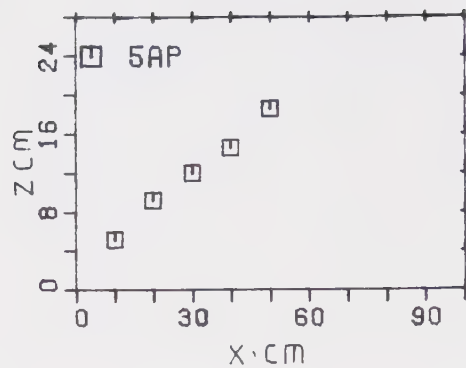
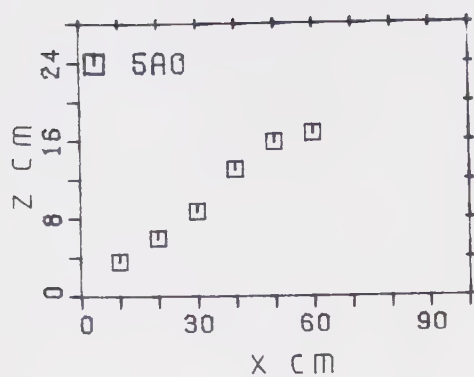




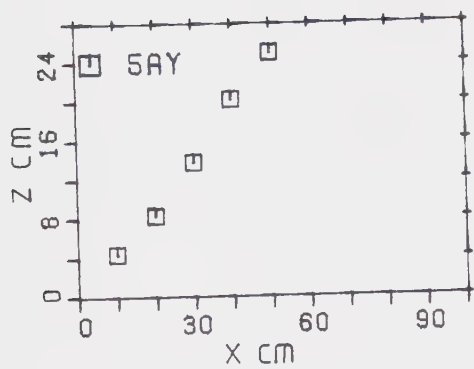
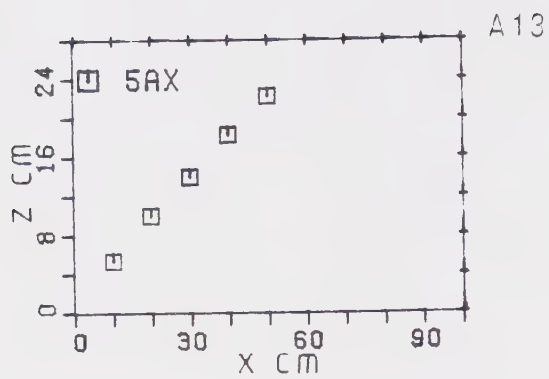
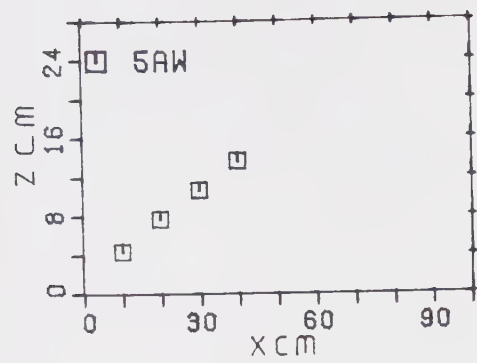




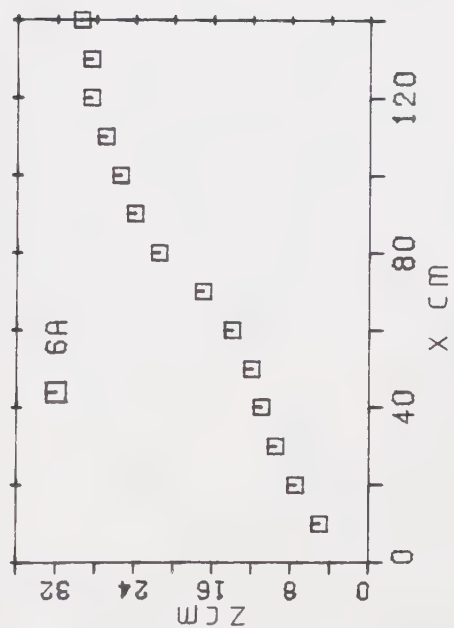
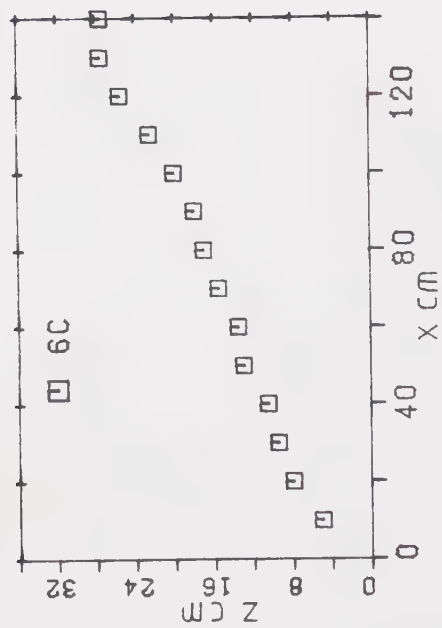






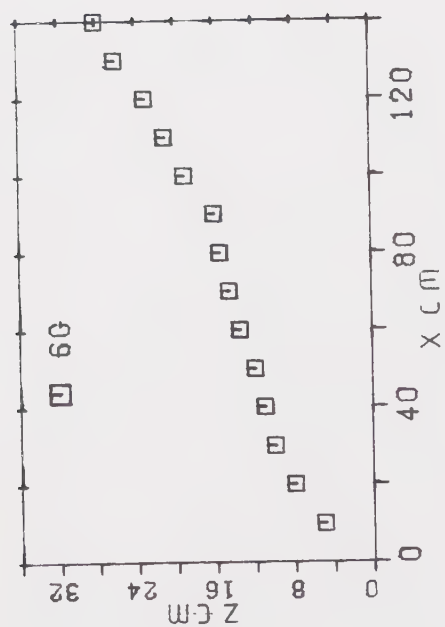
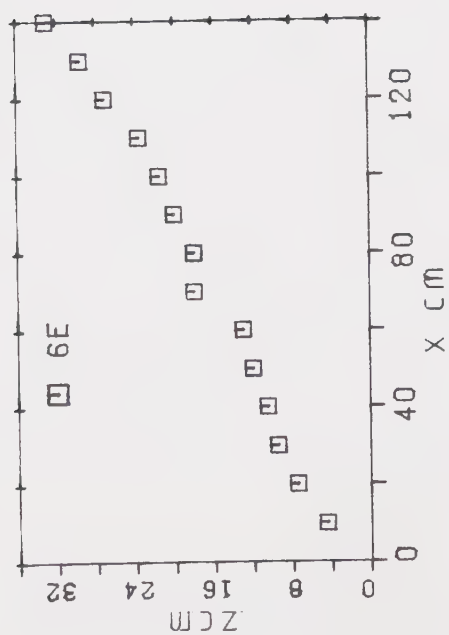
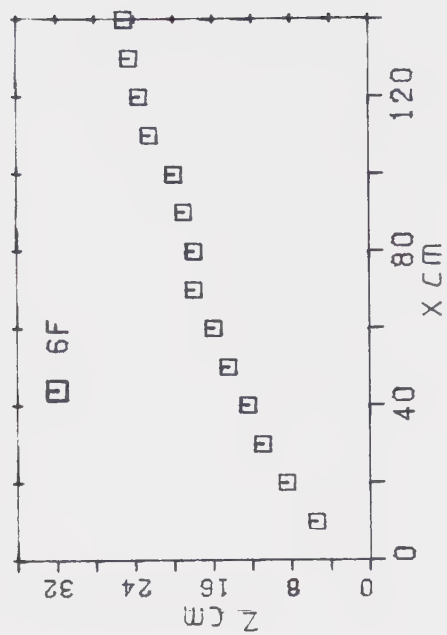






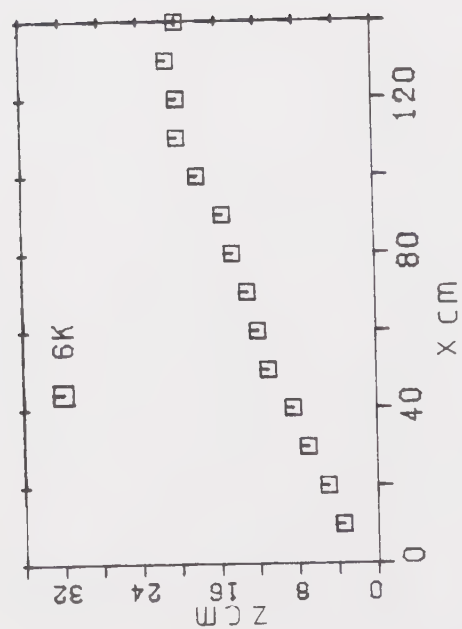
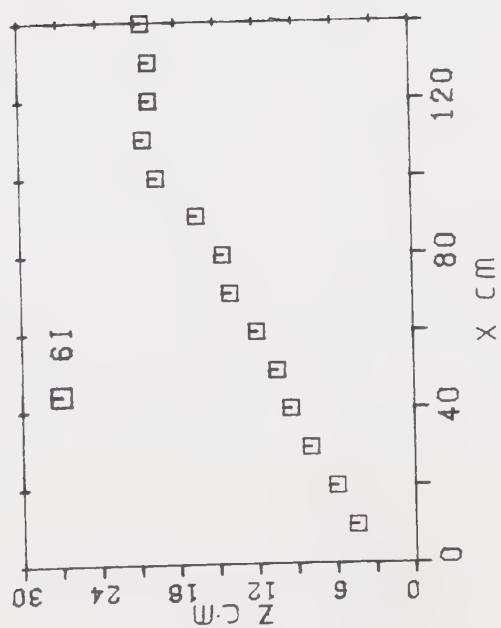
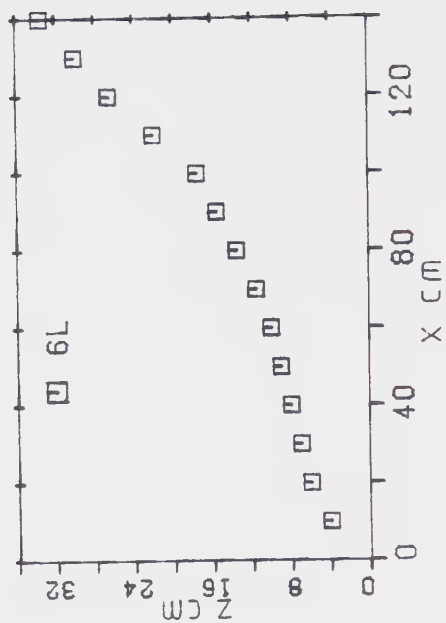
Set6



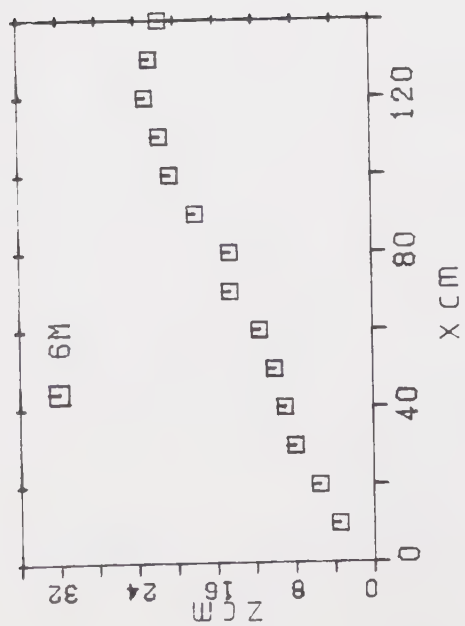
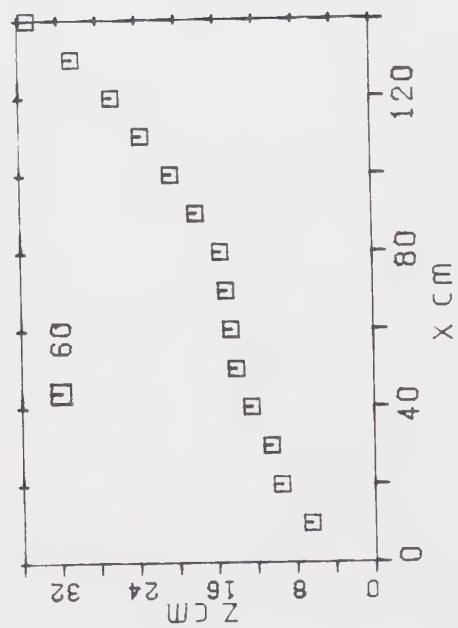
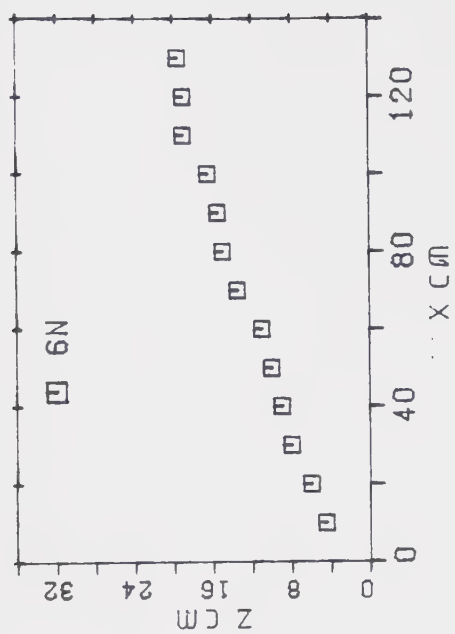




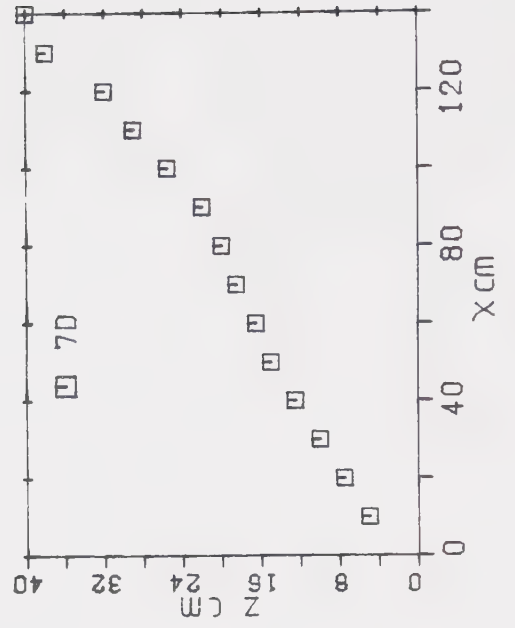
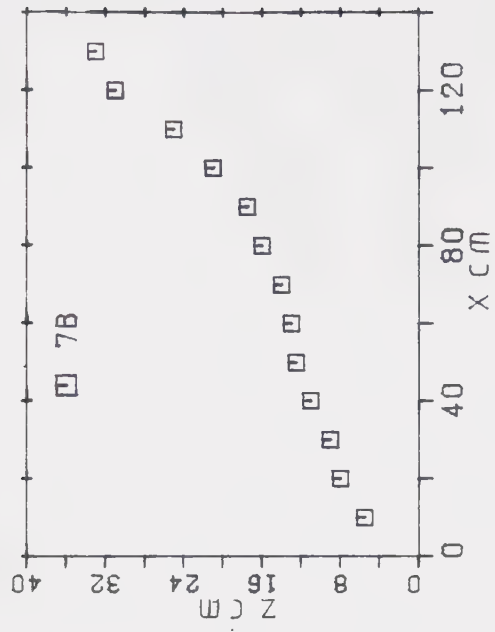




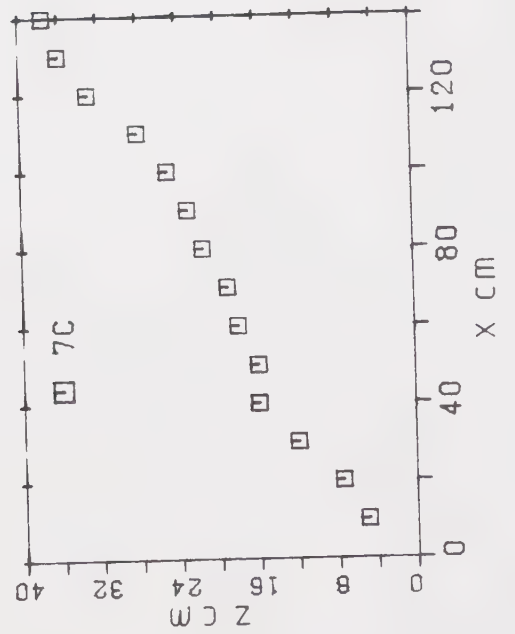
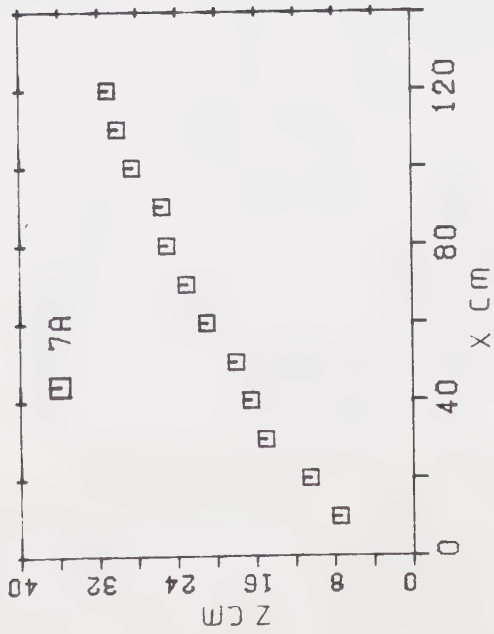








Set 7





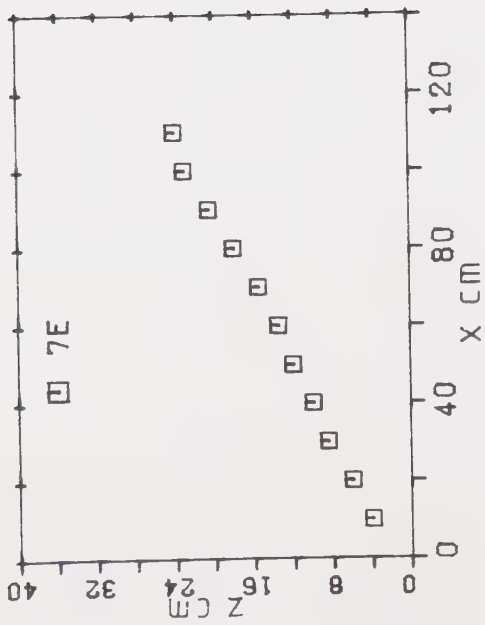
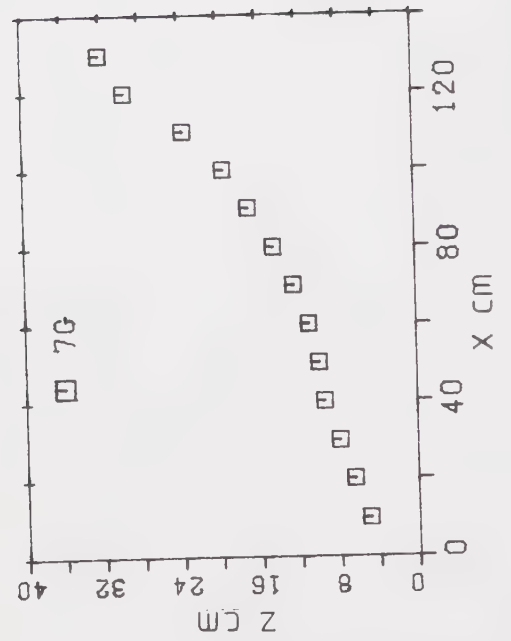
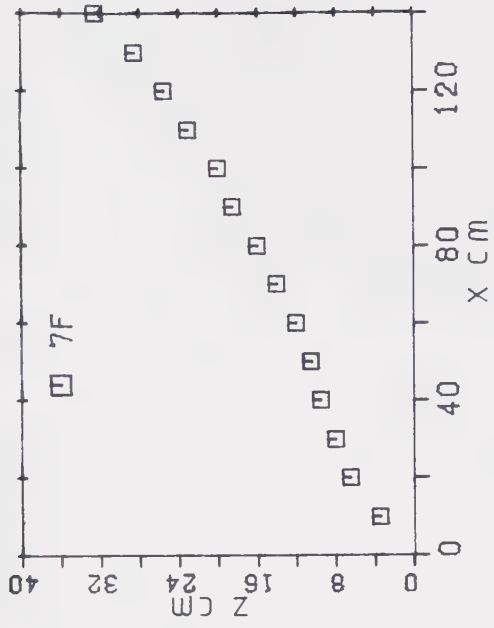






Table A1 Significant Expansion Results

Set	$U_0$ cm/s	$y_t/y_0$	$\tan\theta$	Nozzle
1 a	94.7	0	0.76	*
1 b	92.0	0	0.69	
1 c	86.5	0	0.69	
1 d	83.5	0	0.70	
1 e	70.6	0	0.66	
1 f	120.4	0	0.70	
1 g	265.0	0	0.44	round
2 a	99.8	0.3	0.5	
3 a	141.3	0.32	?	round
3 b	77.3	0.40	?	
3 c	86.5	0.45	?	
3 d	92.1	0.5	?	
3 e	80.5	0.55	?	
3 f	83.5	0.56	?	
3 g	94.7	0.62	?	
4 a	86.5	0.61	0.02	
4 b	89.3	0.62	0.055	
4 c	11.6	0.67	0.095	
4 d	89.3	0.73	0.045	
4 e	86.5	0.73	0.025	
4 f	75.7	0.73	0.06	
4 g	253.7	0.74	0.14	round



Set	$U_0$ cm/s	$y_t/y_0$	$\tan\epsilon$	Nozzle
4 h	137.0	0.78	0.04	sm. rect.
4 i	94.7	0.82	0.08	
4 j	89.3	0.84	0.04	
4 k	89.3	0.84	0.06	
4 l	86.5	0.85	0.05	
4 m	136.1	0.86	0.18	round
4 n	102.3	0.90	0.07	
4 o	135.0	0.94	0.08	
4 p	113.8	0.98	0.155	
5 a	92.0	1.02	0.145	
5 b	92.0	1.06	0.115	
5 c	86.5	1.08	0.10	
5 d	92.1	1.17	0.14	
5 e	89.3	1.23	0.135	
5 f	74.0	1.23	0.21	
5 g	83.5	1.36	0.17	
5 h	181.0	1.42	0.12	sm. rect.
5 i	132.4	1.5	0.2	round
5 j	256.1	1.5	0.23	round
5 k	99.8	1.61	0.16	
5 l	92.1	1.72	0.20	
5 m	92.0	1.78	0.215	
5 n	70.6	1.85	0.22	
5 o	83.5	1.96	0.22	



Set	$U_0$ cm/s	$y_t / y_0$	$\tan \theta$	Nozzle
5 p	99.8	1.98	0.19	
5 q	249.4	2.1	0.23	round
5 r	159.0	2.2	0.22	sm. rect.
5 s	86.5	2.28	0.27	
5 t	109.0	2.34	0.20	sm. rect.
5 u	80.5	2.42	0.24	
5 v	97.3	2.44	0.25	
5 w	92.1	2.49	0.26	
5 x	83.5	2.64	0.21	
5 y	130.6	2.76	0.31	round
5 z	107.0	2.83	0.24	
5 aa	228.5	2.9	0.29	round
5 ab	67.0	2.98	0.23	
5 ac	79.0	3.31	0.26	sm. rect.
5 ad	178.0	3.46	0.23	sm. rect.
5 ae	109.4	3.79	0.24	
5 af	74.0	3.82	0.23	
5 ag	70.6	3.83	0.36	
5 ah	130.6	4.10	0.21	round
5 ai	224.1	4.20	0.25	round
5 aj		4.28	0.34	
5 ak	77.3	4.38	0.25	
5 al	59.1	4.40	0.215	
5 am	77.4	4.62	0.21	



Set	$U_o$ cm/s	$y_t / y_o$	$\tan \theta$	Nozzle
5 an	74.0	4.7	0.22	round
5 ao	217.4	5.0	0.26	
5 ap		5.2	0.33	
5 aq	77.4	5.3	0.28	
5 ar		5.8	0.32	
5 as	127.8	5.8	0.25	round
5 at	144.2	6.1	0.3	
5 au		6.21	0.21	
5 av		7.9	0.36	
5 aw		8.2	0.30	
5 ax		9.2	0.42	
5 ay		13.6	0.5	
6 a	11.1	1.0	0.21	
6 b	4.0	1.0	0.235	
6 c	15.8	1.0	0.18	
6 d	23.5	1.0	0.19	Lake
6 e	18.6	1.0	0.21	
6 f	32.3	1.0	0.18	
6 g	23.7	1.0	0.18	
6 h	22.6	1.0	0.18	
6 i	13.7	1.0	0.17	
6 j	17.7	1.0	0.2	
6 k	4.6	1.0	0.16	
6 l	8.2	1.0	0.14	





Set	$U_o$ cm/s	$y_t / y_o$	$\tan \theta$	Nozzle
6 m	2.3	1.0	0.17	
6 n	15.3	1.0	0.15	
6 o	32.5	1.0	0.2	
			@0.184	
7 a	3.44	1.0	0.18	
7 b	6.4	1.0	0.195	
7 c	1.79	1.0	0.26	
7 d	6.0	1.0	0.26	
7 e	2.3	1.0	0.20	
7 f	4.0	1.0	0.20	
7 g	8.6	1.0	0.14	
			@0.20	

\* unless otherwise noted the nozzle is rectangular.



## APPENDIX B - Velocity and Shear Stress data



Table B1 Velocity Run Flow Parameters

Run	x cm	$y_t$ cm	$y_o$ cm	$U_o$ cm/s	$U_{no}$ cm/s	$U_i$ cm/s	$U_s/U_{ro}$	$x/y_t$	$y_o/y_o$
1	20	2.77	2.5	95.	72.5	49.	.68	7.22	1.11
	30				60.	41.	.68	10.83	
	40				52.	39.5	.76	14.44	
	50				48.	37.5	.78	18.05	
2	20	3.78	2.5	92.	75.5	31.	.41	5.29	1.51
	30				60.5	32.5	.54	7.94	
	40				53.5	32.	.6	10.58	
	50				43.5	30.5	.70	13.23	
3	20	4.05	2.5	98.	79.5	32.	.40	4.94	1.65
	30				65.5	33.	.50	7.41	
	40				56.0	34.	.61	9.88	
	50				46.5	33.5	.72	12.35	
	60				42.5	26.	.61	15.82	



Run	x cm	y cm	y, cm	U <sub>y</sub> cm/s	u <sub>no</sub> cm/s	U <sub>y</sub> cm/s	U <sub>y</sub> /U <sub>s</sub>	x/y <sub>z</sub>	y <sub>z</sub> /y <sub>0</sub>
4	20	3.2	2.5	100.	78.	47.	.60	6.25	1.28
	30				68.5	45.	.66	9.38	
	40				59.5	43.5	.73	12.5	
	50				53.	39.5	.74	15.63	
	60				48.	40.5	.84	18.75	
	30	4.63	2.5	84.	55.0	31.5	.57	6.48	1.85
5	40				46.	24.	.52	8.64	
	50				41.5	27.	.65	10.8	
	20	3.1	2.5	84.5	70.5	47.	.66	6.45	1.24
	30				61.0	43.	.70	9.68	
	40				53.5	41	.77	12.9	
	50				47.5	37.5	.79	16.13	
6	60				42.5	35.	.82	19.35	
	30	11.1	2.5	61.9	41.5	4.4	.11	2.7	4.44
	40				35.	4.	0.11	3.6	
	50								
	60								
	30								
7	40								





Run	x cm	y cm	$y_0$ cm	$U_0$ cm/s	$u_{\text{me}}$ cm/s	$U_2$ cm/s	$U_3/U_2$	$x/y_0$	$y_0/y_D$
8	50				30.	3.5	.12	4.5	
	60				25.	3.0	.12	5.4	
	80				18.	4.	.22	7.2	
	20	7.86	2.5	79.2	65.	.13	2.5	3.14	
	30				53.5	9.5	.18	3.8	
	40				42.3	10.5	.25	5.1	
9	50				35.	12.	.34	6.4	
	60				29.5	14.	.47	7.6	
	20	4.35	2.5	80.8	68.5	23.0	.34	4.6	1.74
	30				57.5	25.5	.44	6.9	
	40				47.0	27.5	.58	9.2	
	50				40.	28.	.7	11.5	
10	60				35.	26.5	.76	13.8	
	20	3.35	2.5	85.1	72.5	42.	.58	6.0	1.34
	30				58.5	37.5	.64	9.0	

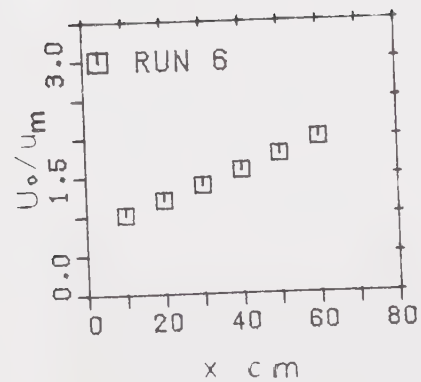
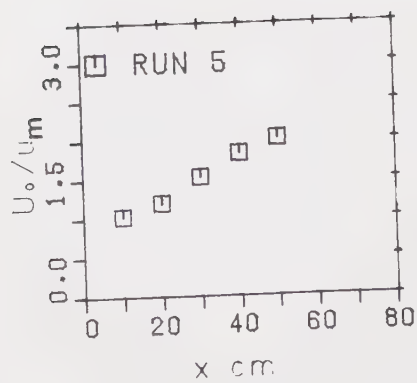
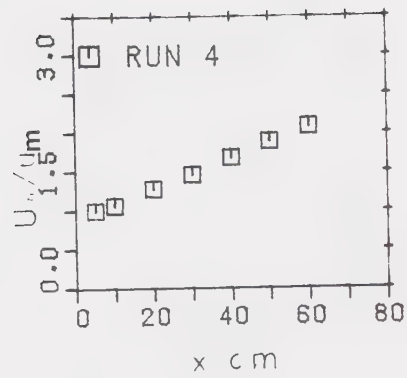
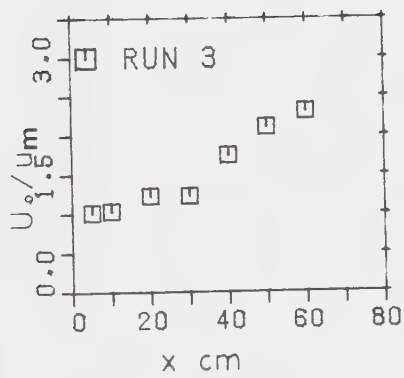
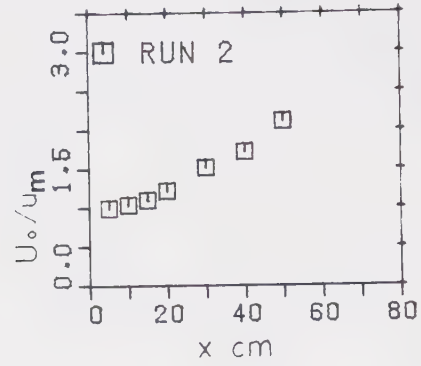
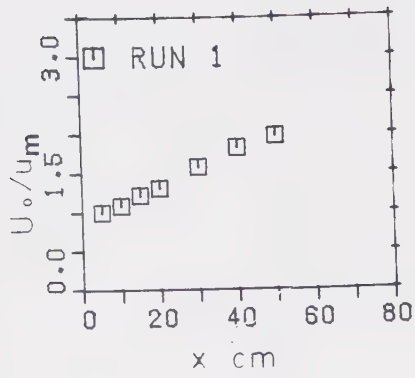


Run	x cm	y cm	y <sub>3</sub> cm	U <sub>3</sub> cm/s	U <sub>10</sub> cm/s	U <sub>3</sub> cm/s	U <sub>3</sub> /U <sub>10</sub>	x/y <sub>3</sub>	y <sub>3</sub> /y
11	40				48.5	35.0	.72	11.9	
	50				41.5	32.	.77	14.9	
	60				37.	29.	.78	17.9	
	30	7.	2.54	187.3	94.	11	.12	4.29	2.76
12	40				89.	24.5	28	5.71	
	50				70.	28.5	.41	7.14	
	60				59.5	32.5	.55	8.57	
	30	4.93	2.54	191.2	115.5	54.5	.47	6.09	1.94
	40				91.	58.	.64	8.11	
	50				70.	47.	.67	10.14	
	60				60.	46.	.77	12.17	

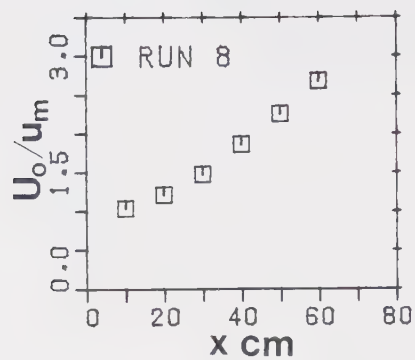
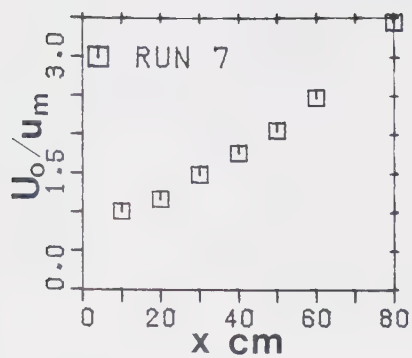


Figure B1 Proportionality of velocity decay

B6







}

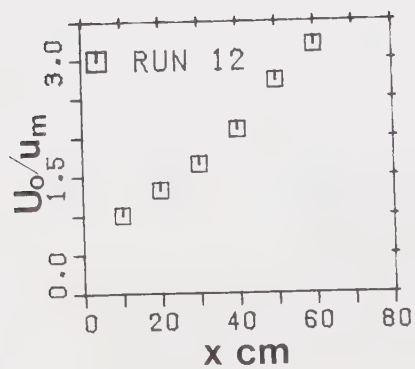
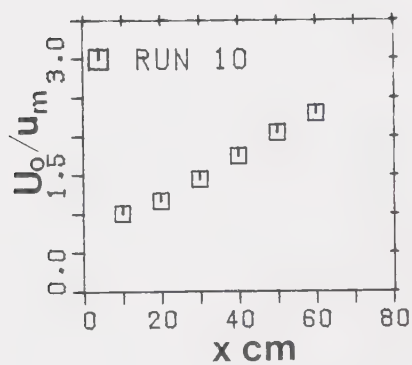
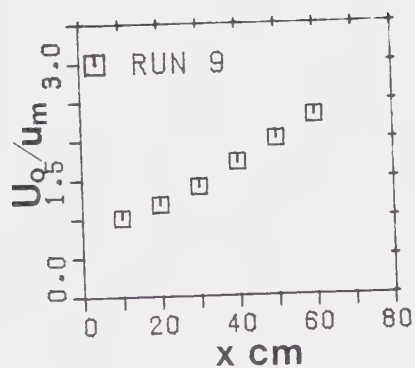
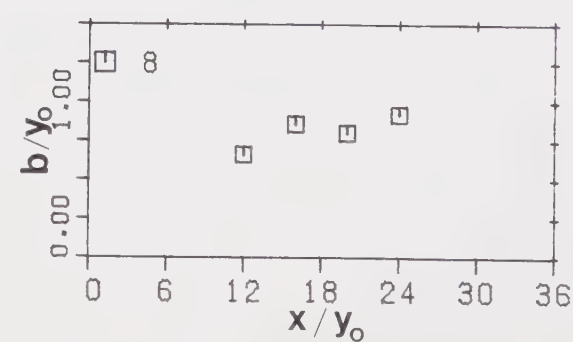
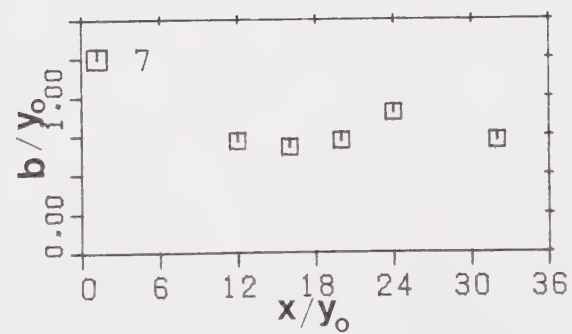
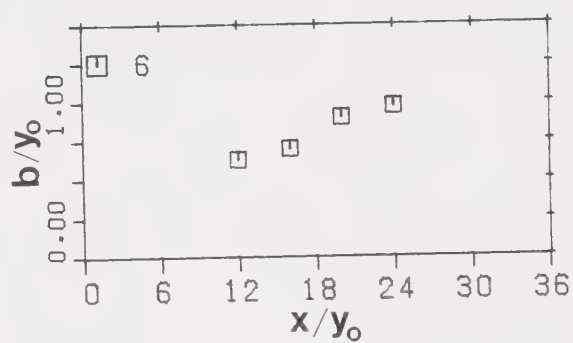
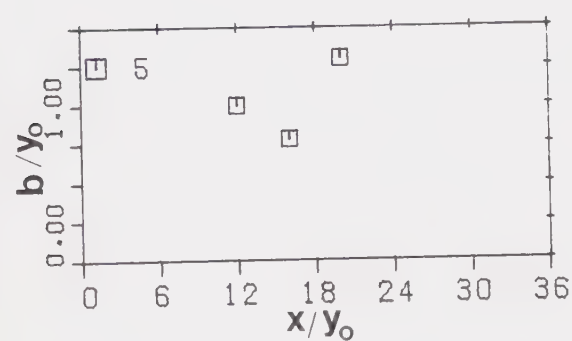
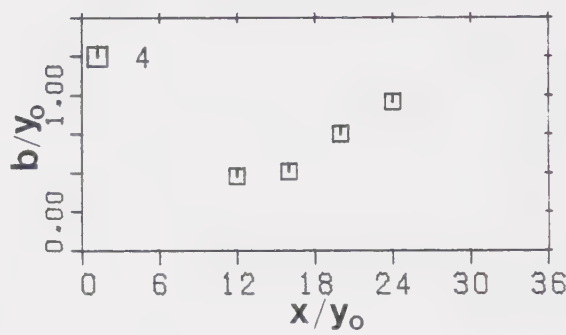
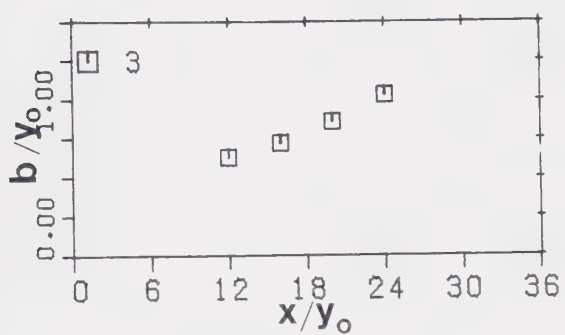
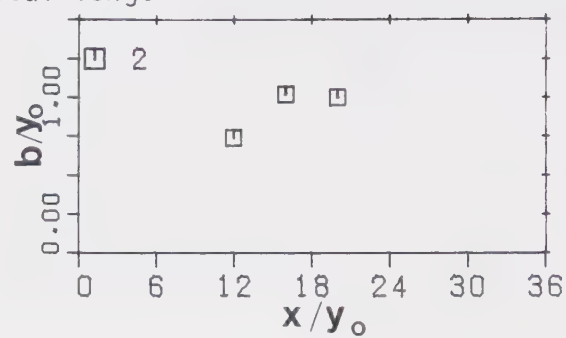
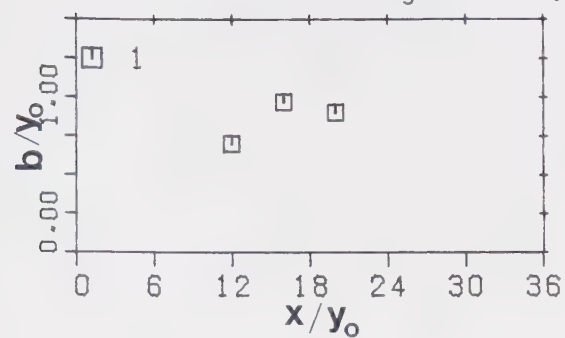


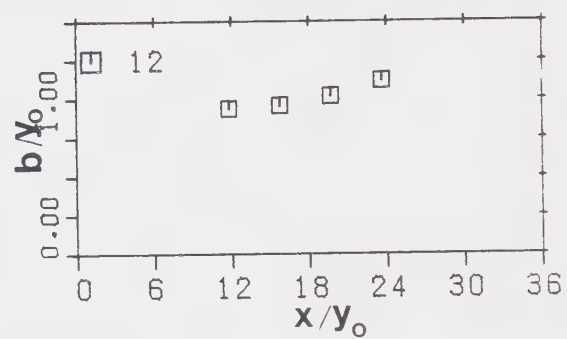
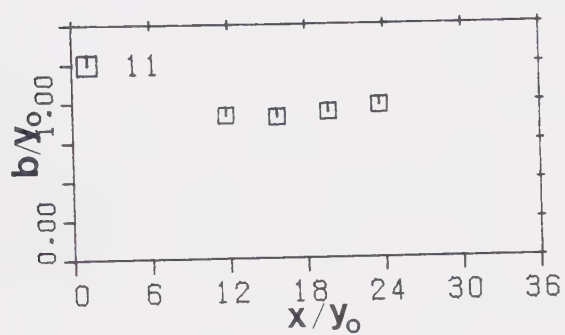
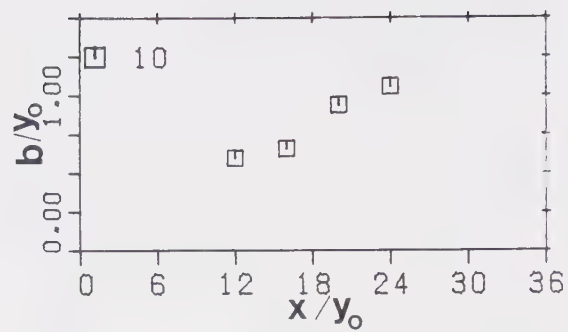
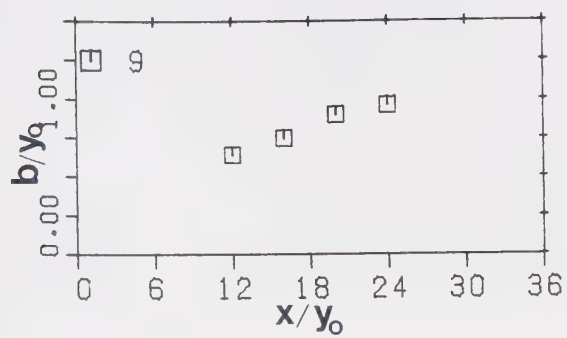




Figure B2 Vertical length scale









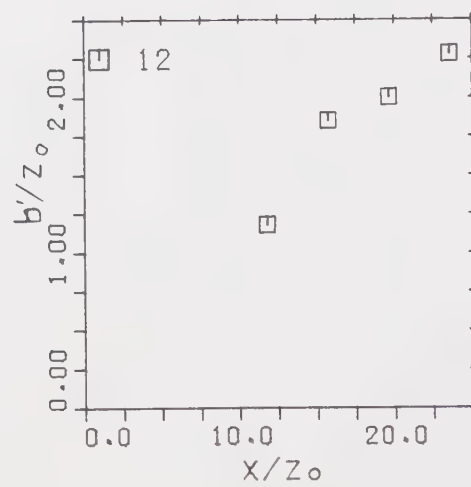
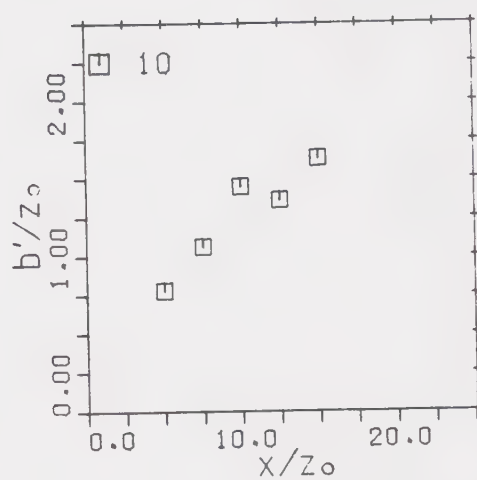
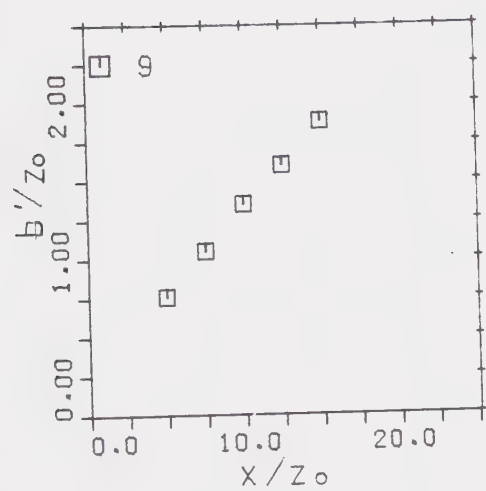
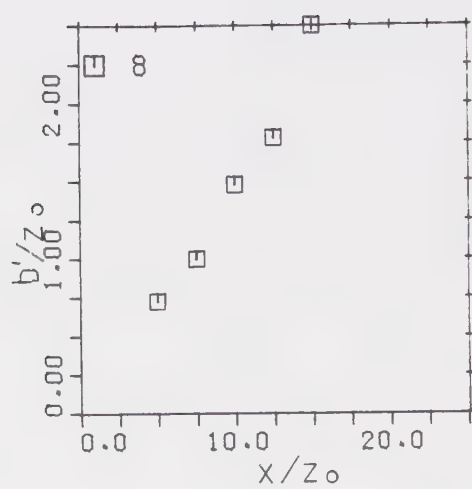
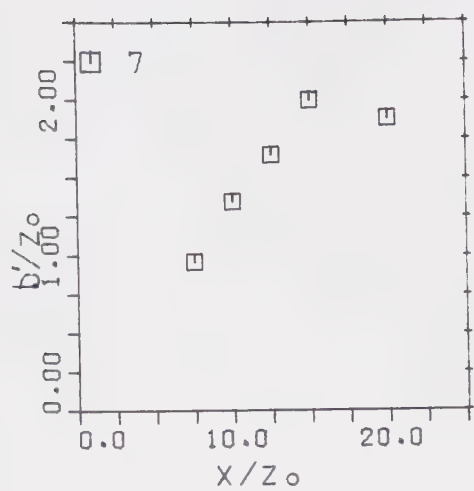


Figure B3 Transverse length scale



Table B2 Centreline Shear Stress

Run	x cm	$\tau_{mo}$ N/m <sup>2</sup>	$x/\sqrt{A}$	$C_F \times 10^{-3}$	$C'_F \times 10^{-3}$
6	10	2.10	3.16	6.10	5.88
	20	1.65	6.32	6.64	4.62
	30	1.38	9.49	7.42	3.87
	40	1.07	12.65	7.48	3.0
	50	.88	15.81	7.8	2.46
	60	.72	18.97	7.97	2.02
7	10	1.09	3.16	5.76	5.69
	20	.895	6.32	6.37	4.67
	30	.775	9.49	9.00	4.04
	40	.628	12.65	10.25	3.28
	50	.477	15.81	10.60	2.49
	60	.311	18.97	9.95	1.62
	80	.208	25.3	12.84	1.08
8	10	1.78	3.16	6.08	5.68
	20	1.39	6.32	6.58	4.43
	30	1.16	9.49	8.11	3.7
	40	0.848	12.65	9.48	2.7
	50	.628	15.81	10.23	2.0
	60	.446	18.97	10.25	1.42
9	10	1.825	3.16	5.7	5.59
	20	1.65	6.32	7.03	5.05
	30	1.4	9.49	8.47	4.29





Run	x cm	$\tau_{mo}$ N/m <sup>2</sup>	$x/\sqrt{A}$	$C_F \times 10^{-3}$	$C'_F \times 10^{-3}$
10	40	1.0	12.65	9.05	3.06
	50	.74	15.81	9.25	2.27
	60	.6	18.97	9.8	1.84
	10	2.22	3.16	6.29	6.13
	20	1.78	6.32	6.77	4.92
	30	1.4	9.49	8.18	3.87
11	40	0.95	12.65	8.08	2.62
	50	.65	15.81	7.55	1.80
	60	.55	18.97	8.04	1.52
	10	5.0	4.44	2.89	2.85
	20	4.4	8.88	4.19	2.51
	30	2.85	13.33	6.45	1.62
12	40	2.25	17.77	5.68	1.28
	50	1.63	22.21	6.65	0.93
	60	1.3	26.65	7.34	0.74
	10	5.35	4.44	3.00	2.93
	20	4.85	8.88	4.68	2.65
	30	4.21	13.33	6.31	2.3
	40	2.52	17.77	6.09	1.38
	50	1.62	22.21	6.61	.89
	60	1.34	26.65	7.44	.73



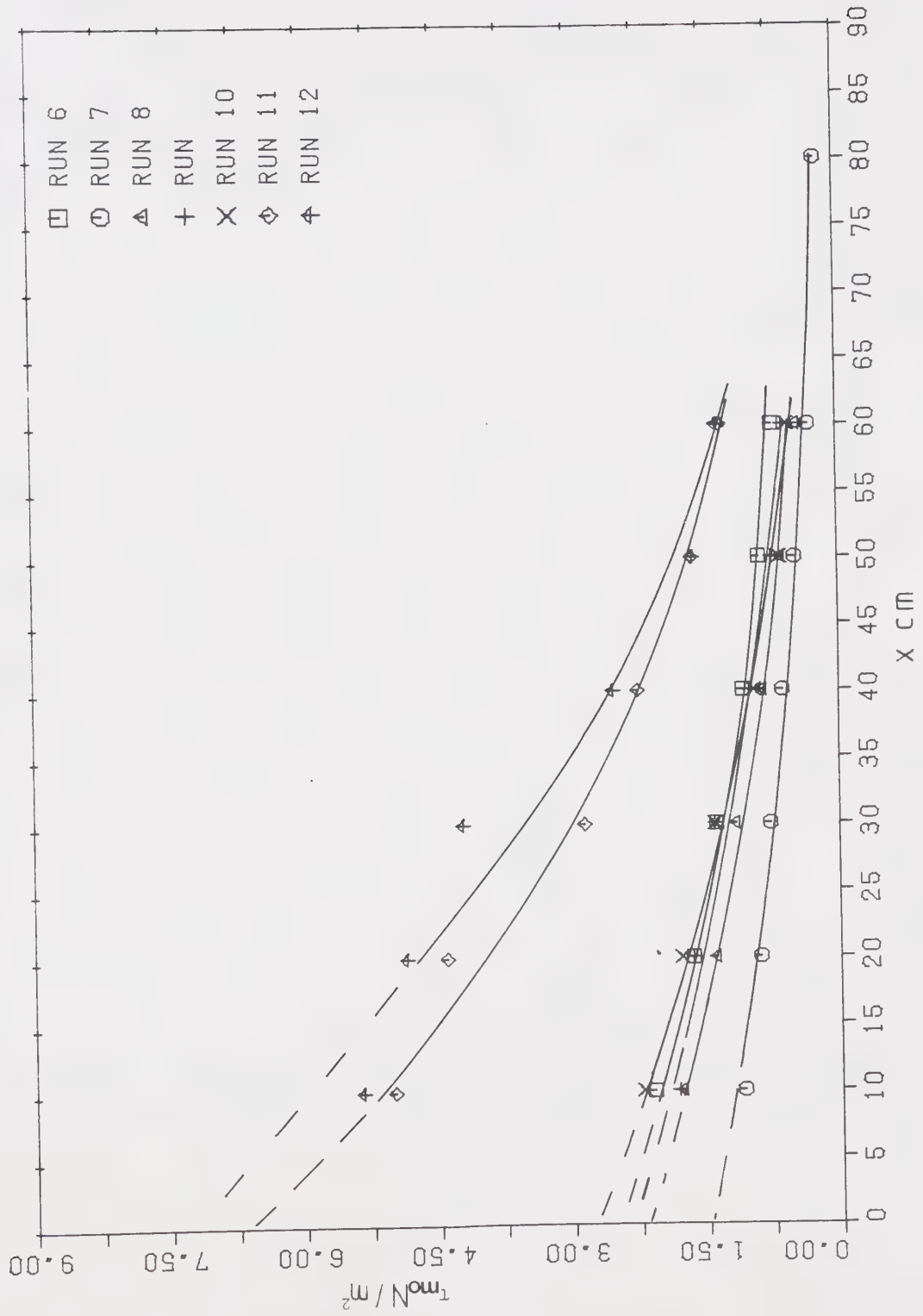
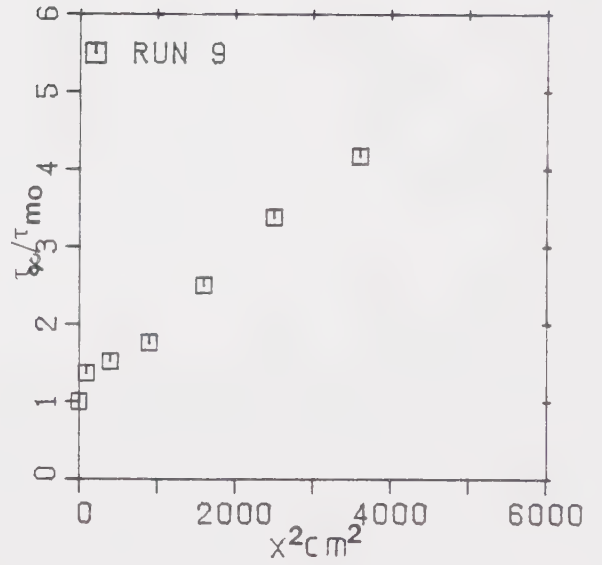
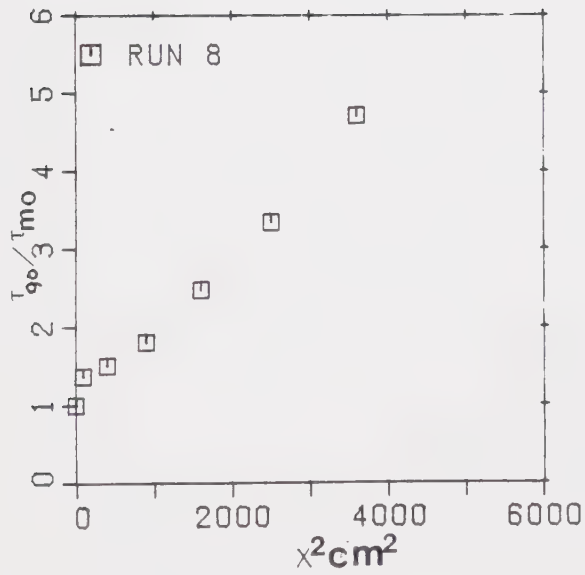
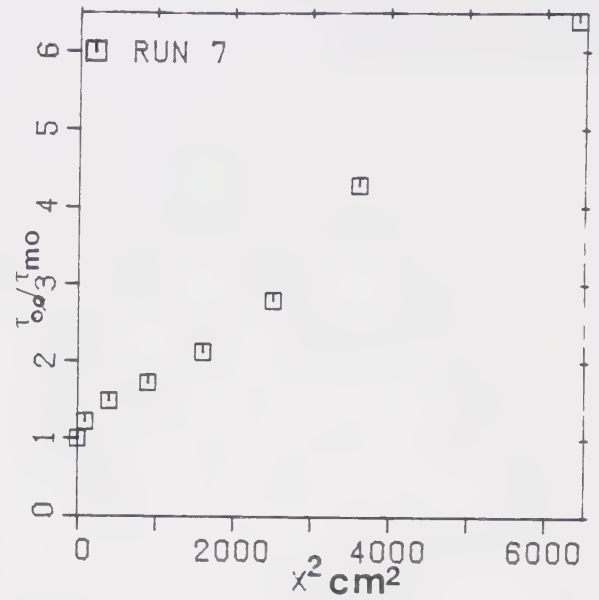
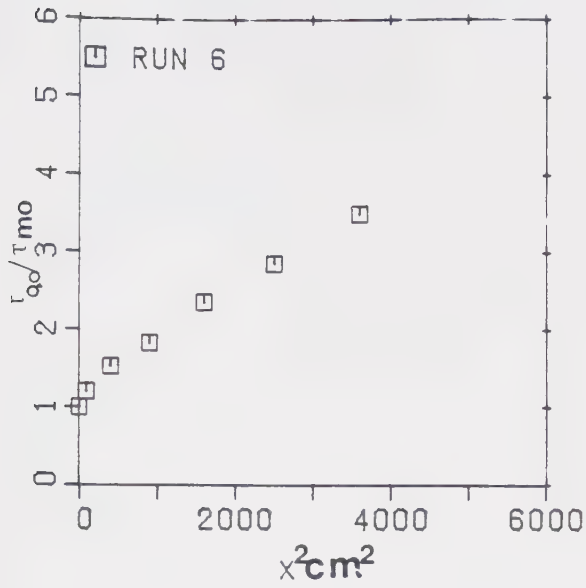


Figure B4 Centreline shear stress

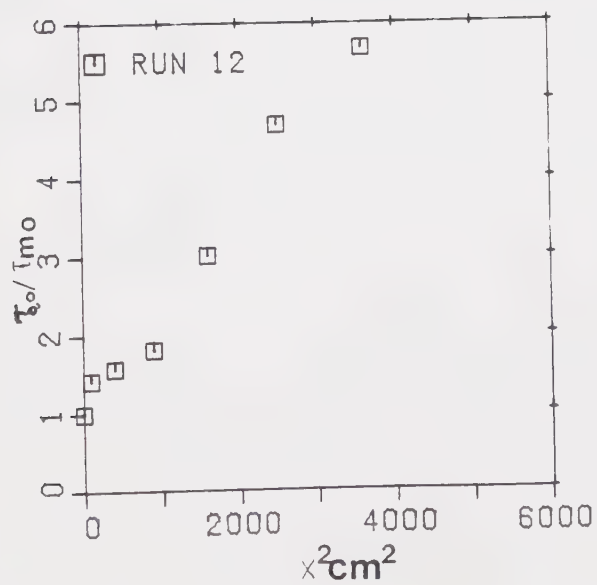
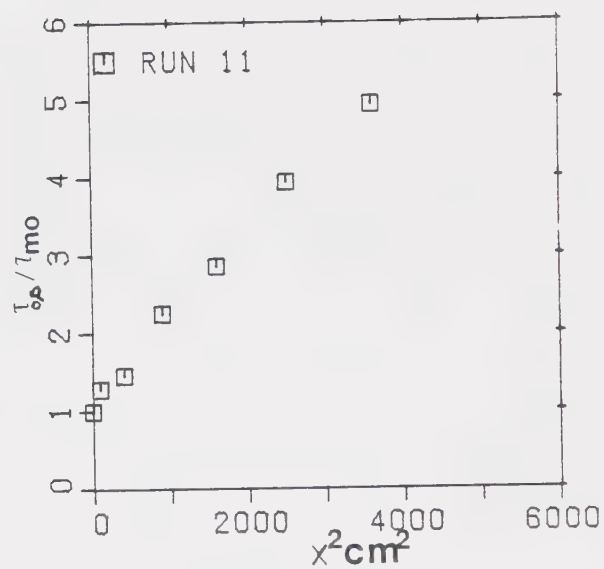
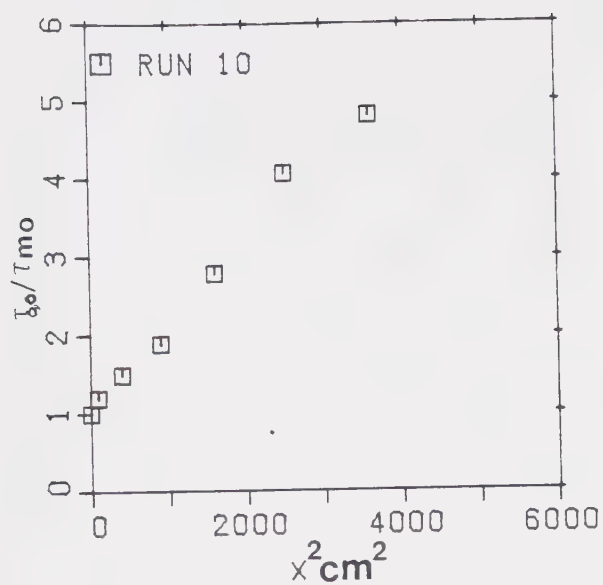


Figure B5 Inverse proportionality of shear stress with  $x^2$

B14











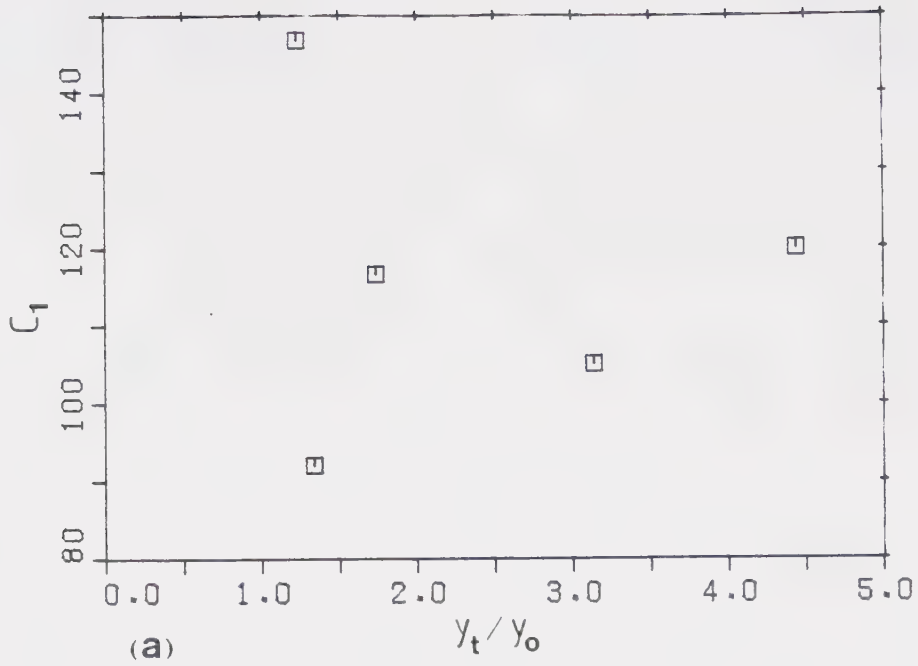
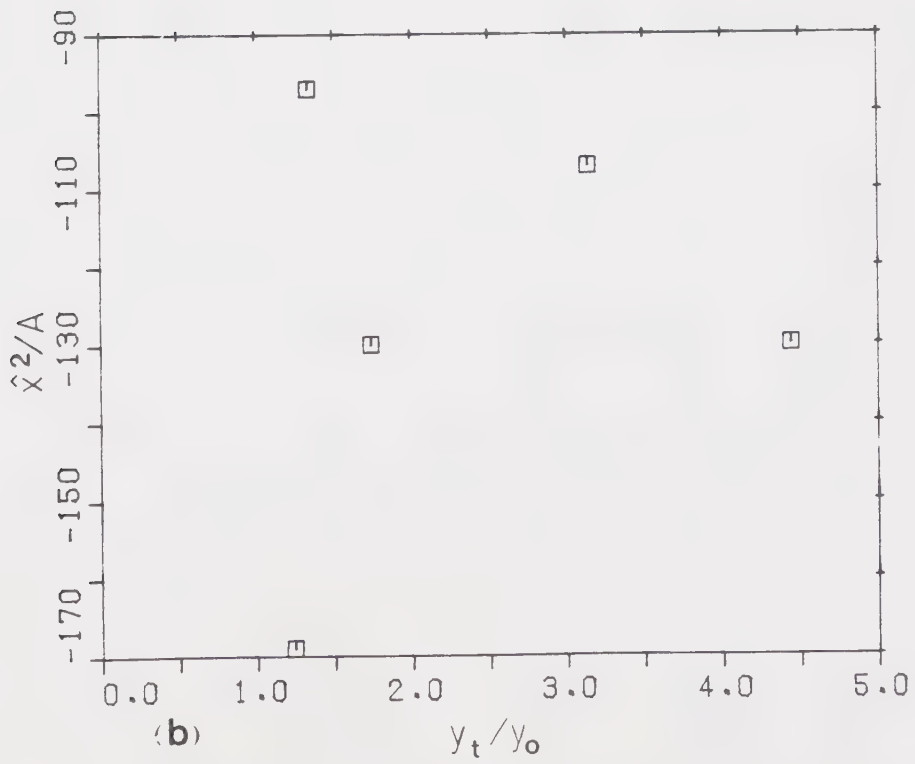
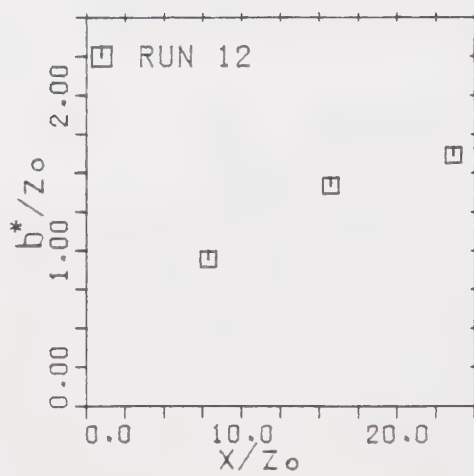
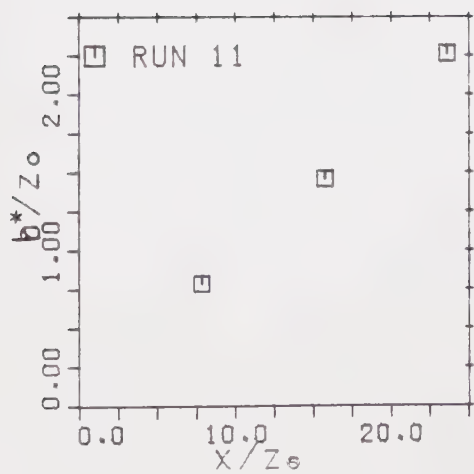
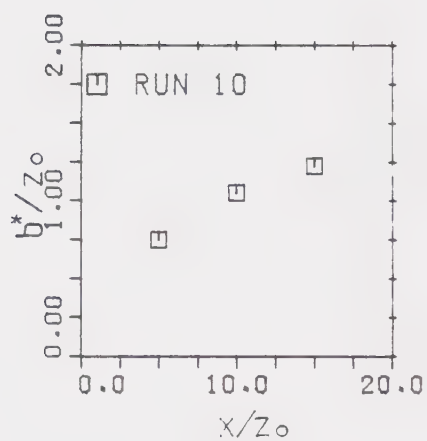
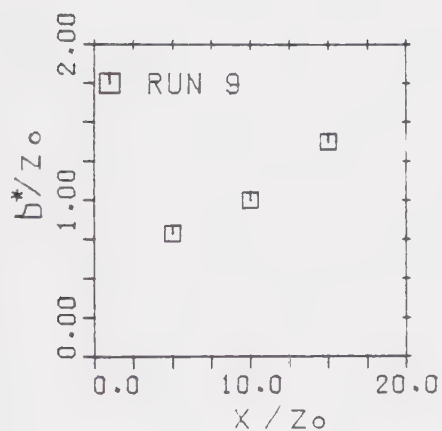
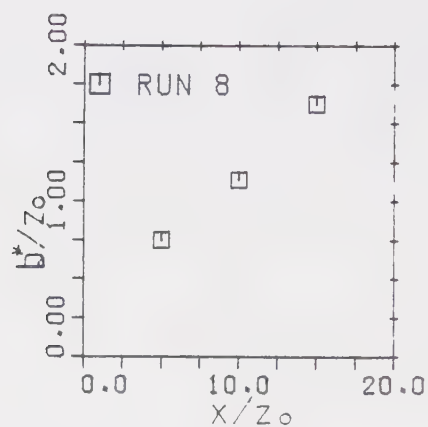
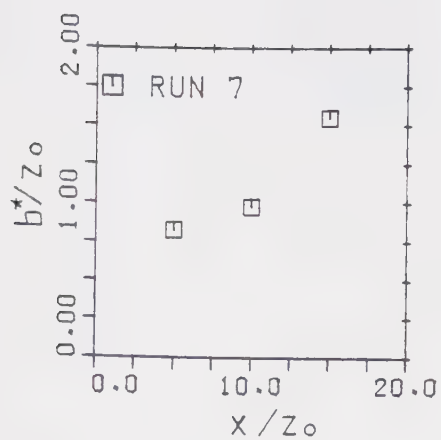


Figure B6 Lack of correlation of shear stress decay with

tailwater depth;  $\frac{\tau_{0,0}}{\tau_{m0}} = \frac{C_1}{(x^2 - \hat{x}^2)/A}$





Figure B7 Growth of length scale  $b^*$



## APPENDIX C - Jet with Scour data



Figure C1 Jet expansion

C2

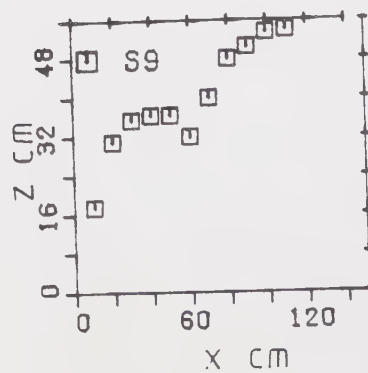
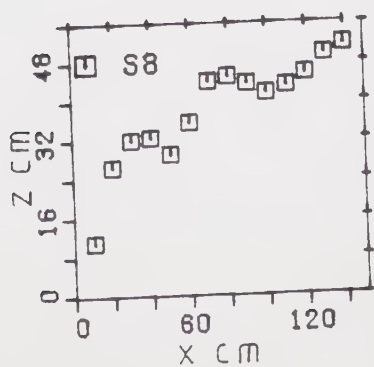
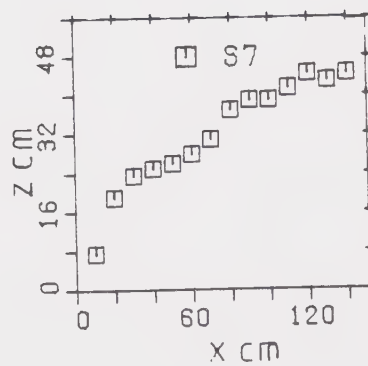
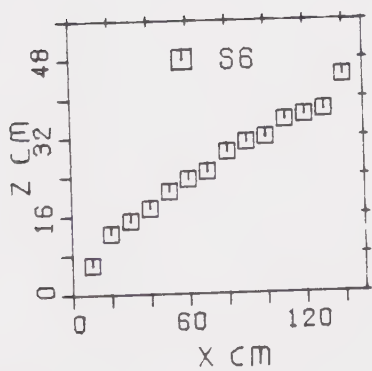
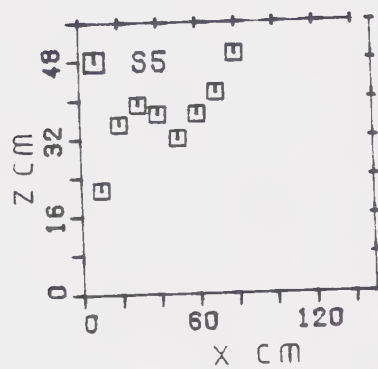
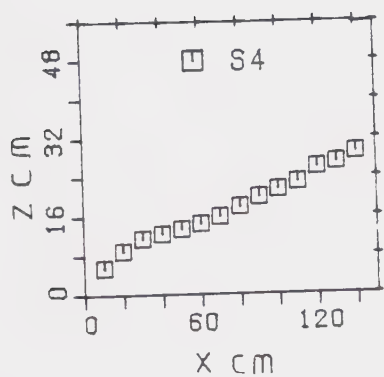
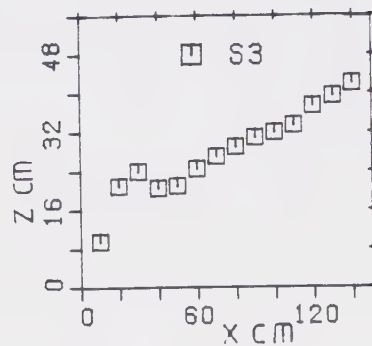
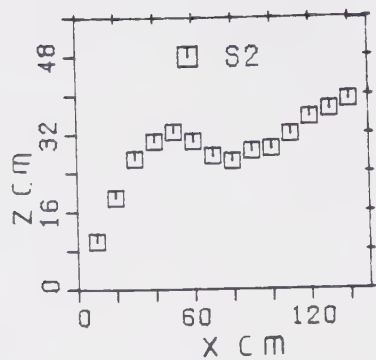






Table C1 Scour Hole Parameters

Run	$x_{\infty}$ cm	$\epsilon_{m\infty}$ cm	$y_0$ cm	$x_{\infty}/y_0$	$\epsilon_{m\infty}/y_0$	$F_d$
S2	16.	5.1	3.47	4.61	1.47	5.5
S3	10.05	3.65	3.38	2.97	1.08	4.46
S4	7.3	1.93	3.38	2.16	.57	2.10
S5	24.5	8.9	3.51	6.98	2.54	7.87
S6	8.5	3.1	3.41	2.49	.91	3.77
S7	12.5	3.8	3.38	3.70	1.12	4.27
S8	24.	7.1	3.53	6.8	2.01	6.8
S9	25.5	9.0	3.59	7.10	2.51	9.57















**B30332**